Technische Universität München

Fakultät für Medizin

III. Medizinische Klinik für Hämatologie und Internistische Onkologie

Klinikum rechts der Isar

Activated gp130 signaling selectively targets B cell differentiation to drive malignant transformation

Anna Katharina Scherger

Vollständiger Abdruck der von der Fakultät für Medizin der Technischen Universität München zur Erlangung des akademischen Grades eines

Doktors der Naturwissenschaften (Dr. rer. nat.)

genehmigten Dissertation.

Vorsitzender:	Prof. Dr. Carsten Schmidt-Weber
Prüfende der Dissertation:	1. apl. Prof. Dr. Ulrich Keller
	2. Prof. Angelika Schnieke, Ph.D.

Die Dissertation wurde am 05.03.2020 bei der Technischen Universität München eingereicht und durch die Fakultät für Medizin am 14.07.2020 angenommen.

Meiner verstorbenen Oma Gretel gewidmet

Parts of this work have been published in:

Scherger AK, Al-Maarri M, Maurer HC, Schick M, Maurer S, Öllinger R, Gonzalez-Menendez I, Martella M, Thaler M, Pechloff K, Steiger K, Sander S, Ruland J, Rad R, Quintanilla-Martinez L, Rose-John S, Wunderlich FT, Keller U:

Activated gp130 signaling selectively targets B cell differentiation to promote transformation of mature B cell lymphoma and plasmacytoma.

JCI Insight. 2019 Aug 8;4(15)

Contents

Abbreviations V
Abstract 1
1 Introduction 2
1.1 IL-6/gp130/JAK/STAT signaling 2
1.1.1 Interleukin-6 (IL-6) 2
1.1.2 Janus kinases (JAKs) 3
1.1.3 Signal transducers and activators of transcription (STATs) 4
1.2 IL-6 downstream signaling 4
1.2.1 The chimeric receptor protein Leucine zipper + glycoprotein 130, L-gp130 5
1.3 B cell development 6
1.3.1 Early B cell development 6
1.3.1 Late B cell development 7
1.4 B cell lymphomas 9
1.5 Plasma cell disorders 10
1.5.1 Plasmacytomas 10
1.5.2 Multiple Myeloma 11
1.6 The IL-6/gp130/JAK/STAT3 axis in MM 13
1.7 Treatment of MM patients 13
1.7.1 Standard treatment 14
1.7.2 Novel treatment options currently studied 14
1.8 Mouse models of MM 15
1.8.1 Genetically engineered mouse models 15
1.8.2 Xenograft models 16
1.8.3 Other mouse models of malignant transformation 17
1.9 The Cre/loxP system 18
1.9.1 Conditional gene targeting by the Cre/loxP system 18
1.10 Objectives 20
2 Materials and Methods 21
2.1 Materials 21
2.1.1 Chemicals and Reagents 21
2.1.2 Consumables 23
2.1.3 Instruments 24
2.1.4 Growth media and buffer compositions 26
2.1.5 Enzymes 30
2.1.6 Primers 30

2.1.7 Antibodies ... 31
2.1.8 Molecular weight markers for DNA and proteins ... 32
2.1.9 Plasmids ... 32
2.1.10 Kits ... 32
2.1.11 Software programs ... 32
2.1.12 Mouse strains ... 33
2.2 Methods ... 35
2.2.1 Molecular biology techniques ... 35
2.2.1.1 Mouse genotyping by PCR ... 35
2.2.1.2 Agarose gel electrophoresis ... 35
2.2.1.3 Isolation of genomic DNA from tumor material ... 35
2.2.1.4 Analysis of IgH rearrangements ... 36
2.2.1.5 RNA extraction from eukaryotic cells ... 36
2.2.1.6 Reverse transcription (RT) ... 36
2.2.1.7 Quantitative real time PCR (qRT-PCR) ... 37
2.2.2 Protein biochemistry ... 37
2.2.2.1 Cell lysis ... 37
2.2.2.2 SDS-PAGE and immunoblotting ... 38
2.2.2.3 Stripping of membranes ... 38
2.2.2.4 Collection of serum and serum electrophoresis ... 38
2.2.3 Cell culture and cell-based assays ... 39
2.2.3.1 Cell culture methods ... 39
2.2.3.2 Preparation and culture of murine embryonic fibroblasts ... 39
2.2.3.3 Generation of retrovirus and infection of MEFs ... 39
2.2.3.4 Freezing and thawing of cells ... 40
2.2.4 Animal experiments ... 40
2.2.4.1 Keeping and breeding of mice ... 40
2.2.4.2 Fetal liver cell transplantation ... 40
2.2.4.3 Serial transplantation of tumor cells ... 40
2.2.4.4 Sheep red blood cell (SRBC) immunization ... 41
2.2.4.5 Necropsy ... 41
2.2.5 Immunological methods ... 41
2.2.5.1 Flow cytometry ... 41
2.2.5.2 Enzyme-linked Immunosorbent Assay (ELISA) ... 42
2.2.5.3 Magnetic cell separation ... 42
2.2.6 Histological and immunohistochemical analyses ... 42
2.2.7 Transcriptome analysis ... 43
2.2.7.1 RNA isolation from tumor material for RNA-sequencing ... 43

2.2.7.2 RNA-sequencing 43
2.2.8 Bioinformatical analyses 43
2.2.8.1 Statistical analysis of high-throughput gene expression data 43
2.2.8.2 Differential gene expression analysis 43
2.2.8.3 Derivation of a *CD19;L-gp* gene expression signature 44
2.2.8.4 Data acquisition and pre-processing 44
2.2.8.5 Gene set collection 44
2.2.8.6 Single sample gene set enrichment (ssGSEA) 45
2.2.8.7 Differential expression of immunoglobulin heavy and light chain genes 45
2.2.9 Statistical analysis 45
3 Results 46
3.1 Generation of R26 fl rx *L-gp130* mice 46
3.2 Gating strategy to define distinct B cell subsets by flow cytometry 48
3.3 Constant gp130 signaling promotes B cell differentiation in young *CD19;L-gp* mice 49
3.4 Establishment of the Lgp-130 signature 51
3.5 Activation of gp130 signaling in B cells leads to mature B cell malignancies 54
3.6 Serial transplantability of the disease 58
3.7 Activation of gp130 during or post the GC reaction results in delayed tumor formation 58
3.8 Immunization of *Cγ1;L-gp* mice leads to the formation of a GC but does not promote tumor development 60
3.9 Activation of gp130 overcomes the lymphoma phenotype of B cell–targeted *Myc* by enforcing plasmacytic differentiation 61
3.10 Conditional gp130 activation in hematopoietic stem/progenitor cells results in a highly aggressive B cell malignancy 65
3.11 RNASeq of tumor material from diseased mice reveals clustering of genotypes 69
3.12 The L-gp130 signature is represented during progression of human MM 70
4 Discussion 72
4.1 Forced activation of gp130 signaling within the B cell compartment results in STAT3 activation, accumulation of mature B cell subsets, and malignant transformation 72
4.2 *CD19;L-gp* show collaboration with the oncogene *Myc* but not with the tumor suppressor *Trp53* .. 74
4.3 Conditional gp130 activation during late B cell differentiation results in B cell tumors with a long latency 75
4.4 Gp130 activation in hematopoietic stem/progenitor cells leads to a rapid and aggressive B cell malignancy 76
4.5 The L-gp130 signature in human MM 77
4.6 Limitations of the novel transgenic mouse models of MM 78
5 Summary 81
6 References 82
7 List of tables 104

8 List of figures 104
9 List of publications 105
9.1 Articles in peer-reviewed journals 105
9.2 Conference contributions 106
10 Acknowledgements 107

Abbreviations

α	alpha (anti)
β	beta
γ	gamma
µg	10^{-6} gram
µl	10^{-6} liter
µmol	10^{-6} Mol
µM (µmol/l)	10^{-6} Mol/liter
aa	amino acid
ABC DLBCL	activated B cell diffuse large B cell lymphoma
ACK	ammonium chloride–potassium bicarbonate
AID	activation-induced cytidine deaminase
AKT	AKT serine/threonine kinase 1
AML	acute myeloid leukemia
Amp	Ampicillin resistance gene
ANOVA	analysis of variance
APC	allophycocyanin
APRIL	A proliferation-inducing ligand
APS	ammonium persulfate
ARF	alternative reading frame
ASCT	autologous stem cell transplantation
ATP	adenosine-5'- triphosphate
BAFF	B cell activating factor
BC	B cell
Bcl-2, 6	B-cell lymphoma 2, 6
Bcl-XL	B-cell lymphoma extra large
BCMA	B-cell maturation antigen
BCR	B cell receptor
bio	biotin
BL	Burkitt's lymphoma

Blimp1	B lymphocyte induced maturation protein 1
BM	bone marrow
BMM	bone marrow microenvironment
bp	base pair
BSA	bovine serum albumin
BSF-2	B cell stimulatory factor-2
° C	degree celsius
C	control, carboxy-terminus
CAG	chicken β-actin promoter coupled to the CMV enhancer
CAR	chimeric antigen receptor
CBD	cytokine binding domain
CD	cluster of differentiation
CDK4	cyclin-dependent kinase 4
cDNA	complementary DNA
CLP	common lymphoid progenitor
cm	centimeter
c-MAF	musculoaponeurotic fibrosarcoma
CMP	common myeloid progenitor, counts per million
CNTF	ciliary neurotrophic factor
CO_2	carbon dioxide
CPM	counts per million
CRAB	hypercalcemia, renal insufficiency, anemia, bone lesions
Cre	causes recombination, recombinase from phage PI
CSR	class-switch recombination
Ct	threshold cycle
CT-1	cardiotropin-1
Cy	cyanine dye
D	diversity
DBD	DNA-binding domain
DEG	differentially expressed genes

dest.	destillata
DLBCL	diffuse large B cell lymphoma
DMEM	Dulbecco´s Modified Eagle Medium
DMSO	dimethyl sulfoxide
DNA	desoxyribonucleic acid
dNTP	2'-Desoxyribonucleosid-5'-triphosphat
DTA	diphtheria toxin fragment A
DTT	dithiothreitol
DZ	dark zone
E13.5	embryonic day 13.5
Eμ	enhancer of immunoglobulin M (μ) gene
E.coli	escherichia coli
EDTA	ethylenediaminetetraacetic acid
e.g.	exempli gratia
EGTA	ethylene glycol-bis(2-aminoethylether)-N,N,N′,N′-tetraacetic acid
ELISA	Enzyme-linked Immunosorbent Assay
env	envelope
ERK	Extracellular-signal regulated kinase
et al.	et alii
EtBr	ethidium bromide
FACS	fluorescence activated cell scanning/sorting
Fas	Fas cell surface death receptor
FCS	fetal calf serum
FDC	follicular dendritic cells
FDR	false discovery rate
f.e.	for example
FELASA	Federation of European Laboratory Animal Science Associations
FERM	four-point-one, ezrin, radixin, moesin
FGFR3	fibroblast growth factor receptor 3
FI	fluorescence intensity

FITC	fluorescein isothiocyanate
FL, fl	follicular lymphoma, fetal liver, floxed
FL-HSPC	fetal liver hematopoietic stem/progenitor cell
floxed	loxP sites flanked
FNIII	fibronectin type III-like domains
Frt	flp recognition target
FSC	forward scatter
Fwd	forward
g	gravity (9,81 m/s^2), gram
gag	group-specific antigen
GAPDH	glyceraldehyde 3-phosphate dehydrogenase
GAS	gamma activated sequence
GC	germinal center
gDNA	genomic DNA
GEM	genetically engineered mouse
GEO	Gene Expression Omnibus Database
GFP	green fluorescent protein
gp	glycoprotein
gp130	glycoprotein 130 kDa
Gran	granulocytes
Gy	gray (1 Gy=1 J/kg)
h	hour
H&E	hematoxylin-eosin
HBSS	Hank’s Balanced Salt Solution
HCL	hydrochloric acid
HEPES	4-(2-hydroxyethyl)-1-piperazineethanesulfonic acid
HRP	horseradish peroxidase
HSC	hematopoietic stem cells
HSPC	hematopoietic stem and progenitor cells
hu	human

i.e.	id est
IFN	interferon
Ig	Immunoglobulin
IgH	Ig heavy chain
Ighg1	immunoglobulin heavy constant gamma 1
IgL	Ig light chain
IHC	immunohistochemistry
IL	interleukin
IL-6R	interleukin 6 Receptor
IMiDs	immunomodulatory drugs
INK4a	inhibitor of Cdk4
i.p.	intraperitoneal injection
IRES	internal ribosomal entry site
IRF4	interferon regulatory factor-4
i.v.	intravenous injection
J	joining
JH	janus homology domain
Jun	jun oncogene
kb	kilobases, 1000 base pairs
kDa	kilodalton
Ki67	Kiel 67
KO	knock out
JAK	Janus kinase
L	ladder, liter
LAH	long arm of homology
L-gp/L-gp130	Leucine zipper + glycoprotein 130
LIF	leukemia inhibitory factor
Lin	lineage, linear
LN	lymph node
log	logarithmic

LOH	Loss of heterozygosity
loxP	locus of X over in PI, recognition sequence of Cre
LSK	$Lin^{-}Sca1^{+}c\text{-}kit^{-}$
LZ	Light zone, leucine zipper
Lymph	lymphocytes
mA	milli Ampère
MALT	mucosa-associated lymphoid tissue
MAPK	mitogen-activated protein kinase
Mcl-1	myeloid cell leukemia-1
MCS	multiple cloning site
MDM2	Murine Double Minute 2 homolog
MEF	murine embryonic fibroblast
$MgCl_2$	magnesium chloride
MGUS	monoclonal gammopathy of undetermined significance
MIG	MSCV IRES GFP
min	minute
ml	milliliter
MM	multiple myeloma
mM (mmol/l)	10^{-3} mol/liter
MPO	myeloperoxidase
MPP	multipotent progenitor
mRNA	messenger RNA
MSCV	murine stem cell virus
MTOR	mechanistic target of rapamycin
MYC	myelocytomatosis oncogene
MZ	marginal zone
N	amino-terminus
n	number
NaB	disodium tetraborate
NaCl	sodium chloride

NaF	sodium fluoride
$NaVO_4$	sodium orthovanadate
NEAA	non-essential amino acids
neo	neomycin resistance gene
NES	normalized enrichment scores
NF-κB	nuclear factor κB
NHEJ	non-homologous end-joining
NK	natural killer
NLS	nuclear localization sequence
nm	10^{-9} meter, nanometer
NMZL	nodal marginal zone lymphoma
NTD	N-terminal domain
ORF	open reading frame
o/n	overnight
OS	overall survival
OSM	oncostatin M
p	phosphorylated
Pax5	paired box protein 5
PB	peripheral blood, pacific blue
PBS	phosphate buffered saline
PBST	PBS + 1 % Tween
PC	plasma cell
PCA	principal component analysis
PCR	polymerase chain reaction
PE	phycoerythrin
PerCP	peridinin chlorophyll protein complex
Pen/Strep	penicillin/streptomycin
pH	pondus Hydrogenii
PI	propidium iodide
PI3K	phosphatidylinositol 3-Kinase

PIAS	protein inhibitors of activated STATs
PIM	Proviral Integration Site for Moloney Murine Leukemia Virus
pmol	10^{-12} mol, picomol
PMSF	phenylmethylsulphonyl fluoride
POEMS	polyneuropathy, organomegaly, endocrinopathy, monoclonal gammopathy, and skin changes
pol	polymerase
PRDM1	PR domain containing 1
pre-B	precursor B cell
pro-B	progenitor B cell
PVDF	polyvinylidene fluoride
qRT-PCR	quantitative real time PCR
R26	Rosa26 locus
RAF	rapidly accelerated fibrosarcoma
RAG1/2	recombinase activating genes 1 and 2
RAS	rat sarcoma
rel	relative
rev	reverse
RNA	ribonucleic acid
RNASeq	RNA-sequencing
ROX, rox	carboxy-X-rhodamine, locus of recombination by Dre
rpm	rounds per minute
RPMI	Roswell Park Memorial Institute medium
RT	reverse Transcriptase, room temperature
rx	rox-flanked
SAH	short arm of homology
SBP	solitary bone plasmacytoma
SCID	severe combined immunodeficiency
SDS-PAGE	sodium dodecyl sulfate polyacrylamide gel electrophoresis
sec	second
SEM	standard error of the mean

SEP	solitary extramedullary plasmacytoma
SH2	Src homology 2
SHM	somatic hypermutation
sIL-6R	soluble IL-6 receptor
SLAMF7	signaling lymphocytic activation molecule F7
SMZL	splenic marginal zone lymphoma
SOCS	suppressors of cytokine signaling
SPF	specific-pathogen-free
SPL	spleen
SRBC	sheep red blood cells
S-S	disulfide bridge
SSC	side scatter
ssGSEA	single sample gene set enrichment analysis
STAT	signal transducer and activator of transcription
STOP	stop sequence
SV40	simian virus 40
t	translocation
TAD	transactivation domain
TEMED	N,N,N',N'-Tetramethylendiamine
TfH	T follicular helper cell
TG	transgene
TP53	tumor protein 53 (human)
Trp53	transformation related protein 53 (mouse)
Tris	2-Amino-2-(hydroxymethyl)propane-1,3-diol
TSO	template switch oligo
Tween 20	poly(oxyethylen)n-sorbitan-monolaurate
TUM	Technical University Munich
Tyk2	tyrosine kinase 2
Tyr	tyrosine
U	unit

UMIs	unique molecular identifiers
UTR	untranslated region
UV	ultra violet
V	volt, variable
VIPER	virtual inference of protein activity by enriched regulon analysis
Vol	volume
w/	with
WBC	white blood cell
WNT	wingless/integrated
w/o	without
WSS	Westphal Stop sequence
WT	wildtype
x	times
XBP-1	X-box binding protein 1
XIAP	X-linked inhibitor of apoptosis protein
Y	tyrosine
YFP	yellow fluorescent protein
ZsGreen	Zoanthus sp. Green fluorescent protein
*	significance
%	percent
+	positive expression
-	negative expression

Abstract

The IL-6/gp130/JAK/STAT3 axis is crucial for the regulation of normal B cell and T cell functions, and for coordinated activity of the innate and adaptive immune system. However, aberrant IL-6/gp130/JAK/STAT3 signaling is associated with a wide range of cancer entities as well as with acute and chronic inflammation. Notably, this axis has been described as a prevalent event in hematological malignancies, including acute and chronic leukemia, and multiple myeloma. Although advancements have been made in understanding the pathogenesis of these severe diseases and novel targeted therapies have been introduced, still not all patients can be cured. Thus, there is an urgent need for the development of new mouse models that would help to better analyze the influence of this pathway on specific tumorigenic processes.

In this study, the role of conditional gp130/JAK/STAT3 activation was examined in transgenic mouse models by targeting constitutively active, cell-autonomous gp130 activity to distinct B cell subsets, as well as to the entire hematopoietic system by making use of the Cre-loxP-system. Thereby constitutive activation of gp130 signaling within the entire B cell compartment promoted differentiation of B cells towards a mature stage in young mice. RNA-sequencing analysis of these animals revealed the L-gp130 signature with activation of IL-6/JAK/STAT3, PI3K/AKT/MTOR, WNT, MYC, as well as BCR and NF-kappaB signaling pathways.

Regardless of when activated during B cell differentiation, constitutive active gp130 signaling eventually led to the development of mature B cell lymphomas and plasma cell disorders with features of multiple myeloma. The tumors in the different compound mice occurred with full penetrance only at different latencies while infiltrating $CD138^+$ cells represented a central characteristic in every tumor.

Notably, a collaboration of the oncogene *Myc* and gp130 signaling in B cells in a HSPC-FL transplantation approach was demonstrated. Here, gp130 activity abrogated the differentiation block induced by a B cell-targeted *Myc* transgene and resulted in complete penetrance of the gp130-associated CD138-positive plasma cell phenotype. However, a collaboration of gp130 activity in B cells and the partial knockdown of the tumor suppressor p53 was not seen.

Moreover, constitutive active gp130 signaling in hematopoietic stem cells likewise resulted in the growth of largely mature, aggressive B cell cancers, again with a high penetrance of CD138-positive tumors and features of multiple myeloma.

Taken together, this study reveals that gp130 signaling selectively provides a strong growth and differentiation advantage for mature B cells and directs lymphomagenesis specifically towards terminally differentiated B cell cancers while also showing serial transplantability.

1 Introduction

1.1 IL-6/gp130/JAK/STAT signaling

1.1.1 Interleukin-6 (IL-6)

Interleukin-6 (IL-6) is a pleiotropic cytokine that acts on various cells and is produced by nearly all stromal cells and cells of the immune system (Hunter and Jones 2015). It belongs to the group of long-chain α-helix-bundle cytokines (Bazan 1990) and uses the IL-6 receptor (IL-6R) for signal transduction. The IL-6R is composed of an 80 kDa IL-6 binding molecule termed gp80, CD126 or IL-6Rα and the ubiquitously expressed 130 kDa common receptor subunit, glycoprotein 130 (gp130, CD130) (Yamasaki, Taga et al. 1988, Taga, Hibi et al. 1989, Hibi, Murakami et al. 1990). Gp130 does not only mediate signal transduction by IL-6 itself but by many other members of the IL-6 family of cytokines, including leukemia inhibitory factor (LIF), ciliary neurotrophic factor (CNTF), oncostatin M (OSM), interleukin-11 (IL-11), and cardiotropin-1 (CT-1) (Gearing, Comeau et al. 1992, Ip, Nye et al. 1992, Liu, Modrell et al. 1992, Yin, Taga et al. 1993, Pennica, Shaw et al. 1995).

There are two types of signaling through the IL-6R. During the classical signaling, binding of IL-6 to the 80 kDa cell membrane receptor IL-6Rα leads to the formation of a complex with the ubiquitously expressed common receptor unit, glycoprotein gp130 thus activating the signaling cascade. In contrast, trans-signaling includes a soluble IL-6 receptor (sIL-6R, gp55), that is either produced by alternative splicing of the IL-6R mRNA or shed from the surface of IL-6R-expressing cells (Lust, Donovan et al. 1992, Mullberg, Schooltink et al. 1993). This sIL-6R, which has been found in body fluids such as urine and blood (Novick, Engelmann et al. 1989), first binds to IL-6 and then to the membrane receptor gp130 hence leading to signal transduction (**Figure 1**) (Jones, Horiuchi et al. 2001, Ataie-Kachoie, Pourgholami et al. 2013).

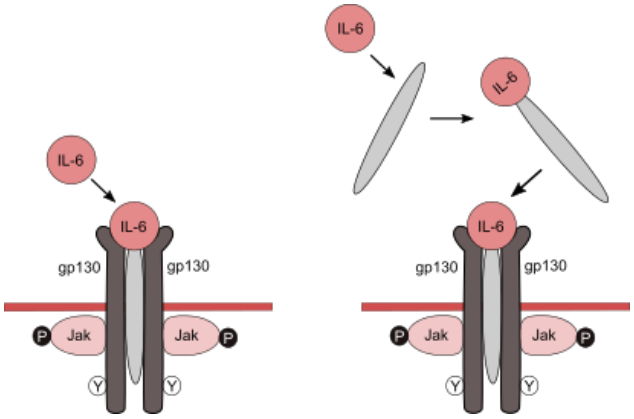

Figure 1: Classical IL-6 signaling (left) and trans-signaling (right). Left: binding of IL-6 to its transmembrane receptor IL-6R leads to the dimerization of the signal transducing receptor subunit gp130, termed classical IL-6 signaling. Right: IL-6 first binds to sIL-6R and this complex then binds to gp130 in a reaction called trans-signaling. Abbreviations: circled Y: tyrosine, white P in black circle: phosphate (adapted from (Heinrich, Behrmann et al. 1998, Lee, Buhimschi et al. 2011)).

Originally identified as a factor essential for differentiation of B cells into antibody producing plasma cells (PCs), IL-6 was initially described as B cell differentiation factor or B cell stimulatory factor-2 (BSF-2) (Hirano, Yasukawa et al. 1986, Akira, Taga et al. 1993). Apart from its important role in B cells, IL-6 also displays a wide range of biological functions in regards of the immune response, inflammation, and hematopoiesis, as well as in the endocrine and nervous systems. It therefore promotes T-cell growth and differentiation, megakaryocyte maturation, the development of osteoclasts, and acute-phase protein synthesis in hepatocytes. Furthermore, IL-6 acts as a growth factor in multiple myeloma (MM)/plasmacytoma and other cancers and promotes the growth of hematopoietic stem cells (Sehgal 1989, Heinrich, Castell et al. 1990, Hirano 1990, Van Snick 1990, Hirano 1992, Hirano 1994).

1.1.2 Janus kinases (JAKs)

Binding of IL-6 to its receptor and subsequent dimerization of gp130 leads to phosphorylation and activation of Janus kinases (JAKs). JAKs comprise a family of four non-receptor tyrosine kinases in mammals, namely Jak1, Jak2, Jak3, and Tyk2. They are over 1,1000 amino acids (aa) in length, ranging in molecular weights from 120 to 140 kDa. Whereas the expression of Jak3 is constrained to cells of the myeloid and lymphoid lineages, Jak1, Jak2, and Tyk2 are ubiquitously expressed (reviewed in (Leonard and O'Shea 1998, Yamaoka, Saharinen et al. 2004)). JAKs have been shown to associate with a proline-rich region in each intracellular domain that is termed box1/box2 region and is adjacent to the cell membrane (Ihle 2001). JAKs possess seven defined regions of homology called Janus homology domains 1 to 7 (JH1-7) at which JH1 at the carboxyl terminus represents the typical eukaryotic tyrosine kinase domain. Adjacent to JH1 lies the JH2 enzymatically inactive pseudokinase domain that regulates catalytic activity of JH1 (Yeh, Dondi et al. 2000). JAKs moreover contain an SH2-like domain (JH3-JH4) and a FERM (four-point-one, ezrin, radixin, moesin) homology domain (JH6-JH7) at their amino terminus (**Figure 2**). The Src homology 2 (SH2) domain is for binding to phosphorylated tyrosine residues and the FERM domain mediates the interaction with receptor complexes (reviewed in (Kisseleva, Bhattacharya et al. 2002, Yamaoka, Saharinen et al. 2004, Thomas, Snowden et al. 2015)). Upon ligand stimulation, receptors undergo conformational changes putting JAKs into proximity of each other, thus enabling activation by autophosphorylation (Remy, Wilson et al. 1999).

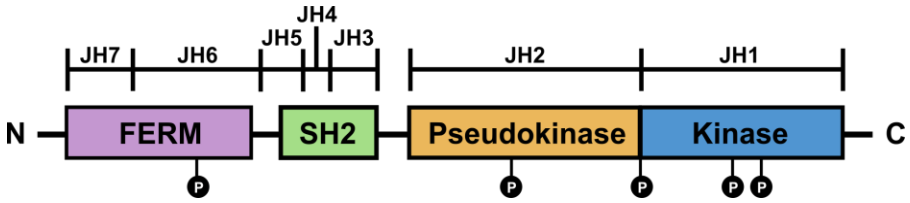

Figure 2: Schematic structure of Janus kinases (JAKs) with their functional domains. Abbreviations: N: amino-terminus, C: carboxyl-terminus, JH: Janus homology, FERM: four-point-one, ezrin, radixin, moesin, SH2: Src homology 2 domain, white P in black circle: phosphate (adapted from (Yamaoka, Saharinen et al. 2004)).

1.1.3 Signal transducers and activators of transcription (STATs)

Once activated, JAKs phosphorylate the tyrosine residues on the IL-6 receptor, thus providing docking sites for the phosphorylation and activation of cytoplasmic transcription factors called signal transducer and activator of transcription (STATs) (Heinrich, Behrmann et al. 2003). Seven STAT proteins have been identified in mammals, namely STAT1, STAT2, STAT3, STAT4, STAT5A, STAT5B, and STAT6 with sizes ranging from 750 to 850 aa, all sharing a common structural motif (**Figure 3**) (Darnell 1997). The N-terminal portion of STATs and the adjacent coiled-coil domain represent protein-protein interaction sites providing contacts for transcription factors and other regulatory proteins. These domains are followed by a DNA-binding region, displaying the central element of the molecule and determining DNA sequence specificity of the individual STATs. A linker region that participates in DNA-binding leads to the SH2 domain that is essential for the recruitment of STATs to phosphorylated receptors and for reciprocal SH2-phosphotyrosine interactions between monomeric STATs to form dimers. The C-terminal end is composed of a transactivation domain (TAD) required for activation of transcription (Shuai, Horvath et al. 1994, Becker, Groner et al. 1998, Chen, Vinkemeier et al. 1998, Bromberg and Darnell 2000). Once STATs are recruited to activated tyrosine kinases on the cytoplasmic part of the IL-6 receptor, they become themselves substrates for tyrosine phosphorylation leading to their homo- or hetero-dimerization and translocation to the nucleus, where they bind specific promoter sequences thus modulating transcription of several genes important for cell growth, differentiation, survival and apoptosis (**Figure 4**) (Heinrich, Behrmann et al. 1998, Buettner, Mora et al. 2002, Levy and Lee 2002).

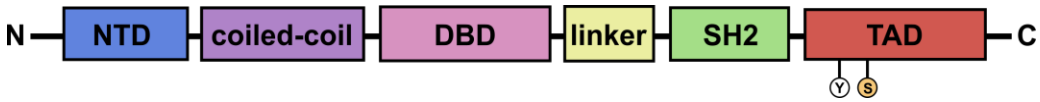

Figure 3: Schematic structure of signal transducers and activators of transcription (STATs) with their functional domains. Abbreviations: N: amino-terminus, C: carboxyl-terminus, NTD: N-terminal domain, DBD: DNA-binding domain, SH2: Src homology 2 domain, TAD: transactivation domain, circled Y: tyrosine, circled S: serine (adapted from (Chen and Khurana Hershey 2007)).

1.2 IL-6 downstream signaling

Central to the IL-6 signaling pathway is the activation of signal transducer and activator of transcription 3 (STAT3), that, following phosphorylation and acetylation, forms a dimer in which the SH2 domain of one phospho-STAT3 (pSTAT3) molecule binds to the phosphorylated Tyr705 of the other and vice versa. Following translocation from the cytoplasm to the nucleus, pSTAT3 dimers can bind to a canonical 8 – 10 bp inverted repeat DNA element that is commonly referred to as an interferon (IFN)-gamma activated sequence (GAS) element (Levy and Lee 2002). This engagement then controls the transcription of a number of genes including the apoptotic regulatory genes B-cell lymphoma-extra large (*Bcl-XL*), myeloid cell leukemia-1 (*MCL-1*), the X-linked inhibitor of apoptosis protein (*XIAP*), the oncogene *MYC*, and the Fas cell surface death receptor (*FAS*) (Darnell 1997).

The termination of this pathway is mediated by endogenous inhibitors including the suppressors of cytokine signaling (SOCS) and protein inhibitors of activated STATs (PIAS). These proteins are produced by activated STAT3 in normal cells under regular physiological conditions to limit IL-6 signaling, thus suggesting the existence of an autoregulatory mechanism for this pathway (Ataie-Kachoie, Pourgholami et al. 2014). STAT3 activation thereby induces expression of SOCS3 thus creating a negative feedback loop to discontinue gp130-dependent signaling (Auernhammer, Bousquet et al. 1999).

Depending on the cell type and cellular environment, IL-6/gp130 signaling is also able to trigger the activation of mitogen-activated protein kinase (MAPK) and phosphoinositide 3-kinase (PI3K) cascades (Costa-Pereira 2014).

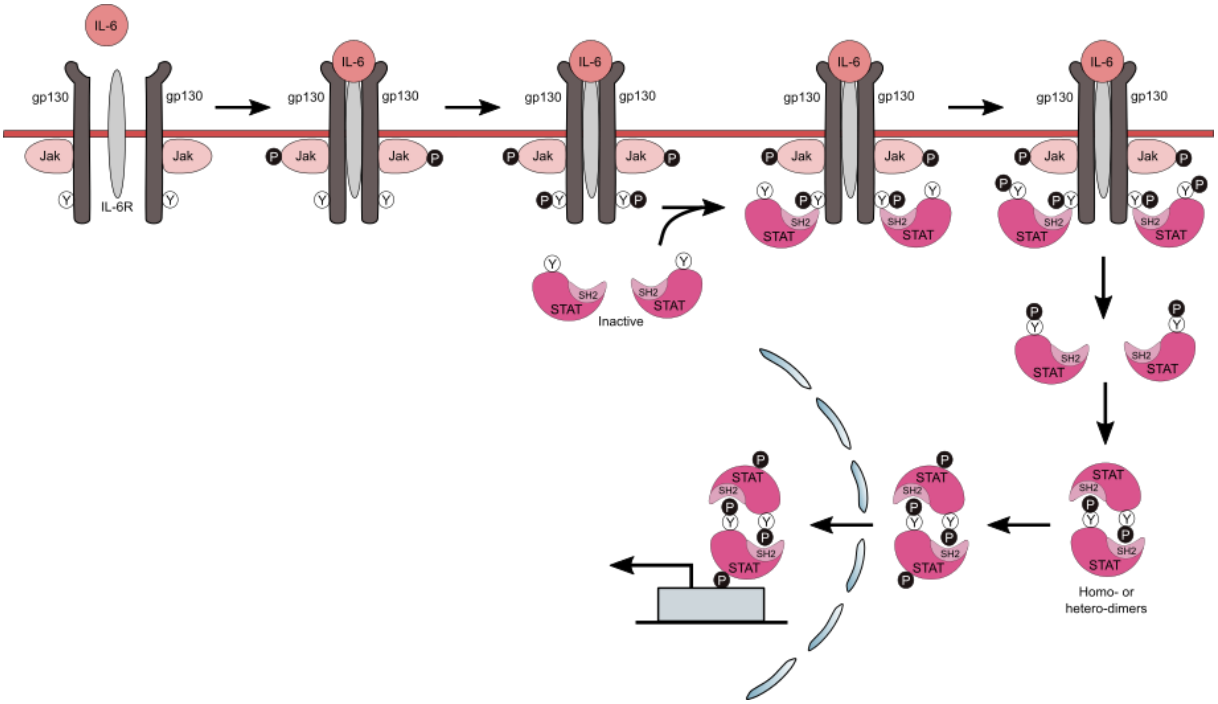

Figure 4: IL-6/gp130/JAK/STAT signaling. Binding of IL-6 to its receptor causes dimerization of two gp130 molecules leading to the activation of associated JAKs. These then phosphorylate the cytoplasmic part of gp130, thus generating docking sites for STATs. STATs also become phosphorylated and translocate into the nucleus as homo- or heterodimers, where they regulate gene transcription. Abbreviations: circled Y: tyrosine, white P in black circle: phosphate (adapted from (Heinrich, Behrmann et al. 1998))

1.2.1 The chimeric receptor protein Leucine zipper + glycoprotein 130, L-gp130

The extracellular part of gp130 consists of an immunoglobulin (Ig)-like domain followed by a cytokine binding domain and three fibronectin III domains. While IL-6 binds to the IL-6R through the binding sites I (Boulanger, Chow et al. 2003), the gp130 dimer is formed by contact of gp130 to the binding sites II and III (Ehlers, Grotzinger et al. 1994). For the design of the constitutive active form of gp130, termed L-gp130 (Leucine zipper + glycoprotein 130), the entire extracellular portion of gp130 was replaced by the human 39-amino acid Jun leucine zipper sequence of the transcription factor Jun (O'Shea, Rutkowski et

al. 1989, Stuhlmann-Laeisz, Lang et al. 2006). The transmembrane and cytoplasmic domains of the gp130-receptor were left intact and the subsequent chimeric gp130 protein is comprised of 343 aa and the molecular mass was calculated to be 43.4 kDa (**Figure 5**) (Stuhlmann-Laeisz, Lang et al. 2006). It was shown that L-gp130 is constitutively active and therefore able to induce STAT3 and ERK1/2 phosphorylation as well as transcriptional activation of gp130 target genes without the addition of IL-6 *in vitro* (Stuhlmann-Laeisz, Lang et al. 2006) and *in vivo* (Dechow, Steidle et al. 2014).

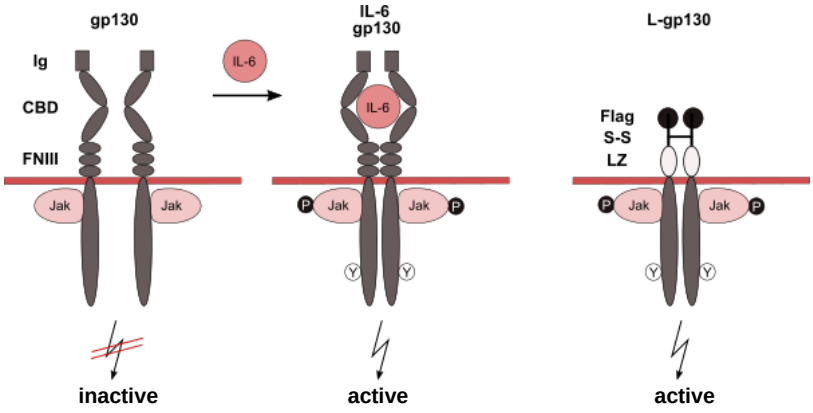

Figure 5: Schematic illustration of gp130 and the chimeric L-gp130. Scheme of the gp130 receptor with the extracellular domain consisting of an Ig-like domain (Ig), cytokine binding domain (CBD), and three fibronectin type III-like domains (FNIII). In the chimeric receptor protein L-gp130, the entire extracellular region was replaced by the leucine zipper (LZ) region of the human *c-jun* gene and stabilized by an additional disulfide bridge (S-S). A FLAG-tag (Flag) was inserted between signal peptide and leucine zipper (adapted from (Stuhlmann-Laeisz, Lang et al. 2006)).

1.3 B cell development

1.3.1 Early B cell development

B cells are produced continuously throughout the lifespan, originating from the fetal liver during embryonic life followed by the development from hematopoietic stem cells that reside in the bone marrow (BM) (reviewed in (Dorshkind 2002, Georgopoulos 2002, Busslinger 2004)). After differentiation via the multipotent progenitor (MPP) and common lymphoid progenitor (CLP) stage (Kondo 2010), early B cell development in the BM relies on the establishment of a functional B cell receptor (BCR) being formed through the rearrangement of V (variable), D (diversity), and J (joining) gene segments at the immunoglobulin (Ig) heavy and light chain loci (Tonegawa 1983, Alt, Yancopoulos et al. 1984). Recombinase activating genes 1 and 2 (RAG1/2) dependent joining of a D and J_H segment at the Ig heavy chain (IgH) locus is the earliest of these developmental stages forming a so-called pro-B cell expressing the surface marker CD19 (Del Nagro, Otero et al. 2005), followed by a V_H to DJ_H rearrangement (Schatz, Oettinger et al. 1989, Oettinger, Schatz et al. 1990). After successful V_HDJ_H recombination, the resulting heavy chain is conjugated to a surrogate Ig light chain (IgL) to establish the pre-BCR, which is then transferred to the cell surface and includes the signal-transducing components Ig-α and Ig-β (CD79-a and CD79-b). Signaling through the pre-BCR is critical for sustained differentiation

into pre-B cells (Pillai and Baltimore 1987, Karasuyama, Rolink et al. 1994). Efficient light chain rearrangement at either the Ig kappa or lambda light chain locus then constitutes a complete BCR and combined with the μ chain forms an IgM molecule that is expressed on the cell surface, hence defining the immature B cell stage.

The molecular mechanisms leading to the formation of a functional BCR are equal in human and mice (LeBien 2000). The only difference lies in the contribution of the common γ chain cytokine interleukin 7 (IL-7). Whereas murine pro- and pre-B cells are reliant on the expression of IL-7 for survival and differentiation, human B cell progenitors are IL-7 independent (Namen, Lupton et al. 1988, Noguchi, Yi et al. 1993, Prieyl and LeBien 1996, Puel, Ziegler et al. 1998). Once immature, B cells leave the BM as transitional B cells and finalize their maturation in the periphery.

1.3.1 Late B cell development

Mature B cells express IgD on their surfaces and are referred to as naïve if they have not yet been exposed to an antigen (Loder, Mutschler et al. 1999). These essential steps in early B cell development from commitment of lymphoid progenitors to the B lymphocyte lineage via the pro-, pre-, immature up to the mature stage of B cell differentiation are regulated by Paired box protein 5 (Pax5). Pax5 also maintains B cell identity by preventing premature entry into the PC transcriptional program (Barberis, Widenhorn et al. 1990, Cobaleda, Schebesta et al. 2007, Fuxa and Busslinger 2007). Mature B cells further differentiation into follicular B cells, marginal zone (MZ) B cells, and germinal center (GC) B cells is then determined by the diverse microenvironmental influences of the spleen, lymph nodes (LNs), and pleural cavity (Pieper, Grimbacher et al. 2013, Rickert 2013).

GCs are histological structures where naïve B cells upon antigen encounter get activated by interaction with $CD4^+$ T cells and are targeted by Ig gene remodeling processes termed somatic hypermutation (SHM) and class-switch recombination (CSR). Both events are driven by expression of activation-induced cytidine deaminase (AID), which deaminates cytidine residues to uridines in the VDJ and switch regions of the Ig gene (Neuberger, Lanoue et al. 1999, Muramatsu, Kinoshita et al. 2000, Nussenzweig and Nussenzweig 2010, Pavri and Nussenzweig 2011, Victora and Nussenzweig 2012). Furthermore, GC B cells express the activation markers GL7 as well as Fas and the transcription factor B cell lymphoma 6 (Bcl-6) that is mandatory for their development (Cattoretti, Chang et al. 1995). Bcl-6 directly binds to Prdm1 and therefore represses the production of B lymphocyte induced maturation protein 1 (Blimp1) thus preventing premature entry into PC differentiation (Vasanwala, Kusam et al. 2002, Tunyaplin, Shaffer et al. 2004). The GC is comprised of a dark zone (DZ), with highly proliferating B cells, termed centroblasts, and a light zone (LZ) in which so-called centrocytes are intermingled with follicular dendritic cells (FDC), T cells and macrophages (Victora and Nussenzweig 2012). Centroblasts in the DZ are large-sized B cells that lack surface Ig and undergo SHM of their IgH and IgL genes, whereas the non-proliferative centrocytes residue in the LZ, are smaller-sized, re-express surface Ig and are submitted to CSR (MacLennan 1994, Klein and Dalla-Favera 2008). CSR changes the IgH class from

IgM to IgG, IgA, or IgE, whereas SHM causes Ig-variable-region mutations, thus creating a B cell pool with increased (or decreased) affinity for a particular antigen (Muramatsu, Kinoshita et al. 2000). In healthy B cells, GC commitment is triggered by the oncogene *MYC*. After its suppression in the GC dark zone, an increase in Myc expression in the light zone selects B cells for re-entry into the GC dark zone to undergo further rounds of proliferation and SHM (Tarlinton and Smith 1997, Wolniak, Shinall et al. 2004, Dominguez-Sola, Victora et al. 2012). While negatively selected cells in the GC reaction die via apoptosis, positively selected clones leave the GC and differentiate into memory B cells or long-lived PCs.

Long-lived PCs survive for about 30 days in the BM, express the surface marker Syndecan-1 (CD138) and possess the ability to produce high-affinity antibodies of different isotype classes (Berek, Berger et al. 1991, Jacob, Kelsoe et al. 1991, MacLennan 1994, Aref, Goda et al. 2003, Zhan, Tian et al. 2003, Victora and Nussenzweig 2012). In addition to IL-6 (Hirano, Yasukawa et al. 1986, Akira, Taga et al. 1993), this PC transcriptional program is mainly regulated by the expression of Blimp1, which directly suppresses *MYC* (Lin, Wong et al. 1997), as well as interferon regulatory factor-4 (*IRF-4*), and X-box binding protein 1 (*XBP-1*), all essential transcription factors in terminal B cell differentiation (reviewed in (Reimold, Iwakoshi et al. 2001)). Survival of PCs in the BM is mediated by IL-6, A proliferation-inducing ligand (*APRIL*) as well as B cell activating factor (*BAFF*) that are produced by stromal cells and various hematopoietic cells such as eosinophil (Sze, Toellner et al. 2000, Shapiro-Shelef and Calame 2004, Shapiro-Shelef and Calame 2005, Nutt, Hodgkin et al. 2015).

However, not all antigen-activated B cells ultimately enter the GC reaction. Following T cell contact, a subset of selected B cells travels as plasmablasts to particular areas in the LNs, known as the medullary chords, where they differentiate into short-lived PCs that secrete antibodies with low affinity for the invading pathogen and die within three days. This secreted Ig is not somatically hypermutated, and is mostly IgM (**Figure 6**) (Jacob and Kelsoe 1992, Hallek, Bergsagel et al. 1998).

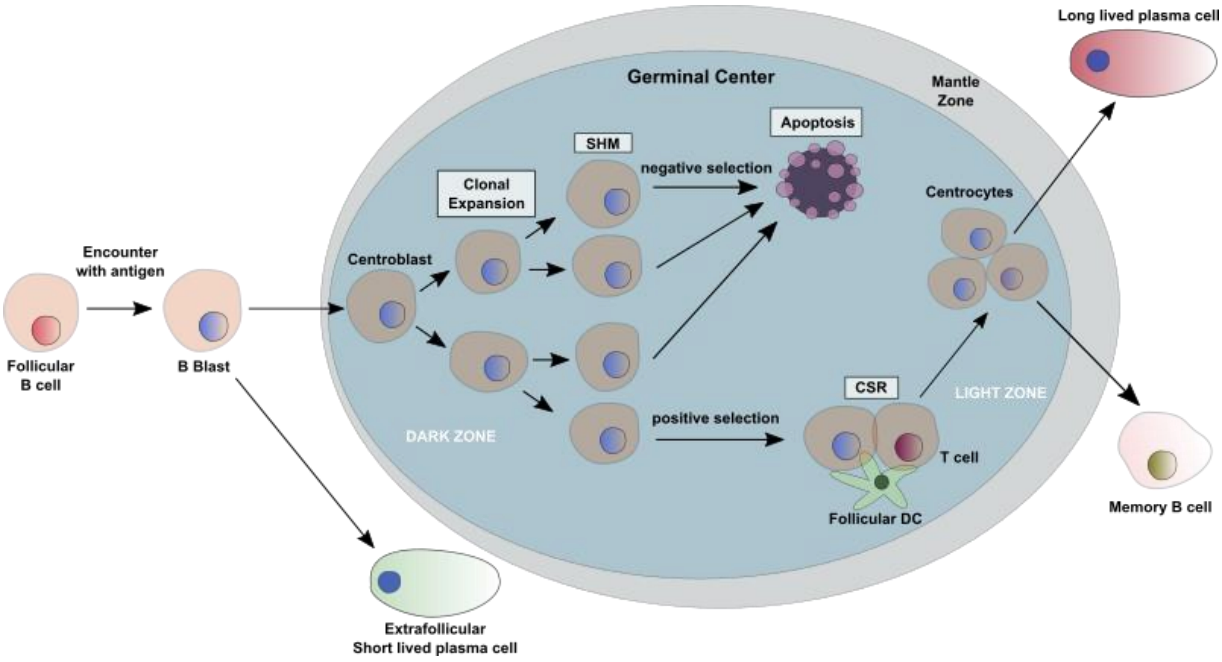

Figure 6: The Germinal Center (GC) reaction. Upon antigen encounter, activated B cells either differentiate into short-lived extrafollicular PCs responsible for the early production of IgM antibodies or differentiate into large blasts called centroblasts, and initiate the so-called germinal center (GC) reaction. Centroblasts undergo clonal expansion and somatic hypermutations (SHM), and those that are positively selected experience class switch recombination (CSR) and differentiate into smaller centrocytes and, finally, long-term memory or PCs (Allen, Okada et al. 2007) (adapted from (Samitas, Lotvall et al. 2010)).

1.4 B cell lymphomas

Chromosomal translocations and oncogenic mutations can occur during the complex machinery of antibody diversification, making B cells particularly prone to malignant transformation. The pathways normal B cells use to sense antigens, are frequently disrupted in B cell malignancies either through gain-of-function mutations that activate signaling effectors, loss-of-function mutations that inactivate negative regulators of signaling, or autocrine receptor activation. This may then lead to constitutive stimulation of prosurvival pathways or the simultaneous activation of several interconnected signaling pathways (Shaffer, Young et al. 2012). As depicted above, recombination of V, D, and J gene segments assembles IgH and IgL genes during B cell development in the BM. This process is driven by the two enzymes RAG1 and RAG2, ultimately leading to breaks in double-stranded DNA. These breaks are subsequently resolved by DNA repair processes (non-homologous end-joining, NHEJ). However, they display a source of chromosomal translocations in different types of B cell lymphomas (Jung, Giallourakis et al. 2006). When a functional BCR is then built and the B cell enters the GC reaction, two before described modifications of B cell DNA alter the BCR: SHM and CSR, both dependent on AID activity (Muramatsu, Kinoshita et al. 2000). Although those genetic changes are indispensable for a normal immune response, they are also prone to DNA damage making the GC reaction another presumable source for the development of many types of B cell lymphomas (Allen, Okada et al. 2007, Lenz and Staudt 2010).

Therefore, it is well understood that GC B cells are the origin of diffuse large B cell lymphoma (DLBCL) of the GC subtype, follicular lymphoma (FL), and Burkitt's lymphoma (BL) in humans. These lymphoma entities carry the differentiation program of the normal B cell they arise from, but are malignantly transformed due to above described oncogenic abnormalities that often disrupt this usual program (Alizadeh, Eisen et al. 2000, Shaffer, Rosenwald et al. 2001, Klein, Tu et al. 2003). On the contrary, DLBCL of the ABC subtype is a post–GC cancer being characterized by mutated Ig V genes (Lossos, Alizadeh et al. 2000) and exhibiting a gene expression signature comprising many PC–associated genes, such as *XBP-1* and *IRF-4* (Wright, Tan et al. 2003). Unlike multiple myeloma (MM), ABC DLBCL maintains expression of many mature B cell genes, suggesting that its blockage in plasmacytic differentiation takes place at the plasmablast stage and is due to the loss of Blimp1 activity, a key transcription factor indispensable to drive mature B cells into terminal differentiation and cell-cycle arrest (Turner, Mack et al. 1994, Shapiro-Shelef, Lin et al. 2003, Shapiro-Shelef, Lin et al. 2005).

Marginal zone (MZ) B cells are situated at the interface between the circulation and the lymphoid tissue and presumably display the cells of origin for several indolent types of B cell lymphomas that progress in the SPL (f.e. splenic marginal zone lymphoma (SMZL)), in the LN (nodal marginal zone lymphoma (NMZL)) or at extranodal sites such as the mucosa-associated lymphoid tissue (MALT lymphoma) (Bende, van Maldegem et al. 2009).

1.5 Plasma cell disorders

Plasma cell disorders, also known as plasma cell dyscrasias, are a heterogeneous group of diseases arising from the proliferation of neoplastic monoclonal PCs which often produce a monoclonal Ig protein referred to as M-protein spike (Drappatz and Batchelor 2004). The disorders cover a wide spectrum of clinical manifestations ranging from more indolent and benign processes to highly aggressive conditions that require immediate intervention. Plasma cell dyscrasias comprise: monoclonal gammopathy of undetermined significance (MGUS), multiple myeloma (MM), Waldenström macroglobulinemia (WM), plasmacytoma, plasma cell leukemia, POEMS syndrome (polyneuropathy, organomegaly, endocrinopathy, monoclonal gammopathy, and skin changes), primary amyloid light-chain (AL) amyloidosis, and heavy-chain diseases (Sobol and Stiff 2014, Lee 2016, Swerdlow, Campo et al. 2017).

1.5.1 Plasmacytomas

Solitary plasmacytomas comprise 2 – 5 % of all plasma cell disorders and are characterized by a localized accumulation of neoplastic monoclonal PCs without the evidence of a systemic plasma cell proliferative disease (Knowling, Harwood et al. 1983). With a disease onset at the median age of 55 years, plasmacytomas can be categorized into two groups depending on their location. Patients with solitary bone plasmacytomas (SBP) present with a single area of bone destruction due to clonal malignant PCs primarily affecting the axial skeleton especially the vertebrae while patients suffering from

solitary extramedullary plasmacytoma (SEP) harbor a mass of abnormal PCs outside the bone in soft tissue (Dimopoulos, Moulopoulos et al. 2000, Dimopoulos and Hamilos 2002, Soutar, Lucraft et al. 2004). The differentiation criteria for both SBP and SEP from MM is the absence of CRAB characteristics (hypercalcemia, renal failure, anemia, and multiple bone lesions). SBP is diagnosed by a skeletal survey confirming a solitary bone lesion as well as by a BM examination revealing normal morphology or a very low infiltration of clonal PC (less than 10 %), and lack of myeloma-related organ dysfunction (Durie and Salmon 1975, Dimopoulos, Moulopoulos et al. 2000, Soutar, Lucraft et al. 2004, Rajkumar, Dimopoulos et al. 2014). The existence of monoclonal Ig protein has been reported for 60 % of SPB and less than 25 % of SEP patients but only at low levels of less than 30 g/l. The treatment of choice for plasmacytoma is local radiotherapy. However, over 50 % of patients progress to MM within two years after treatment (reviewed in (Dimopoulos, Moulopoulos et al. 2000, Soutar, Lucraft et al. 2004)). In comparison to patients suffering from SEP, SBP patients have a poor prognosis and a significantly higher risk to develop MM (reviewed in (Kilciksiz, Karakoyun-Celik et al. 2012)). Although SEP can arise throughout the body, almost 90 % develop in the head and neck, especially in the upper respiratory tract. The gastro-intestinal tract represents the next most frequent site of SEP (reviewed in (Soutar, Lucraft et al. 2004)).

1.5.2 Multiple Myeloma

Multiple myeloma (MM) also belongs to the group of plasma cell disorders and is a highly aggressive type of B cell lymphoma that displays the second most common hematologic malignancy accounting for approximately 1 % of all neoplasms and for 13 % of hematologic cancers worldwide. It represents a disease of old people with most patients being diagnosed at the age of 70 years and older (Palumbo and Anderson 2011). The disease is thought to arise from malignantly transformed post-GC PCs that invade the BM with a low proliferative rate and extended life span (Hallek, Bergsagel et al. 1998, Matsui, Wang et al. 2008). A 10 – 15 % involvement of monoclonal PCs in the BM identified by aspiration or biopsy is required for the definitive diagnosis of MM (George and Sadovsky 1999). Due to the abnormal infiltration of malignant cells into the BM, B cells, T cells, and macrophages of MM patients undergo immunologic alterations resulting in an increased susceptibility to infections, particularly those caused by pneumococcus, tetanus and diphtheria organisms (Munshi 1997). The abnormal PCs that accumulate in the BM produce high amounts of monoclonal Ig or Ig fragments in the serum and/or urine (M-protein spike) (**Figure 7**). Over 90 % of all MM patients present with an M-protein in the α_2, β or γ regions in the serum or urine at the time of diagnosis of greater than 30 g/l (George and Sadovsky 1999, International Myeloma Working 2003, Kyle and Rajkumar 2006, Galson, Silbermann et al. 2012). The Ig is mostly of the IgG, IgM or IgA and rarely of the IgE or IgD subtype or alternatively represents kappa or lambda light chain fragments (called Bence Jones protein) and causes hyperviscosity as well as end-organ damage (reviewed in (Michels and Petersen 2017)). Furthermore, 80 – 90 % of patients present with multiple bone lesions due to the inhibition of osteoblasts and activation of osteoclasts during their course of disease and this feature remains a major source of morbidity and mortality (Roodman 2004). The typical clinical manifestations of MM are hypercalcemia, renal failure, anemia, and multiple bone lesions (CRAB)

(International Myeloma Working 2003, Kyle and Rajkumar 2004). Although the BM is the primary location of MM, spreading of neoplastic to other organs like the spleen, LNs, the liver or the gastrointestinal tract has been reported (reviewed in (Gutnik and Bacon 1985, Kyle and Greipp 1988)).

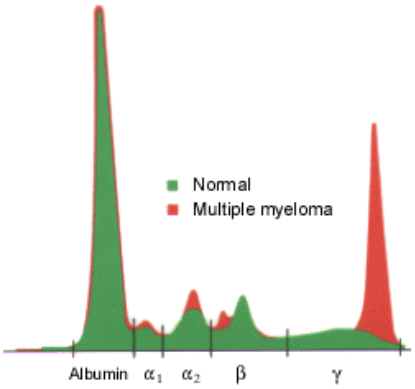

Figure 7: Serum protein electrophoresis. The red line is from an MM patient showing a characteristic M-protein spike. The green line depicts a healthy patient that lacks this feature in the γ-fraction (George and Sadovsky 1999).

MM can occur de novo or evolve from a precursor condition termed monoclonal gammopathy of undetermined significance (MGUS) as a result of accumulating oncogenic events that differ between patients accompanied by changes in the bone marrow microenvironment (BMM) (Morgan, Walker et al. 2012, Botta, Di Martino et al. 2016). Under these circumstances, MGUS progresses to smoldering myeloma, an asymptomatic early form of MM, and finally to symptomatic intramedullary or extramedullary myeloma (EMM) (Kuehl and Bergsagel 2002). While in intramedullary myeloma, proliferation of clonal PCs is restricted to the BM, EMM is defined by the presence of these cells outside the BM. EMM occurs in around 6 % of patients and affects liver, CNS, kidneys, lymph nodes (LNs), and the gastro-intestinal tract amongst others (Soutar, Lucraft et al. 2004, Blade, Fernandez de Larrea et al. 2011, Weinstock and Ghobrial 2013). As described above, MM also frequently develops in patients suffering from plasmacytomas (Dimopoulos, Moulopoulos et al. 2000, Soutar, Lucraft et al. 2004).

In early pathogenesis, MM patients are typically assigned to a hyperdiploid group characterized by trisomies of one or more odd-numbered chromosomes 3, 7, 9, 11, 15, or 17 or to a non-hyperdiploid group, where the majority of patients displays translocations comprising the switch region of the IgH locus on chromosome 14, such as t(4;14), t(11;14) or t(14;16) resulting in deregulation of certain oncogenes like FGFR3 (fibroblast growth factor receptor 3), cyclin D1 or c-MAF (musculoaponeurotic fibrosarcoma) (Chesi, Bergsagel et al. 1998, Fonseca, Blood et al. 2002, Kuehl and Bergsagel 2002, Fonseca, Barlogie et al. 2004, Fonseca, Bergsagel et al. 2009, Kumar, Fonseca et al. 2012). Secondary translocations promote disease progression and comprise complex cytogenetic abnormalities like chromosome 13 deletions, deregulation of the oncogene *MYC*, activating mutations of *RAS* or *B-RAF* or loss of chromosome 17p, which results in loss of the tumor suppressor *Trp53*. Those aberrations result in an altered expression of growth factor receptors as well as adhesion molecules on the surface of MM cells, hence stimulating their proliferation and migration while modifying their interaction with the BMM

(Kuehl and Bergsagel 2002, Korde, Kristinsson et al. 2011, Palumbo and Anderson 2011). One of these surface molecules is the heparan sulfate proteoglycan Syndecan-1 (CD138), which is not only expressed on normal PCs but also highly upregulated on MM cells. Syndecan-1 is important for the connection between (malignant) PCs and the BMM and can thereby support myeloma growth and metastasis (Ridley, Xiao et al. 1993, Reijmers, Groen et al. 2010). Furthermore, it is well known that the cytokine IL-6, derived from either paracrine sources or MM cells themselves, plays a crucial role in the malignant progression of MM by regulating growth and survival of myeloma tumor cells (Kawano, Hirano et al. 1988, Klein, Zhang et al. 1995). Accordingly, 35 % of myeloma patients show significantly elevated serum IL-6 levels (Bataille, Jourdan et al. 1989).

1.6 The IL-6/gp130/JAK/STAT3 axis in MM

MM cells locate to the BM and interact with stromal cells thereby stimulating production of IL-6 leading to inhibition of osteoblastic activity while triggering osteoclast activity. Increased osteoclastic activity plus inhibited osteoblastic activity results in osteoporosis, painful lytic lesions, and hypercalcemia (Chauveau and Choukroun 1996). IL-6 is thereby expressed by MM cells in an autocrine way (Kawano, Hirano et al. 1988, Schwab, Siegall et al. 1991) but the major source are the BM stromal cells that produce high amounts of IL-6 upon stimulation by malignant cells (Caligaris-Cappio, Bergui et al. 1991, Uchiyama, Barut et al. 1993). Elevated serum levels of IL-6 are associated with progression of MM and remain a predictive factor for poor prognosis of the disease (Ludwig, Nachbaur et al. 1991, Pelliniemi, Irjala et al. 1995, Frassanito, Cusmai et al. 2001). In addition to classical IL-6 signaling, MM cells can experience IL-6 trans-signaling, where IL-6 in the circulation or interstitium binds to sIL-6R. Thereby, IL-6 trans-signaling is capable of conferring IL-6 responsiveness to myeloma cells that have lost their IL-6R expression during tumor progression (Rosean, Tompkins et al. 2014). It is thus not surprising that elevated levels of soluble IL-6R in the serum were seen in MM (Kyrtsonis, Dedoussis et al. 1996, Thabard, Barille et al. 1999). Furthermore, constitutively activated IL-6/gp130/JAK/STAT3 signaling directly accounts for the malignant progression of MM by conferring a survival advantage through the prevention of apoptosis, thus allowing the accumulation of long-lived myeloma tumor cells (Catlett-Falcone, Landowski et al. 1999). Additionally, STAT3 phosphorylation and target gene activation have been demonstrated as hallmarks in patients suffering from MM (Dechow, Steidle et al. 2014).

1.7 Treatment of MM patients

During the last couple of years, new therapeutic advances, including novel agents such as immunomodulatory drugs (IMiDs) (thalidomide, lenalidomide and pomalidomide) and proteasome antagonists (bortezomib, ixazomib, carfilzomib), have led to markedly improved overall survival of myeloma patients by targeting both, the tumor cell and its BMM (Hideshima and Anderson 2002, Kumar,

Rajkumar et al. 2008, Rajkumar and Kumar 2016). Proteasome inhibitors disrupt normal degradation of intracellular proteins by the proteasome, thus resulting in cell-cycle arrest, stimulation of apoptosis, and inhibition of angiogenesis (Mitsiades, Mitsiades et al. 2002, Adams 2004). IMiDs promote apoptosis of established neovasculature and prevent angiogenesis as well as cell-cell adhesion, thereby counteracting the protective effect of the BM milieu (Quach, Ritchie et al. 2010).

1.7.1 Standard treatment

Transplant eligible patients without substantial comorbidities and aged below 65 typically receive approx. four cycles of initial chemotherapy that encompasses three drugs, including at least one novel agent (an IMiD or proteasome inhibitor) and steroids. The goal of induction therapy is to reduce the myeloma burden, improve symptoms and allow for successful stem cell collection. This is followed by stem cell collection and high-dose melphalan treatment with consequent autologous stem cell transplantation (ASCT) as consolidation. Currently, the most common induction regimens for newly diagnosed MM patients are bortezomib, thalidomide, and dexamethasone (VTd); bortezomib, lenalidomide, and dexamethasone (VRd); bortezomib, cyclophosphamide, and dexamethasone (VCd); and carfilzomib, lenalidomide, and dexamethasone (KRd). The choice and duration of subsequent maintenance therapy is then frequently driven by the presence or absence of high-risk cytogenetic features (Palumbo and Anderson 2011, Engelhardt, Terpos et al. 2014, Rajkumar and Kumar 2016, Paul, Lipe et al. 2019). Older patients, presenting with more formidable comorbidities, are treated with more moderately dosed chemotherapy only (Rollig, Knop et al. 2015).

1.7.2 Novel treatment options currently studied

In recent years, novel drugs have been approved or are in clinical trials for the treatment of patients suffering from MM. These comprise mainly immunotherapeutic approaches. Two monoclonal antibodies (daratumumab and isatuximab) targeting CD38 that is expressed on the surface of more than 90 % of malignant plasma cells from patients with MM have shown promise in relapsed, refractory MM (Jelinek and Hajek 2016, Lonial, Weiss et al. 2016, Usmani, Weiss et al. 2016, Feng, Zhang et al. 2017). Recently, a four-drug combination (bortezomib, melphalan, prednisone, and the monoclonal anti-CD38 antibody daratumumab) was approved for the treatment of MM patients (Mateos, Dimopoulos et al. 2018) while several other four-drug combinations are currently under evaluation in clinical trials (Paul, Lipe et al. 2019). Elotuzumab, another monoclonal antibody targeting the signaling lymphocytic activation molecule F7 (SLAMF7), has also shown activity in relapsed MM (Lonial, Dimopoulos et al. 2015). Both, daratumumab and elotuzumab are currently assessed in the treatment of newly diagnosed MM patients in combination with multiple induction regimens (reviewed in (Paul, Lipe et al. 2019)).

In addition to monoclonal antibodies, several immunotherapies have recently been proposed. They include, amongst others, chimeric antigen receptor T-cell therapy (CAR-T cells), tumor vaccines, immune checkpoint inhibitors as well as antibody-drug conjugates, that combine a monoclonal antibody and

chemotherapy in one drug (Rodriguez-Otero, Paiva et al. 2017). In the last years, a number of other CAR-T cells has been designed to target surface antigens expressed by MM cells. These include CD38 (Suck, Odendahl et al. 2016), CD138 (Jiang, Zhang et al. 2014), and CD269, the B-cell maturation antigen (BCMA) (Tai and Anderson 2015). However, despite their efficacy, CAR-T cells have raised many concerns regarding their short- and long-term toxicities (Brudno and Kochenderfer 2016).

Other promising agents include novel proteasome inhibitors (oprozmib and marizomib), CDK inhibitors (dinaciclib), phosphoinositide 3-kinase (PI3K) inhibitors, histone deacetylase inhibitors (panobinostat, rocilinostat, vorinostat), ABT-199, a selective BCL-2 inhibitor, and LGH-447, a pan PIM kinase inhibitor (Naymagon and Abdul-Hay 2016, Rajkumar and Kumar 2016).

In addition, the IL-6/gp130/JAK/STAT pathway is also being targeted in finding novel treatment approaches to fight MM. Success in pre-clinical data using JAK inhibitors has thereby further prompted early-phase studies. Currently, ruxolitinib, targeting JAK1 and JAK2, is being studied with regimens containing IMiDs, proteasome inhibitors, and monoclonal antibodies (de Oliveira, Fook-Alves et al. 2017, Ghermezi, Spektor et al. 2019). Moreover, the IL-6 inhibitor siltuximab, a chimeric monoclonal antibody which binds IL-6, has been approved for the treatment of multicentric Castleman's disease and is now also being investigated for treatment in MM (Orlowski, Gercheva et al. 2015, Brighton, Khot et al. 2019).

Unfortunately, up till now, nearly all patients will eventually relapse and develop refractory disease, wherefore MM is still seen as an incurable disease.

1.8 Mouse models of MM

Over the past centuries, a variety of pre-clinical mouse models has been generated that recapitulate a broad range of biological features of MM. These systems comprise strains that spontaneously undergo malignant transformation while aging as well as transgenic models of murine MM or immuno-compromised animals receiving orthotopic xenografts of human MM cell lines (Rossi, Botta et al. 2018). However, most of them are limited because of their late disease onset and/or low penetrance.

1.8.1 Genetically engineered mouse models

Genetically engineered mouse (GEM) models are often used for studying human cancer. The genetic profile of these mice is altered in a way that one or several genes which are seemingly involved in malignant transformation are mutated, deleted or overexpressed (Richmond and Su 2008). To date, several GEM models of MM have been generated. The *Eμ-xbp-1s* strain (on a C57BL/6 background) expresses high levels of a spliced isoform of XBP-1 (XBP-1s), a transcription factor that is important for terminal B cell differentiation and known to be implicated in human MM (Munshi, Hideshima et al. 2004), under the control of immunoglobulin V_H promoter and *Eμ* enhancer elements. Some of these animals develop MGUS at around one year of age and few progress into MM in later life showing lytic bone

lesions and monoclonal gammopathy as well as human MM like gene signature with over-expression of Cyclin D1 and MAF (Carrasco, Sukhdeo et al. 2007). In another GEM model, expression of the oncogene *MYC* is targeted to GC B cells in C57BL/6 mice by means of AID-dependent SHM. The majority of these Vk*MYC transgenic animals presents with monoclonal gammopathies as well as PC expansion in the BM (but not in secondary lymphoid organs such as spleen and LNs) and exhibits end organ damage with a median survival of two years. Additionally, serial transplantation of MM cells into syngeneic recipients results in rapid reestablishment of the disease. These characteristics clearly recapitulate human MM in this model. Yet, some Vk*MYC mice also develop other cancers of the B cell lineage (Chesi, Robbiani et al. 2008, Chesi, Matthews et al. 2012). A third GEM model is based on the finding that the c-MAF proto-oncogene was found to be over-expressed in MM in the presence of t(14;16) resulting in an aggressive MM phenotype with short survival (Chesi, Bergsagel et al. 1998). In the *Eμ c-Maf* model regulation of c-Maf by means of the immunoglobulin enhancer is directed to the murine B-cell compartment. At around 50 weeks of age, transgenic mice develop a clonal M spike with hyper-gammaglobulinemia, increased PCs in the BM and cast nephropathy and resemble a plasmacytic or plasmablastic lymphoma phenotype (Morito, Yoh et al. 2011).

Additionally, there are also several transgenic MM models that are based on the activation of the IL-6/IL-6R axis (Dechow, Steidle et al. 2014, Paton-Hough, Chantry et al. 2015, Rossi, Botta et al. 2018), underscoring its importance in proliferation as well as malignant transformation of late B cells. C57BL/6 mice that overexpress IL-6 develop plasmacytosis characterized by an elevated production of Ig (Suematsu, Matsuda et al. 1989); however, development of monoclonal and transplantable plasmacytomas is only seen in IL-6 transgenic mice on a BALB/c background (Suematsu, Matsusaka et al. 1992). In a retroviral murine BM transduction-transplantation model on the same background, expression of *L-gp130* facilitating constitutive IL-6/gp130/JAK/STAT3 activation, induces MM development at a high penetrance and relatively short latency (Dechow, Steidle et al. 2014). The BALB/c strain is prone to developing PC disorders upon adequate stimuli due to a mutation in the inhibitor of Cdk4/alternative reading frame (INK4a/ARF) locus leading to partial disability of the tumor suppressor protein $p16^{Ink4a}$ (Zhang, DuBois et al. 2001). It is therefore of great interest to generate a model resembling human MM on the frequently used C57BL/6 background eliminating the role of the mutation in the INK4a/ARF locus that supports lymphomagenesis.

1.8.2 Xenograft models

Xenograft models of murine MM are based on the engraftment of primary human MM cells or MM cell lines in immuno-compromised mice. To mimic human MM in mice, two different SCID (severe combined immunodeficiency) mouse models for MM have been generated, namely the SCID xenograft and the SCID-hu model. In the SCID xenograft model, human MM cell lines are injected intravenously (i.v.) into immuno-compromised mice. There, the transplanted cells home to the BMM resulting in the reestablishment of MM with osteolytic bone lesions and the existence of serum paraprotein (reviewed in

(Asosingh, Radl et al. 2000)). For the SCID-hu animal model, SCID mice are implanted with bilateral human fetal bone grafts that serve as a niche for interaction of human MM cells with a BMM of human origin. Human MM derived cell lines are then injected directly into the BM cavity of sublethally irradiated SCID-hu mice resulting in the MM cells to infiltrate the marrow cavity of the graft while sparing the murine bone and all other murine normal tissues. With osteolytic lesions of the human bone and the presence of monoclonal human Ig as well as human IL-6 in the PB serum of mice, this model represents a suitable tool to mimic the human disease in mice (Urashima, Chen et al. 1997). The SCID-hu animal model has since been used to investigate the interaction of human MM cells with the BMM. Yaccoby and colleagues were thereby able to show successful engraftment of primary cells from MM patients upon transplantation with development of osteolysis in the implanted human bone and serial transplantability of the disease (Yaccoby, Barlogie et al. 1998, Yaccoby and Epstein 1999).

1.8.3 Other mouse models of malignant transformation

In addition to the described GEM and xenograft models, other approaches have been used to study MM *in vivo*.

It is known that with aging, mice of the C57BL strains recurrently display an idiopathic paraproteinemia that resembles the development and natural history of human MGUS and eventually human MM (van den Akker, de Glopper-van der Veer et al. 1988). C57BL/KaLwRij mice exhibit the highest frequency of idiopathic paraproteinemia amongst the various strains of C57BL mice. Approximately 80 % of C57BL/KaLwRij mice spontaneously evolve a B cell proliferative disorder resembling human MGUS and a very small fraction of around 1 % presents with MM or WM after two years. C57BL/KaLwRij mice developing MM represent what is known as the original 5TMM model. Serial transplantation of BM from the 5TMM model into young naïve syngeneic recipients results in the reestablishment of the disease for multiple generations with characteristics similar to the human disease. The 5TMM models nicely reflect the syngeneic nature of interaction of the MM cells with adhesion molecules and cytokines of the host microenvironment (Radl, De Glopper et al. 1979, Radl, Croese et al. 1988, Radl 1989, Radl 1990, Vanderkerken, De Raeve et al. 1997).

In another model, an abnormal accumulation and proliferation of PCs in the peritoneal cavity is seen upon intraperitoneal (i.p.) injection of pristane mineral oil into BALB/c mice. The plasmacytomas are transplantable into the peritoneum of syngeneic recipients primed with pristane. However, these PC tumors are primarily localized in the peritoneum, LNs, and spleen and not in the BM (Potter 1986).

1.9 The Cre/loxP system

The site-specific DNA recombinase Cre (**c**auses **re**combination) of the bacteriophage PI specifically recognizes 34 bp long sequences, known as loxP (**l**ocus **o**f **X** over in **P**I) (Sternberg and Hamilton 1981, Sternberg, Hamilton et al. 1981). Cre cuts out DNA segments that are flanked by two directly repeated loxP sites as a circular molecule, thereby leaving a single loxP site in the genome (Sauer and Henderson 1988). As Cre recombinase does not require cofactors or accessory molecules in eukaryotic cells (Abremski and Hoess 1984), it appears to be the first choice for gene modifications in the mouse genome. In case that the gene of interest is flanked by loxP sites (i.e. floxed), Cre expression results in the knock down of this gene. If the gene of interest is preceded by a floxed transcriptional stop sequence (STOP), Cre expression will lead to the removal of the stop cassette, thus allowing expression of the gene of interest (Lakso, Sauer et al. 1992). The latter scenario is depicted in **Figure 8** where expression of the transgene L-gp130 is facilitated upon activation of Cre recombinase.

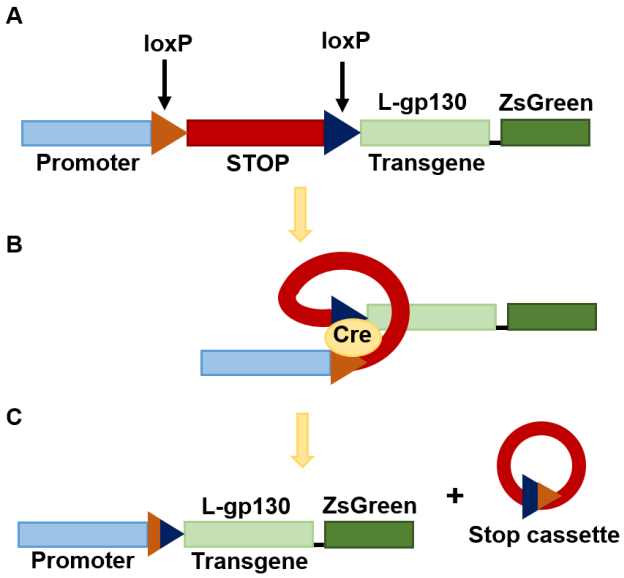

Figure 8: Gene activation by the Cre/loxP system by L-gp130 as the gene of interest. (A) LoxP sites flanking the target sequence, i.e. a stop cassette. Downstream is the gene of interest followed by a reporter gene. (B) LoxP sequences bind to each other by complementary base-pairing; Cre recombinase then gets attached to this structure, cleaves in the middle, catalyzing homologous recombination thereafter. (C) As a result, the target sequence is released from the genomic DNA as a circular DNA molecule and the gene of interest gets expressed (after (Szeberenyi 2013)).

1.9.1 Conditional gene targeting by the Cre/loxP system

Conditional gene targeting is a gene modification being restricted to a specific cell type of the mouse. It requires a mouse strain containing a floxed gene of interest or stop cassette and an additional mouse strain expressing the Cre recombinase under a cell type specific promoter. Breeding of those two strains results in the generation of compound mice, carrying the knockdown or activation of the gene of interest restricted to those cell types, where Cre recombinase is expressed. Conditional mouse mutants are now

widely used to study the function of ubiquitously expressed genes in certain cell types and to circumvent embryonic lethality due to inactivation of a putative indispensable gene (Nagy 2000, Nagy, Mar et al. 2009).

Using the *CD19Cre* strain in the above depicted scenario (**Figure 8**) results in expression of the L-gp130 transgene and therefore activation of IL-6/gp130/JAK/STAT3 signaling from the pro-B cell stage onwards (Rickert, Roes et al. 1997) while breeding with *Cγ1Cre* mice allows conditional gene activation within the GC (Casola, Cattoretti et al. 2006). As *PRDM1Cre* (herein referred to as *Blimp1Cre*) is expressed when B cells leave the GC to differentiate towards the PC stage, L-gp130 expression in compound mice is restricted to plasmablasts and PCs (Kallies, Hasbold et al. 2007) and the *Vav1Cre* strain directs L-gp130 expression to the whole hematopoietic compartment (Ogilvy, Elefanty et al. 1998, Ogilvy, Metcalf et al. 1999). **Figure 9** gives an overview of all Cre-transgenic strains used in this study and depicts when they are active during differentiation.

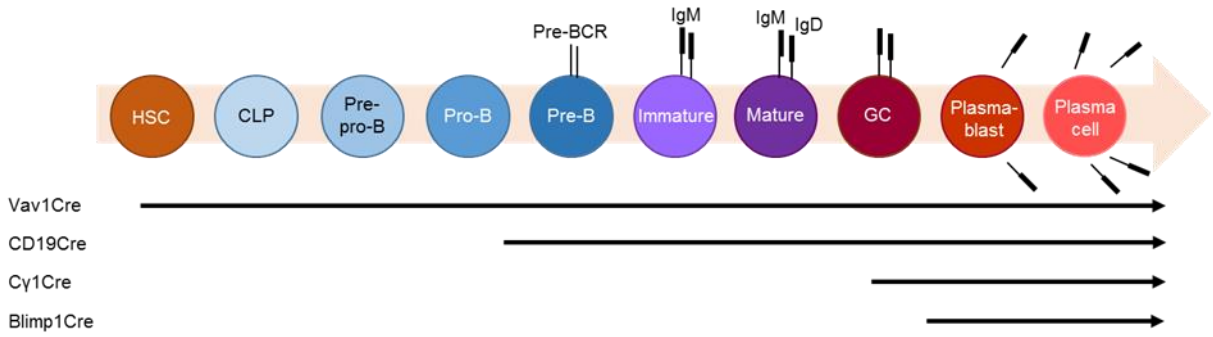

Figure 9: Overview of the Cre-transgenic strains and their expression during B cell development and in hematopoietic stem cells. Breeding of L-gp130 mice to distinct Cre-transgenic strains results in constitutive activation of gp130 signaling during hematopoietic and B cell development. HSC: hematopoietic stem cell, CLP: common lymphoid progenitor, Pre-pro B: pre-pro B cell, Pro-B: pro B cell, Pre-B: pre B cell, Immature: immature B cell, Mature: mature B cell, GC: germinal center B cell, Pre-BCR: pre B cell receptor (after (Giles, Bender et al. 2009)).

The described strains were selected as it is known for decades that IL-6/gp130 signaling is not only important for late B cell differentiation (Hirano, Yasukawa et al. 1986, Akira, Taga et al. 1993) but also directly accounts for the malignant progression of MM (Catlett-Falcone, Landowski et al. 1999). Apart from its central role in B cells, conventional IL-6/gp130 signaling is moreover essential for regulating cellular responses during hematopoiesis (Jenkins, Roberts et al. 2005) and for the differentiation of certain other lymphoid compartments (Park, Nakagawa et al. 2004, Nishihara, Ogura et al. 2007).

1.10 Objectives

B cell malignancies including MM represent frequent cancers and are still considered incurable for a large proportion of patients. Despite significant progress in understanding the pathogenesis of these severe diseases and the introduction of novel targeted therapies, the remission free and overall survival of patients is poor (Guang, McCann et al. 2018). With IL-6/gp130/JAK/STAT3 signaling playing an important role regarding the development and progression of MM, this pathway is of special interest for the future invention of new medications (Catlett-Falcone, Landowski et al. 1999). Although several murine models based on the activation of this axis have been generated, they are limited due to their low penetrance and late disease onset (Dechow, Steidle et al. 2014, Paton-Hough, Chantry et al. 2015, Rossi, Botta et al. 2018). So far, the development of transplantable plasmacytomas has only been shown in IL-6 transgenic mice on a BALB/c background (Suematsu, Matsusaka et al. 1992), a strain that is prone to malignant transformation as it harbors a mutation in the inhibitor of Cdk4/alternative reading frame (INK4a/ARF) locus that results in partial disability of the tumor suppressor protein $p16^{Ink4a}$ (Zhang, DuBois et al. 2001). Therefore, there is an urgent need to develop novel *in vivo* models for mimicking and analyzing the mechanisms of B cell lymphoma and myeloma pathogenesis, and for providing novel tools for testing therapies.

For that reason, the aim of the present study was to create conditional *in vivo* models of activated IL-6/gp130/JAK/STAT3 signaling on the frequently used C57BL/6 background. Constitutively active, cell-autonomous gp130 activity was thereby targeted to B cells, as well as to the entire hematopoietic system by making use of the Cre-loxP system.

First, the murine models allowed the investigation of the IL-6/gp130/JAK/STAT3 axis in B cell development and differentiation. Second, this approach was used to reveal concomitantly activated signaling pathways. Third, diseases that developed in these newly generated models were characterized particularly with regard to bearing resemblance to human MM. Fourth, the collaboration of activated gp130 signaling with second mutations in the development of malignant transformation was assessed.

2 Materials and Methods

2.1 Materials

2.1.1 Chemicals and Reagents

2-Mercaptoethanol, 50 mM	*Thermo Fisher Scientific*
Acetic acid	*Carl Roth GmbH*
ACK Lysis buffer	*Thermo Fisher Scientific*
Acrylamide/Bis-acrylamide solution [30 %]	*Carl Roth GmbH*
Agarose NEEO ultra-quality Roti®Garose	*Carl Roth GmbH*
Ammonium persulfate (APS)	*Sigma-Aldrich*
Bovine Serumalbumin (BSA)	*Sigma-Aldrich*
Bromphenol blue	*Sigma-Aldrich*
Complete Mini (Protease Inhibitor Cocktail)	*Roche*
Deionized water	*B. Braun Melsungen AG*
Dimethyl sulfoxide (DMSO)	*Serva*
dNTP Mix, 10 mM	*Fermentas*
Dithiothreitol (DTT)	*Sigma-Aldrich*
Dulbecco's phosphate buffered saline (DPBS)	*Thermo Fisher Scientific*
Dulbecco's Modified Eagle Medium (DMEM)	*Thermo Fisher Scientific*
Ethanol	*Carl Roth GmbH*
Ethidiumbromid (EtBr) solution [1 %]	*Carl Roth GmbH*
Ethylendiamintetraacetate (EDTA)	*Carl Roth GmbH*
Ethylene glycol-bis(2-aminoethylether)-N,N,N′,N′-tetraacetic acid (EGTA)	*Carl Roth GmbH*
Fetal Calf Serum (FCS)	*PAA Laboratories GmbH*
Formaldehyde solution [36 %]	*Fluka*
Formalin solution [10 %]	*Sigma-Aldrich*
Glycerol	*Sigma-Aldrich*
Glycine	*Carl Roth GmbH*
Hank's Balanced Salt Solution, 10x (HBSS)	*Thermo Fisher Scientific*
4-(2-hydroxyethyl)-1-piperazineethanesulfonic acid (HEPES)	*Thermo Fisher Scientific*
Isoflurane CP® [1 mg/ml]	*CP-Pharma*
Isopropanol	*Carl Roth GmbH*

L-Glutamine, 200 mM	*Thermo Fisher Scientific*
Lipofectamine® 2000	*Thermo Fisher Scientific*
Magnesium chloride ($MgCl_2$)	*Sigma-Aldrich*
Methanol	*J.T. Baker*
Non-essential amino acids (NEAA)	*Thermo Fisher Scientific*
Oligo(dT)12-18 Primer	*Thermo Fisher Scientific*
Opti-Mem® I Reduced Serum Media	*Thermo Fisher Scientific*
Osteosoft®	*Sigma-Aldrich*
Penicillin/Streptomycin (Pen/Strep)	*Thermo Fisher Scientific*
Phenylmethylsulphonyl fluoride (PMSF)	*Sigma-Aldrich*
Phosphate buffered saline (PBS)	*Thermo Fisher Scientific*
Polybrene (Hexadimethrine bromide)	*Sigma-Aldrich*
Ponceau S	*Sarstedt*
Propidium Iodide (PI)	*Thermo Fisher Scientific*
RNase OUT	*Thermo Fisher Scientific*
Sheep red blood cells (SRBC)	*Thermo Fisher Scientific*
Skim milk powder	*Sigma-Aldrich*
Sodium dodecylsulfate (SDS)	*Sigma-Aldrich*
Sodium chloride (NaCl)	*Carl Roth GmbH*
Sodium fluoride (NaF)	*Sigma-Aldrich*
Sodium orthovanadate (Na3VO4)	*Sigma-Aldrich*
Sodium tetraborate decahydrate (Borax)	*Sigma-Aldrich*
SuperSignal West (Pico/Dura/Femto)	*Pierce*
N,N,N′,N′-Tetramethylethan-1,2-diamin (TEMED)	*Sigma-Aldrich*
Tris(hydroxymethyl)aminomethane (TRIS)	*Carl Roth GmbH*
Trypan blue stain solution [0.4 %]	*Thermo Fisher Scientific*
Trypsin-EDTA-Solution, 10x	*Thermo Fisher Scientific*
Tween 20	*Sigma-Aldrich*
Ultra Pure Distilled Water (Aqua dest.)	*Thermo Fisher Scientific*

2.1.2 Consumables

6 *well*-plates	*Greiner Bio-One GmbH*
12 *well*-plates	*Greiner Bio-One GmbH*
BD Plastipak™ 1 ml Sub-Q insulin syringes	*BD Biosciences*
Blood lancets supra	*Megro GmbH & Co KG*
Cell culture dishes	*TPP*
Cell culture flasks T125, T75, T25	*Greiner Bio-One GmbH*
Cell strainers 100 µm	*BD Bioscience*
Combitips advanced® 10 ml	*Eppendorf AG*
CoolCell™ FTS30 Freezing container	*Sigma Aldrich*
Cryo Tubes™	*Corning*
CyAn ADP Lx P8	*Beckman Coulter*
Discardit™ II disposable syringes	*BD Biosciences*
Eppendorf tubes, 1.5 ml and 2 ml	*Sarstedt*
FACS tubes, 5 ml	*BD Biosciences*
Filter vacuum driven bottle top filter	*Millipore*
Kodak films	*Thermo Fisher Scientific*
MACS LS Columns	*Miltenyi Biotech*
Microvette tubes	*Sarstedt*
Parafilm	*Pechiney Plastic Packaging*
PCR-Strips Single Cap 8er-Soft-Strips 0.2 ml	*Biozym Scientific GMBH*
Pipette tips	*Sarstedt*
Pipette filter tips	*Starlab*
PVDF-Membrane	*Bio-Rad Laboratories*
S-Monovette®, EDTA	*Sarstedt*
Sterican® disposable needles	*B. Braun Melsungen AG*
Whatman® Filter Unit Puradisc FP30 0.2 µm and 0.45 µm	*GE Healthcare Life Sciences*
Whatman® Paper	*Biometra*

2.1.3 Instruments

Analytical balance Kern 770	*Kern & Sohn GmbH*
Cage systems IVC	*Tecniplast*
Cell incubator (Heraeus Hera cell 240)	*Heraeus*
Electrophoresis chamber	*Bio-Rad Laboratories*
Elphoscan ES2000 Plus device	*Sarstedt*
Flow cytometer (Cyan ADP Lx P8)	*Coulter-Cytomation*
FACSAria™ III cell sorter	*BD Biosciences*
Fridges and lab freezers	*Liebherr Hausgeräte GmbH*
Dissecting instruments	*Fine Science Tools GmbH*
Epson Perfection 4990 Photo Scanner	*Epson*
GelDoc System Universal Hood II	*Bio-Rad Laboratories*
Glas ware	*Labware SCHOTT AG*
Infrared lamp	*Breuer GmbH*
Light microscope Olympus CK40 and CKX41	*Olympus*
Light microscope Axiovert 25	*Carl Zeiss*
Liquid nitrogen tank Biosafe® MDβ	*Cryotherm*
MACS MultiStand	*Miltenyi Biotec*
Microfuge Heraeus Biofuge fresco	*Heraeus*
Microfuge Heraeus Megafuge 16 RS	*Heraeus*
Microfuge Heraeus Multifuge 3s	*Heraeus*
Microfuge MiniSpin	*Eppendorf AG*
Microcentrifuge Mikro22R	*Hettich Zentrifugen*
Microwave MWS 2820	*Bauknecht Hausgeräte GmbH*
MidiMACS™ Separator	*Miltenyi Biotec*
Multi-Channel Pipettes Research Plus®	*Eppendorf AG*
NanoDrop 2000c	*Thermo Fisher Scientific*
Neubauer hemocytometer	*Paul Marienfeld GmbH*
OPTIMAX X-ray Film Processor	*PROTEC GmbH & Co KG*
pH-meter SevenEasy™	*Mettler Toledo*
Pipetboy	*Integra Biosciences AG*

Pipettes Research Plus®	*Eppendorf AG*
Power Pac 200	*Bio-Rad Laboratories*
Power Pac P25T	*Biometra*
Precision balance Kern EG 2200-2NM	*Kern & Sohn GmbH*
Repeater 4780 and M4	*Eppendorf AG*
qRT-PCR Cycler (ABI Prism 7900 HT)	*Applied Biosystems*
Rotating mixer RM5	*CAT Laboratory Shakers and Mixers*
Safety cabinet HERAsafe® HSP18	*Heraeus*
Scil Vet ABC Blood Counter	*ScilAnimal Care*
SDS-Gelelectrophoresis chamber (Multigel Long)	*Biometra GmbH*
Smart Spec Plus™ Spectrophotometer	*Bio-Rad Laboratories*
SONOPLUS Homogenisator (HD 2070)	*Bandelin electronic*
Sunrise Microplate Reader	*Tecan Life Sciences*
Thermal Cycler Veriti™ 96-well	*Thermo Fisher Scientific*
Thermal Cycler BIOER Gene Touch	*Biozym Scientific GmbH*
Thermomixer comfort	*Eppendorf AG*
Vortex Mixer Genie2	*Scientific Industries*
Vortex Mixer IKA MS1 and Lab Dancer	*IKA® Werke GmbH & Co. KG*
Water bath	*Memmert*
Water bath SUB	*Grant Instruments*
Wet-transfer device	*Bio-Rad Laboratories*

2.1.4 Growth media and buffer compositions

Phoenix Eco media:

DMEM

10 % FCS (heat inactivated)

Storage at 4 °C

MEF media:

DMEM

10 % FCS (heat inactivated)

1 % Pen/Strep

1 % Glutamine

1 % NEAA

0.1 % 2-Mercaptoethanol

Storage at 4 °C

Freeze media:

FCS (heat inactivated)

10 % DMSO

Storage at 4 °C

HF2^{+} buffer:

10 % HBSS, 10x

2 % FCS (heat inactivated)

1 % HEPES

1 % Pen/Strep

deionized water

0.22 µm sterile filtered

Storage at 4 °C

FACS buffer:

PBS

0.5 % BSA

Storage at 4 °C

Formaldehyde buffer for intracellular staining:

1:10 Formaldehyde solution [36 %]

1:1 dilution in FACS buffer

Tail buffer:

1 % SDS

0.1 M NaCl

0.1 M EDTA

0.05 M Tris (pH 8)

315 ml deionized water

NaB buffer (1x):

0.19 % Borax

deionized water

Agarose gel (1 %):

1 % Agarose

NaB buffer (1x)

Boiled in microwave until completely dissolved

1 µg/ml EtBr

Protein lysis buffer:

50 mM HEPES

150 mM NaCl

1 mM EDTA pH 7.5

2.5 mM EGTA pH 7.5

0.1 % Tween 20

1 mM PMSF

1 mM NaF

0.1 mM NaVO4

10 % of one Roche Mini-Complete tablet dissolved in H_2O

PBS-Tween (PBS-T):

1 ml Tween in 1 L PBS

APS (10 %):

10 % Ammoniumpersulfat in Aqua dest.

Separating gel:

10 % Acrylamid/Bisacrylamid

375 mM Tris/HCl, pH 8.8

0.1 % SDS

3 % APS

0.07 % TEMED

Stacking gel:

5 % Acrylamid/Bisacrylamid

125 mM Tris/HCl, pH 6.8

0.1 % SDS

7 % APS

0.14 % TEMED

Loading buffer 5x:

3.88 g DTT

250 mM Tris-HCl 1M ph 6.8

5 g SDS

6.25 g Bromphenol blue (1 %)

50 % Glycerol

50 ml deionized water

SDS-Running buffer 10x:

14.4 % Glycine

3 % Tris

1 % SDS

deionized water

SDS-Running buffer 1x:

1:9 10x Running buffer in H_2O

Transfer buffer:

20 % Methanol

10 % SDS-Running buffer (10x)

deionized Wasser

Amido Black Destain:

10 % Methanol

10 % Acetic acid

80 % deonized water

4 % Formalin solution:

40 % Formalin solution [10 %]

60 % PBS

2.1.5 Enzymes

Phusion High Fidelity DNA Polymerase [2 U/µl]	*Thermo Fisher Scientific*
Proteinase K	*Ambion*

2.1.6 Primers

All oligonucleotides were purchased from Eurofins Genomics.

Primer names	Primer sequence 5` -> 3`
L-gp130	
L-gp130_rev_CAG	TGT CGC AAA TTA ACT GTG AAT C
L-gp130_rev wt	GAT ATG AAG TAC TGG GCT CTT
L-gp130_fwd	AAA GTC GCT CTG AGT TGT TAT C
CD19Cre	
Cre8	CCC AGA AAT GCC AGA TTA
19c	AAC CAG TCA ACA CCC TTC C
19d	AAC CAG TCA ACA CCC TTC C
Vav1Cre	
Vav1Cre_fwd	AGA TGC CAG GAC ATC AGG AAC CTG
Vav1Cre_rev	ATC AGC CAC ACC AGA CAC AGA GAT C
Cɣ1Cre	
Cɣ1_WT_fwd	TGT TGG GAC AAA CGA GCA ATC
Cɣ1_Mutant_fwd	GGT GGC TGG ACC AAT GTA AAT A
Cɣ1_Common	GTC ATG GCA ATG CCA AGG TCG CTA G
Blimp1Cre	
Blimp1Cre_fwd	GCC GAG GTG CGC GTC AGT AC
Blimp1Cre_rev	CTG AAC ATG TCC ATC AGG TTC TTG
Eµ-Myc	
Myc fwd	ACC TCT CCG AAA CCA GGC ACC GCA A
Myc rev	TCT TGC TCG CGC GCT AGT CCT TTC C
p53 KO	
p53 Mutant fwd	CAG CCT CTG TTC CAC ATA CAC T
p53 WT fwd	AGG CTT AGA GGT GCA AGC TG
p53 Common	TGG ATG GTG GTA TAC TCA GAG C

Table 1: Overview of primers used for genotyping in this study

Primer names	Primer sequence 5` -> 3`
L-gp130	
L-gp130 fwd (human)	ATG ATA AAG AAT TGT GCG GCG G
L-gp130 rev (human)	TGT TTA AGC TGT GCC ACC TG
gp130	
gp130 fwd (murine)	CCG TCA TTT TGG ATT TGG CAC A
gp130 rev (murine)	CCT CAC CAG CCC ACA TTC TA
GAPDH	
GAPDH fwd (murine)	AAG GTC ATC CCA GAG CTG AA
GAPDH rev (murine)	CTG CTT CAC CAC CTT CTT GA

Table 2: Overview of primers used for qRT-PCR in this study

2.1.7 Antibodies

Primary antibody	Dilution	Supplier
anti-actin; α-mouse	1/5000 in 5 % MP	*Sigma*
anti-Bcl-2; α-mouse	1/1000 in 5 % BSA	*BD Pharmingen*
anti-Bcl-XL; α-rabbit	1/1000 in 5 % BSA	*Cell Signaling*
anti-gp130; α-rabbit	1/1000 in 5 % MP	*Santa Cruz*
anti-STAT3; α-rabbit	1/1000 in 5 % BSA	*Cell Signaling*
anti-pSTAT3 (tyr705); α-rabbit	1/1000 in 5 % BSA	*Cell Signaling*
anti-phospho-p44/42 MAPK (Thr202/Tyr204)	1/1000 in 5% BSA	*Cell Signaling*
Primary antibody	**Dilution**	**Supplier**
anti-mouse (HRP-linked)	1/10.000	*GE Healthcare*
anti-rabbit (HRP-linked)	1/10.000	*GE Healthcare*

Table 3: Overview of antibodies used for western blot analysis in this study

Antigen	Fluorochrome	Clone	Dilution	Supplier
CD45	Pacific Blue/eFluor450	30-F11	1/200	*eBioscience*
CD45	APC	30-F11	1/200	*eBioscience*
CD19	Pacific Blue/eFluor450	eBio1D3 (1D3)	1/200	*eBioscience*
CD138	PE	281-2	1/200	*BD Biosciences*
CD138	APC	281-2	1/200	*BD Biosciences*
CD95	PECy7	Jo2	1/400	*BD Biosciences*
GL7	PerCP/Cy5.5	GL7	1/400	*BioLegend*
B220	APC-eFluor780	RA3-6B2	1/400	*eBioscience*
B220	PECy7	RA3-6B2	1/400	*eBioscience*
IgM	APC	II/41	1/400	*eBioscience*
IgM	PE	eB121-15F9	1/400	*eBioscience*
IgD	PE	11-26c (11-26)	1/400	*eBioscience*
IgD	Pacific Blue/eFluor450	11-26c (11-26)	1/400	*eBioscience*
CD93	PerCP/Cy5.5	AA4.1	1/200	*eBioscience*
CD11b	APC-eFluor780	M1/70	1/200	*eBioscience*
CD3e	PerCP/Cy5.5	145-2C11	1/200	*eBioscience*
Gr.1	PE	RB6-8C5	1/200	*eBioscience*
ckit (CD117)	APC-eFluor780	2B8	1µl/1Mio cells	*eBioscience*
ckit (CD117)	PE	2B8	1µl/1Mio cells	*eBioscience*
Sca1	PECy7	D7	1µl/1Mio cells	*eBioscience*
Mouse hematopoietic Lineage Cocktail	bio		1µl/1Mio cells	*eBioscience*
Ter119	Pacific Blue/eFluor450	Ter-119	1µl/1Mio cells	*eBioscience*
Streptavidin	Pacific Blue/eFluor450		1µl/1Mio cells	*eBioscience*
pSTAT3 (Y705)	PE	LUVNKLA	0.06µg/sample	*eBioscience*
Isotype IgG2b kappa	PE	eBMG2b	0.06µg/sample	*eBioscience*

Table 4: Overview of antibodies used for flow cytometric analysis in this study

2.1.8 Molecular weight markers for DNA and proteins

Gene Ruler™ 1 kb Plus Ladder	*Thermo Fisher Scientific*
PageRuler™ Plus Prestained Protein Ladder	*Thermo Fisher Scientific*

2.1.9 Plasmids

MSCV-IRES-GFP (MIG)	J. Miller and W. Pear, Philadelphia
MSCV-Cre-YFP	gift from M. Schmidt-Supprian, Munich
MSCV-L-gp130-IRES-GFP	gift from T. Dechow, Munich

2.1.10 Kits

Bio-Rad Protein Assay	*Bio-Rad Laboratories*
CD19 MicroBeads, mouse	*Miltenyi Biotec*
CD138 MicroBeads, mouse	*MiltenyiBiotec*
KAPA Mouse Genotyping Kit	*Kapa Biosystems*
Mouse Immunoglobulin Panel	*SouthernBiotech*
Platinum SYBR Green qPCR SuperMix-UDG	*Invitrogen*
Qiagen® DNeasy Blood & Tissue Kit	*Qiagen*
Qiagen® Omniscript RT Kit	*Qiagen*
Qiagen® Qiashredder	*Qiagen*
Qiagen® RNeasy Plus Mini Kit	*Qiagen*
SBA Clonotyping™ System-AP	*SouthernBiotech*

2.1.11 Software programs

Excel	*Microsoft Office*
FlowJo Version 10	*Tree Star Inc.*
GraphPad Prism Version 7	*GraphPad Inc*
Inkscape Version 0.92	*Inkscape Community*
Magellan Version 7	*Tecan Life Sciences*
Quantity One 1-D Analysis Software	*Bio-Rad Laboratories*
Word	*Microsoft Office*

2.1.12 Mouse strains

Mice used in this study were on a C57BL/6 background. All mice were bred and maintained in microisolators in the animal facility of Technische Universität München under specific-pathogen-free (SPF) conditions according to FELASA recommendations on a 12-h light/dark cycle, receiving food and water *ad libitum*. Animal experiments were performed in accordance with the FELASA guidelines and approvals from the regional animal ethics committee (Regierung von Oberbayern, Munich, Germany).

R26 fl rx *L-gp130* (herein referred to as *L-gp130*)

This novel conditional mouse strain on the frequently used C57BL/6 background was generated by Frank-Thomas Wunderlich and Mona Al-Maarri at the Center for endocrinology, preventive medicine and diabetes at the Max Planck Institute for Metabolism Research in Cologne, Germany. In this strain, compound expression of the chimeric receptor protein L-gp130 (Stuhlmann-Laeisz, Lang et al. 2006) and the fluorescent protein from the CAG promoter is prevented by a loxP- and a rox-flanked stop cassette. The novel B9-36 ROSA26 targeting vector, a derivative of the STOP-EGFP ROSA CAG targeting vector, comprising a short arm of homology (SAH), a chicken beta actin promoter followed by a loxP flanked neo stop and a rox flanked stop cassette was employed. The single AscI site can be used to insert in frame transgenes to the 2A driven *Zoanthus* sp. green fluorescent protein (ZsGreen) construct to monitor Cre- and Dre-mediated recombination. 3' to the 2A ZsGreen cassette, the 4.5 kb long arm of homology (LAH) and negative PGK DTA cassettes are inserted. L-gp130 was amplified from pCDNA L-gp130 with oligos 5AscLGP130 (GGC GCG CCA CCA TGT TGA CGT TGG CAG ACT TGG) and 3AscLGP130 (GGC GCG CCC TGA CCT GAG GCA TGT AGC CGC C) sequenced and inserted into AscI site of B9-36 TV. 40µg of AsiSI linearized B9-36 L-gp130 was transfected into 10^7 Bruce 4 ES cells by electroporation and selected with G418. Isolated single ES clones were screened using Southern blot analysis of EcoRI digested clonal DNA using ROSA26 EcoRI/PacI probe as previously described (Belgardt, Husch et al. 2008). An additional 7.1 kb targeted band appeared with the 15.6 kb WT band in correctly targeted clones. A neo probe confirmed single integration of the transgene. Correctly targeted clones were injected into donor blastocysts to generate chimeric mice that were backcrossed to C57BL/6 mice to obtain R26 fl rx *L-gp130* mice on a pure C57BL/6 background. To create the Cre-activatable *L-gp130* conditional allele, parental mice were crossed to Dre deleter mice (Anastassiadis, Fu et al. 2009). Breeding of this strain to Cre-transgenic mice leads to forced activation of gp130 signaling in the correspondent compartment.

***CD19Cre* (*B6.129P2(C)-Cd19$^{tm1(cre)Cgn}$/J*)**

A Cre recombinase gene was inserted into the first coding exon of the CD19 antigen gene thus abolishing endogenous CD19 gene function and placing Cre expression under the control of the endogenous CD19 promoter/enhancer elements. Cre recombinase expression in this strains is seen from the earliest stages throughout B-lymphocyte development and differentiation (Rickert, Roes et al. 1997).

***Cγ1Cre* (*B6.129P2(Cg)-Ighg1$^{tm1(cre)Cgn}$/J*)**

This transgenic mouse model expresses Cre recombinase from the endogenous *Ighg1* (immunoglobulin heavy constant gamma 1) locus restricting Cre recombinase activation to GC B cells. The expression of a bicistronic mRNA consisting of the Ig gamma 1 constant region (C*γ*1) and Cre recombinase was made possible by the introduction of an Internal Ribosome Entry Site (IRES)-Cre-frt-flanked neomycin cassette into the 3' UTR of the Ig gamma 1 constant region gene between the last membrane coding region and its polyadenylation site (Casola, Cattoretti et al. 2006).

***PRDM1-Cre* (*B6.Cg-Tg(Prdm1-cre)1Masu/J*; herein referred to as *Blimp1Cre*)**

In this strain, Cre recombinase is expressed under the control of the mouse Prdm1 (PR domain containing 1; Blimp1) promoter. The exon 1 and 2 coding region of the targeted mouse gene were replaced by a nuclear localization sequence (NLS) followed by the Cre sequence and a transcriptional stop cassette (Ohinata, Payer et al. 2005). Blimp1 gets upregulated upon exit from the GC reaction and its expression is therefore seen in PCs (Turner, Mack et al. 1994).

***Vav1-iCre* (*B6.Cg-Commd10$^{Tg(Vav1-icre)A2Kio}$/J*; herein referred to as *Vav1Cre*)**

This transgenic line expresses Cre recombinase under the control of the mouse vav 1 oncogene (*Vav1*) promoter therefore directing expression of an optimized variant of Cre recombinase (iCre) to hematopoietic cells (and their progenitors) (Ogilvy, Elefanty et al. 1998, Ogilvy, Metcalf et al. 1999, Shimshek, Kim et al. 2002, de Boer, Williams et al. 2003).

Eμ-Myc (B6.Cg-Tg(IghMyc)22Bri/J)

In this strain, the murine oncogene *Myc* (*c-Myc*) is under control of the Eμ immunoglobulin heavy chain enhancer restricting its expression to the B cell lineage. *Eμ-Myc* transgenic mice frequently develop aggressive pre-/immature B cell lymphomas early in life mimicking the human BL phenotype (Adams, Harris et al. 1985).

***Trp53 knockout* (*B6.129S2-Trp53^{tm1Tyj}/J*; herein referred to as *p53 KO*)**

In this transgenic strain, exons 2 – 6 (including the start codon) of the *Trp53* gene are replaced by a neomycin cassette leading to the knockout of the gene. Mice homozygous for the mutation develop lymphomas and sarcomas at three to six months of age. Heterozygous mice show tumor formation at about ten months of age (Jacks, Remington et al. 1994).

Ly5.1 (B6.SJL-Ptprc^{a} Pepc^{b}/BoyJ; CD45.1)

In contrast to WT C57BL/6 inbred strains expressing the *Ptprc^{b}* (CD45.2 or Ly5.2) allele, this C57BL/6 congenic strain carries the differential pan leukocyte marker *Ptprc^{a}*, commonly known as CD45.1 or Ly5.1 (Shen, Saga et al. 1985). It is commonly used in transplant studies and therefore served as BM support in the FL-HSPC transplantation approach in the present study.

2.2 Methods

2.2.1 Molecular biology techniques

2.2.1.1 Mouse genotyping by PCR

Genotyping of mice is based on the polymerase chain reaction (PCR) that allows for *in vitro* amplification of specific DNA sequences by repeated cycles of DNA-denaturation, annealing of specific primers and elongation by a thermoresistant DNA polymerase (Mullis and Faloona 1987). Products can then be visualized on an agarose gel to control for the presence of transgenes.

DNA was isolated from ear punches or embryonic tissue (see chapter 2.2.3.2) by digestion in Tail buffer with 200 µg/ml Proteinase K at 55 °C, 750 rpm o/n in a thermo shaker. The next day, the reaction was stopped by heat inactivation at 99 °C for 5 min. After centrifugation at 4 °C at 13000 rpm in a table centrifuge, supernatants were collected and 1 µl was used for genotyping using the KAPA Mouse Genotyping Kit.

Reaction mix, 20 µl in H_2O:
1 µl DNA
1 µl each Primer (100 pmol/µl)
10 µl Kapa Genotyping Mix
Ad 20 µl H_2O

The temperature for denaturation was 94 °C, annealing temperatures varied between 56 – 65 °C depending on the melting temperature of the primers, and elongation was carried out at 72 °C for 1 – 2 min depending on the length of the sequence.

Primers used for genotyping are depicted in **Table 1**.

2.2.1.2 Agarose gel electrophoresis

In an agarose gel, DNA is separated in an electric field dependent on its size. Visualization is then realized by addition of ethidium bromide (EtBr), a fluorescent agent that intercalates into DNA (Waring 1965). In this study, 1 % agarose gels were used. Therefore, agarose was dissolved in the appropriate volume of electrophoresis buffer (1X NaB), boiled, supplemented with EtBr and cooled down in a gel chamber. DNA samples were then loaded into gel pockets together with a marker (DNA ladder) prior to electrophoresis. EtBr stained DNA visualized under UV-light.

2.2.1.3 Isolation of genomic DNA from tumor material

Genomic DNA was isolated from tumor/tissue samples using the Qiagen® DNeasy Blood & Tissue Kit according to manufacturer's instructions.

2.2.1.4 Analysis of IgH rearrangements

IgH rearrangements were amplified by PCR from genomic DNA (chapter 2.2.1.3) as follows: MsVHe-AH-forward (TCGAGTTTTTCAGCAAGATGAGGTGCAGCTGCAGGAGTCTGG) was combined with JH4e-New-AH-reverse (ATCTTCTAGAAAGATGTCCCTATCCCATCATCCAGGG) to amplify rearrangements involving JH1-4. All samples were amplified by PCR for 35 cycles with Phusion High Fidelity DNA Polymerase (2 U/µl) with the following conditions: 2 mM $MgCl_2$; melt at 98 °C for 10 mins, anneal at 72 °C for 1 min, extend at 72 °C for 10 mins and then visualized on a 1 % agarose-gel. Genomic DNA from *Eμ-Myc* LN was used for monoclonal and oligoclonal controls.

2.2.1.5 RNA extraction from eukaryotic cells

For analysis of gene expression on transcriptional level, mRNA needs to be extracted using RNase-free solutions because of omnipresent RNases. In this study, total RNA was extracted from MEFs with the Qiagen® RNeasy Mini Kit according to the manufacturer's instructions. Isolation of total RNA from MEFs was realized in a two-step protocol: the tissue lysate was first homogenized using a QIAshredder, followed by RNA extraction with help of the RNeasy Mini Kit that depends on reversible binding of RNA to silica-membrane spin columns as stated above. To obtain a higher RNA purity, the optional DNAse digestion steps were performed as suggested by the manufacturer.

RNA concentration in the final eluates was measured spectrophotometrically on a Nanodrop.

2.2.1.6 Reverse transcription (RT)

Reverse transcriptases are enzymes of viral origin, synthesizing complementary DNA (cDNA) on the basis of an RNA template in a reaction called reverse transcription (RT) (Baltimore 1970, Temin and Mizutani 1970, Spiegelman, Watson et al. 1971). The resulting cDNA is the source for different gene expression analyses such as quantitative real time PCR (qRT-PCR).

To obtain cDNA, 1 µg of extracted RNA (see chapter 2.2.1.5) was reversely transcribed using the Qiagen® Omniscript RT Kit with RNase Out and oligo(dT) primers, which allow specific transcription of mRNA via annealing to polyA-tails according to the manufacturer's protocol:

cDNA was synthesized at 37 °C for 60 min with heat inactivation of the enzyme at 93 °C for 5 min.

Reaction mix: 1 µg RNA in 12 µl RNase-free H_2O

2 µl 10x Puffer RT

2 µl dNTPs

2 µl oligo-dT (1:5 dilution)

1 µl RNase out (1:4 dilution)

1 µl Reverse Transcriptase

2.2.1.7 Quantitative real time PCR (qRT-PCR)

qRT-PCR is a PCR-based method using fluorochromes to monitor the amount of amplified DNA in real time after each PCR cycle (Bustin and Mueller 2005). SYBR Green is a commonly used qRT-PCR dye that unspecifically binds to double-stranded DNA to form a DNA-SYBR Green complex absorbing blue and emitting green light. Fluorescence intensity hence correlates with the amount of DNA, thus allowing quantification of gene expression in relation to reference genes (Schneeberger, Speiser et al. 1995, Zipper, Brunner et al. 2004). In this study, analysis was performed on an ABI Prism 7900HT cycler using the Platinum SYBR-Green Q PCR SuperMix-UDG according to the manufacturer's instructions with cDNA from MEFs (see chapter 2.2.3.2) in triplicates as templates. Data analysis was done by comparing Ct values with a control sample set as 1 and normalized to the expression of GAPDH.

Primer sequences are listed in **Table 2**.

Reaction mix: 15.6 µl Power SYBR Green PCR Master Mix
0.5 µl ROX
1 µl Primer (forward and reverse, each 10 µM)
1.8 µl cDNA
8.0 µl H_2O

Program: 95 °C 1 min
95 °C 15 sec
60 °C 1 min } 40 x
95 °C 15 sec
60 °C 1 min
95 °C 15 sec } Melt curve

2.2.2 Protein biochemistry

2.2.2.1 Cell lysis

Cell pellets were lysed in ice-cold lysis buffer containing protease inhibitors for 15 minutes on ice followed by sonication (4 cycles with 10 sec at 30 % power). Cell debris was removed by centrifugation at full speed for 5 min at 4 °C in a microcentrifuge and supernatants were collected. Protein was quantified using the Bio-Rad Protein Assay Dye Reagent according to the manufacturer's instructions (Bradford 1976). Protein absorption was measured at 750 nm on the Smart Spec Plus Spectrophotometer. 15 µg protein were taken up in 5X loading dye, boiled at 95 °C for 5 min to denaturate proteins via SDS and stabilize the sample.

2.2.2.2 SDS-PAGE and immunoblotting

SDS polyacrylamide gel electrophoresis (SDS-PAGE) is a gel-based technique for the separation of proteins in an electric field due to their electrophoretic mobility. In the presence of SDS, tertiary structures are overcome and proteins are coated in negative charge, thus migrating according to their molecular weight (Smith 1984). SDS-PAGE is followed by immunoblotting to detect membrane-bound proteins by making use of specific antibodies.

15 µg of protein samples and a molecular weight marker were loaded onto a 10 % SDS polyacrylamide gel and electrophoretically separated in 1X Running Buffer in an electrophoresis chamber at 30 V and RT o/n. The gel was then blotted onto a Methanol-activated PVDF membrane (0.45 µm) in a wet-transfer device using Transfer buffer at 4 °C and 1000 mA for 2 h. After blocking with BSA or skim milk in PBST for 1 h at RT, membranes were incubated o/n at 4 °C with primary antibodies in BSA or skim milk in PBST on a roller mixer as indicated on the respective data sheet. Membranes were then washed twice with PBST and incubated with secondary anti-rabbit or anti-mouse IgG antibody conjugated to HRP for 1 h at RT. Following three additional washing steps with PBST, membranes were visualized on Kodak films with Pierce™ ECL Western Blotting Substrate according to the manufacturers' instructions. The ECL method is based on chemiluminescent HRP substrates, creating signals at the site of bound secondary antibody.

2.2.2.3 Stripping of membranes

To re-probe a PVDF membrane with another antibody, the previously bound primary and secondary antibodies were stripped off the membranes using Amido Black Stain solution for 10 min at RT followed by three washing steps with PBST and incubated again with the new antibodies.

Primary and secondary antibodies and their dilutions used in this study are listed in **Table 3**.

2.2.2.4 Collection of serum and serum electrophoresis

Up to 300 µl of whole blood from mice were collected in Microvette tubes and allowed to clot for 30 min at RT. The clot was removed by subsequent centrifugation in a table centrifuge at 2.000 x g for 10 min at 4 °C. The supernatant was collected and stored at – 20 °C. Serum protein electrophoresis was performed on an Elphoscan ES2000 Plus device. 25 µl mouse serum was applied to a cellulose acetate strip. After separation, the resulting protein fractions were stained with Ponceau S and quantified by densitometric scanning.

2.2.3 Cell culture and cell-based assays

2.2.3.1 Cell culture methods

Cells were kept in a humidified incubator at 37 °C and 5 % CO_2.

2.2.3.2 Preparation and culture of murine embryonic fibroblasts

Preparation and culture of murine embryonic fibroblasts (MEFs) has been described elsewhere (Jozefczuk, Drews et al. 2012). MEFs of the following genotypes were prepared and cultured in this study: *L-gp130*$^{fl/fl}$, *L-gp130*$^{fl/+}$, *L-gp130*$^{+/+}$ (i.e. WT). Genotyping was performed on heads of isolated embryos as described in chapter 2.2.1.1 and 2.2.1.2.

2.2.3.3 Generation of retrovirus and infection of MEFs

The ecotropic packaging cell line PhoenixEco was used for the generation of retrovirus in order to deliver exogenous DNA into murine cells upon transfection with Lipofectamine™ 2000. Lipofectamine is a cationic liposome substance that forms complexes with negatively charged nucleic acid molecules thus allowing their translocation into the cell by overcoming the electrostatic repulsion of the cell membrane (Dalby, Cates et al. 2004). Retrovirus genomes generally comprise three open reading frames (ORF) that encode for proteins essential for virus production: env (envelope), gag (group-specific antigen), and pol (polymerase). gag codes for core and structural proteins of the virus, pol codes for reverse transcriptase, protease and integrase, and env codes for the retroviral coat proteins (Coffin 1992).

For transfection, PhoenixEco cells were seeded at a density of 4 x 10^6 cells in 5 ml PhoenixEco media in a 10 cm cell culture dish and kept at 37 °C o/n. Per dish, 30 µl of Lipofectamine™ 2000 were mixed with 750 µl Opti-MEM® I Reduced Serum Media and incubated for 5 min at RT. In the meantime, 20 µg of plasmid DNA was given to 750 µl Opti-MEM® I Reduced Serum Media, combined with the Lipofectamine mixture and incubated for 30 min at RT. Media was removed from PhoenixEco cells and replaced by 3.5 ml fresh media followed by addition of 1.5 ml DNA/Lipofectamine complexes per dish. After 6 h incubation, the media was changed to MEF media. Supernatants containing retroviral particles were then collected after 24, 36, and 48 h post transfection and filtered through a 0.45 µm Whatman® Filter Unit.

The day before, MEFs were seeded at low densities (i.e. 6 x 10^5 cells in T25 cell culture flasks in 5 ml MEF media) to allow for their proliferation as a prerequisite for retroviral infection of adherent cells (Miller, Adam et al. 1990). MEFs were infected three times at 12-h intervals with retroviral supernatant supplemented with 8 µg/ml polybrene. Polybrene is a cationic polymer used to increase infection efficiency (Davis, Morgan et al. 2002). MEFs were then sorted for GFP/YFP positivity on the BD FACSAria™ III cell sorter for further analyses.

Plasmids used for transfection are listed in the Materials section 2.1.9.

2.2.3.4 Freezing and thawing of cells

Cells can be cryoconserved using a cryoprotectant such as dimethyl sulfoxide (DMSO). DMSO enters the cell thus avoiding crystallization, damage, and cell lysis (McGann and Walterson 1987). For long term storage, MEFs as well as freshly isolated cells from mouse necropsies were pelleted, resuspended in freeze media (FCS supplemented with 10 % DMSO), and aliquoted in cryotubes at a concentration of up to 1 x 10^8 cells/ml. Cryotubes were transferred to a – 80 °C freezer in a freezing container assuring a cooling rate of 1°C/min to prevent damage to the cell membrane that is caused by a rapid freezing process. After at least 24 h at – 80 °C, the cells were transferred to liquid nitrogen for long-term storage.

For thawing of the cells, it is mandatory to rapidly wash out the DMSO that can be toxic to the cell at prolonged exposure times. Accordingly, cells were rapidly thawed at 37 °C and DMSO was washed out with $HF2^+$ buffer.

2.2.4 Animal experiments

2.2.4.1 Keeping and breeding of mice

WT C57BL/6J mice for transplantation experiments were purchased from Charles River Laboratories or Janvier Laboratories. The novel conditional L-gp130^{fl} mouse model was bred to the different Cre-transgenic strains, described in chapter 3.2, to activate gp130/JAK/STAT3 signaling at distinct stages of hematopoietic and B cell development. Recipient as well as compound mice were monitored for signs of morbidity and tumor development by daily observation and physical examination. For experiments littermates were used as control animals unless otherwise indicated.

2.2.4.2 Fetal liver cell transplantation

L-g130$^{fl/fl}$ mice were bred to *CD19Cre$^{+/+}$* and *Eμ-Myc$^{+/-}$* mice and subsequent offspring was again mated and females were monitored for vaginal plugs. Fetal liver hematopoietic stem/progenitor cells (FL-HSPC) were obtained on embryonic day 13.5 (E13.5) and genotyping was done on isolated embryonic DNA (see chapter 2.2.1.1 and 2.2.1.2). C57BL/6 FLC recipient mice received myeloablative irradiation (8.5 Gy) and were transplanted with 1.2 × 10^6 syngeneic FL-HSPC together with 0.2 x 10^6 Ly5.1 BM support in total via tail vein injection.

2.2.4.3 Serial transplantation of tumor cells

For serial transplantation, *CD19;L-gp* mice were sacrificed upon arrival of the defined endpoints of the study and 1 x 10^6 tumor cells were transplanted into sublethally irradiated (4.5 Gy) syngeneic recipients.

2.2.4.4 Sheep red blood cell (SRBC) immunization

Intravenous sheep red blood cell (SRBC) injection has been shown to initiate a GC reaction (Zhang, Tech et al. 2018). Therefore, *Cγ1;L-gp* mice were injected i.v. with 1 x 10^8 SRBCs in PBS to activate gp130/JAK/STAT3 signaling and analyzed 11 d after immunization.

2.2.4.5 Necropsy

Upon reaching the previously defined end points of the study, mice were sacrificed using isoflurane. Blood samples were collected into 1.2 ml heparinized tubes and blood cells were counted on a Scil Vet ABC. Mesenteric tumors as well as SPL and LN were dissected from the surrounding tissues and divided for further analyses: one part was fixed in 4 % Formalin solution for 48 h for immunohistochemical (IHC) analyses, the other part was passed through 100 µm cell strainers, washed in $HF2^+$ buffer and frozen viably for further analyses. Femurs and tibias were also isolated. While one tibia was fixed in 4 % Formalin solution for 48 h followed by storage in Osteosoft for two weeks for subsequent IHC analyses, the BM from the additional bones was flushed out using $HF2^+$ buffer, homogenized and passed through a filcon before being frozen viably. If samples immediately underwent flow cytometric analysis, ammonium chloride–potassium bicarbonate (ACK) lysis buffer was used to lyse erythrocytes prior to staining.

2.2.5 Immunological methods

2.2.5.1 Flow cytometry

Flow cytometry is a laser-based technique used to simultaneously analyze different cell characteristics on a single cell level. In a hydrodynamic field, single cells are illuminated by a laser beam and pass a set of light detectors that measure fluorescent signals e.g. autofluorescence or fluorochrome-coupled antibodies as well as physical properties such as size and granularity of single cells (Orfao, Ruiz-Arguelles et al. 1995). For extracellular staining, cells were incubated with fluorescently labeled antibodies in FACS buffer for 30 min on ice in the dark. Unbound antibodies were removed by subsequent washing with FACS buffer. Viability distinction was realized by resuspending the cell pellet with propidium iodide (PI) at a concentration of 1 µg/ml in FACS buffer. Before analysis on a Cyan ADP Lx P8, cells were passed through a filcon to remove remaining tissue clumps. FlowJo Software Version 10 was used for data analysis.

Gating strategy for distinct B cell subsets is shown in **Figure 13**. Mouse Hematopoietic Lineage Biotin Cocktail was used together with antibodies against c-kit, Sca-1, and Ter119 for defining LSK and MPP compartments in the BM. Gating for these populations has been described elsewhere (Istvanffy, Kroger et al. 2011).

2.2.5.1.1 Intracellular flow cytometry for pSTAT3

After extracellular staining with fluorescently labeled antibodies against CD45, CD19, and CD3, splenocytes from *Vav;L-gp* mice and age-matched controls were washed twice with FACS buffer and fixed in warm Formaldehyde solution (4 %) for 10 mins at 37 °C followed by permeabilization in 90 % ice-cold Methanol for 30 mins on ice. After subsequent washing with FACS buffer for two times, cells were incubated with the intracellular pSTAT3 antibody for 1 h on ice in the dark, washed again and resuspended in FACS buffer for flow cytometric analysis. IgG2b kappa was used as an isotype control.

Antibodies for flow cytometry and their dilutions are listed in **Table 4**.

2.2.5.2 Enzyme-linked Immunosorbent Assay (ELISA)

ELISA is an assay technique for detecting and quantifying soluble antigens (Engvall and Perlmann 1971, Van Weemen and Schuurs 1971). In a so-called sandwich ELISA, antibodies are immobilized to a solid surface capable of binding antigens from a sample. Those antigens are bound by a second antibody coupled to an enzyme. Added substrate is then converted by the enzyme into a detectable signal that correlates with the quantity of the antigen. In the present study, basal Ig concentrations of IgM and IgG_{total} were determined by ELISA applying the SBA Clonotyping™ System-AP and the Mouse Immunoglobulin Panel on serum samples (see chapter 2.2.2.4) from diseased mice and controls. Optical densities were measured on a Sunrise Microplate Reader with Magellan 7 software.

2.2.5.3 Magnetic cell separation

Murine B cells and PCs were magnetically purified from tumor material as well as from young *CD19;L-gp* and C57BL/6 WT spleens using CD19 and/or CD138 MicroBeads according to the manufacturer's protocol.

Purification was afterwards controlled by flow cytometry.

2.2.6 Histological and immunohistochemical analyses

Histological and IHC analyses was performed by Prof. Dr. Leticia Quintanilla de Fend at the Institute of Pathology (University of Tübingen) and Prof. Dr. Katja Steiger at the Institute of Pathology (TUM). IHC describes the detection of antigens in tissue sections using specific antibodies. Samples were fixed in 4 % Formalin solution and stored in PBS thereafter. Paraffinized samples were then sent to the Institute of Pathology in Tübingen, where the samples were cut into sections using a microtome and processed according local standard protocols.

Hematoxylin and eosin (H&E) staining was performed following standard protocols.

2.2.7 Transcriptome analysis

2.2.7.1 RNA isolation from tumor material for RNA-sequencing

RNA was isolated from samples with an infiltration of > 60 % ZsGreen$^+$ tumor cells using the Qiagen® RNeasy Plus Mini Kit according to the manufacturer's protocols. Where infiltration rate was lower, CD19$^+$ cells were collected by MACS separation (see chapter 2.2.5.3) and RNA was isolated thereafter. The latter also accounted for splenocytes from young *CD19;L-gp* as well as C57BL/6 WT controls.

RNA concentration in the final eluates was measured spectrophotometrically on a Nanodrop.

2.2.7.2 RNA-sequencing

Library preparation for bulk 3'-sequencing of poly(A)-RNA was done as described previously (Parekh, Ziegenhain et al. 2016). Briefly, barcoded cDNA of each sample was generated with a Maxima RT polymerase using oligo-dT primer containing barcodes, unique molecular identifiers (UMIs) and an adapter. 5' ends of the cDNAs were extended by a template switch oligo (TSO) and after pooling of all samples full-length cDNA was amplified with primers binding to the TSO-site and the adapter. cDNA was tagmented with the Nextera XT kit (Illumina) and 3'-end-fragments finally amplified using primers with Illumina P5 and P7 overhangs. In comparison to Parekh et al. the P5 and P7 sites were exchanged to allow sequencing of the cDNA in read1 and barcodes and UMIs in read2 to achieve a better cluster recognition. The library was sequenced on a NextSeq 500 (Illumina) with 75 cycles for the cDNA in read1 and 16 cycles for the barcodes and UMIs in read2. Data was processed using the published Drop-seq pipeline (v1.0) to generate sample- and gene-wise UMI tables (Macosko, Basu et al. 2015). Reference genome (GRCm38) was used for alignment. Transcript and gene definitions were used according to the ENSEMBL annotation release 75. RNASeq was done by R. Öllinger.

2.2.8 Bioinformatical analyses

2.2.8.1 Statistical analysis of high-throughput gene expression data

High-throughput gene expression data from the conditions indicated in the text were carried out using the R environment for statistical computing (v3.4.0) (R-Core-Team 2016). Analysis of RNASeq data was done in collaboration with H.C. Maurer.

2.2.8.2 Differential gene expression analysis

Genome-wide differential gene expression analysis for RNASeq data was carried out using the *voom-limma* framework as implemented the R package *limma* (Ritchie, Phipson et al. 2015). This yielded moderated t- and F-statistics for two and three group comparisons, respectively, and a false discovery rate (FDR) < 0.1 was considered significant.

2.2.8.3 Derivation of a *CD19;L-gp* gene expression signature

First, a differential gene expression analysis was carried out between WT B cells and B cells with Cre-mediated L-gp130 activation (*CD19;L-gp*) as described above, yielding to a total of 2094 genes which were differentially expressed at a FDR < 0.05. The top 100 genes induced and repressed by L-gp130 activation, respectively, were used to build a two-tailed gene set and information on their effect size (log_2 fold change) was added as an additional weight for ssGSEA, thus yielding a *L-gp130 signature regulon*. When using the L-gp130 signature regulon, positive enrichment scores indicate similarity to *CD19;L-gp* B cells whereas negative enrichment scores indicate similarity to WT B cells.

2.2.8.4 Data acquisition and pre-processing

B cell development: gene expression data from studies comparing different stages of B cell development using the Affymetrix GeneChip Human Genome U133 Plus 2.0 platform were retrieved from ArrayExpress and Gene Expression Omnibus (GEO), respectively. Specifically, the accession numbers were E-MEXP-2360 (Jourdan, Caraux et al. 2009), E-MEXP-3034 (Jourdan, Caraux et al. 2011), E-MEXP-3945 (Jourdan, Cren et al. 2014), and GSE15271 (Caron, Le Gallou et al. 2009).

CEL files were retrieved for all studies and normalized using the *GCRMA* R package (Wu 2014).

MM: Normalized gene expression data from Keats et al. (Keats, Fonseca et al. 2007) were retrieved from the Multiple Myeloma Genomics Portal (Liefeld 2008).

For all microarray datasets, probes were collapsed at the gene level by keeping the probe with the highest median expression. Genes with an interquartile range of zero were removed from the analysis.

2.2.8.5 Gene set collection

Gene sets were retrieved from the MSigDb v6.0 (Subramanian, Tamayo et al. 2005, Liberzon, Birger et al. 2015) modules HALLMARK, C2 canonical pathways, C3 transcription factor targets and C6 oncogenic signatures and were categorized as follows: (i) B cell signaling pathways whose names contain ‘B_CELL’ or ‘BCR’ (n = 10), (ii) NF kappa B signaling pathways containing ‘KAPPAB', or ‘NFKB’ (n = 22), (iii) Downstream signaling pathways containing ‘MAPK’, ‘ERK’, ‘PI3K’, ‘AKT’ or ‘MTOR’ (n = 43), (iv) Hippo signaling containing ‘HIPPO’ or ‘YAP’ (n = 5), (v) Developmental pathways containing ‘WNT’, ‘NOTCH’, ‘TGF’, ‘HEDGEHOG’, ‘SHH’ or ‘BMP’ (n = 40) and (vi) MYC and STAT3 signaling containing ‘MYC’, ‘IL6’, ‘IL6ST’ or ‘STAT3’ (n = 18). In order to determine STAT3 activity as opposed to mere STAT3 expression among different B cell development stages, the expression of STAT3 target genes rather than STAT3 itself was considered as described below. STAT3 target genes were retrieved from the TTRUST (Han, Cho et al. 2018) database.

2.2.8.6 Single sample gene set enrichment (ssGSEA)

Single sample GSEA (ssGSEA) was used to determine the activity of selected pathways or regulatory genes per individual sample as implemented in the VIPER (virtual inference of protein activity by enriched regulon analysis) framework (Alvarez 2014). VIPER is capable to account for separate tails of a gene set, e.g. up- and downregulated genes from a signature between conditions, and furthermore, considers the absolute ranking of genes as well by using the aREA algorithm (Alvarez, Shen et al. 2016).

First, raw counts from RNASeq were normalized to account for different library sizes, and the variance was stabilized by transforming the data to $\log_2$ CPM (counts per million) using the *edgeR* (Robinson, McCarthy et al. 2010) R package. Then ssGSEA was carried out using the indicated gene sets and regulons, respectively, and the *viper (eset.filter = FALSE, method = 'scale', min.size = 10)* function from the eponymous R package (Alvarez 2014). VIPER yields normalized enrichment scores (NES) per sample which are normally distributed and based on the assumption that in the null situation, the target genes are uniformly distributed in the gene expression signature.

Differential enrichment analysis of gene sets and regulatory gene activity between conditions was carried out using the *limma* R package (Ritchie, Phipson et al. 2015) and a FDR < 0.1 was considered significant. If only one pathway or signature was compared across conditions, significance was assessed using Welch's *t* test and ANOVA assuming unequal variance as implemented in the R *stats* package, respectively, depending on whether two or more conditions were compared. Single sample enrichment results for select pathways were depicted in a heatmap using the pheatmap R package (Kolde 2015).

2.2.8.7 Differential expression of immunoglobulin heavy and light chain genes

Immunoglobulin (Ig) light (*Igkc, Iglc1, Iglc2, Iglc3, Iglc4*) and heavy (*Igha, Ighm, Ighd, Ighg2b, Ighg3, Ighg1, Ighg2c*) chain genes were examined for their differential expression between WT and tumor tissues from *Vav;L-gp* mice as well as from *CD19;L-gp* mice with PC and Mature phenotypes, respectively. Expression levels are shown as counts CPM on a log2 scale and false discovery rates were retrieved from a linear model fit using the R package *limma* (Ritchie, Phipson et al. 2015).

2.2.9 Statistical analysis

All statistical tests were performed using the statistical functions of Microsoft Excel or GraphPad Prism7. All values are expressed as mean ± SEM, and a *P* value less than 0.05 was considered significant (**P* < 0.05, ***P* < 0.005, ****P* < 0.0005, and *****P* < 0.0001). The 2-tailed Student's *t* test was used to compare quantitative data between two independent samples. When comparing three or more groups, a one-way analysis of variance (ANOVA) statistical test was used to analyze the differences between group means followed by the Tukey's test. Survival data were analyzed using the Mantel-Cox test.

3 Results

This study was conducted in the research group of Prof. Dr. Ulrich Keller at Klinikum rechts der Isar (TUM) in the Department of Internal Medicine III supported by the help from collaboration partners. To warrant a comprehensive understanding of the project, relevant data acquired by other researchers is also shown here; the respective contributions are indicated in the text and/or figure legends.

3.1 Generation of R26 fl rx *L-gp130* mice

To create an *in vivo* tool for aberrant gp130 downstream signaling, a novel mouse model allowing conditional expression of L-gp130 was designed by Frank-Thomas Wunderlich and Mona Al-Maarri at the Center for endocrinology, preventive medicine and diabetes at the Max Planck Institute for Metabolism Research in Cologne, Germany. The ROSA26 knock-in mouse strain, where compound L-gp130 and ZsGreen expression from the CAG promoter is prevented by a loxP- and a rox-flanked stop cassette were generated on the frequently used C57BL/6 background. The strategy to insert the floxed L-gp130-2A-ZsGreen cassette under control of the CAG promotor into the mouse ROSA26 locus is shown in **Figure 10** and further details are stated in the Materials and Methods section. Crossing these mice to deleter Dre mice removed the rox-flanked stop cassette in the germline, thereby generating a Cre-dependent *L-gp130* allele.

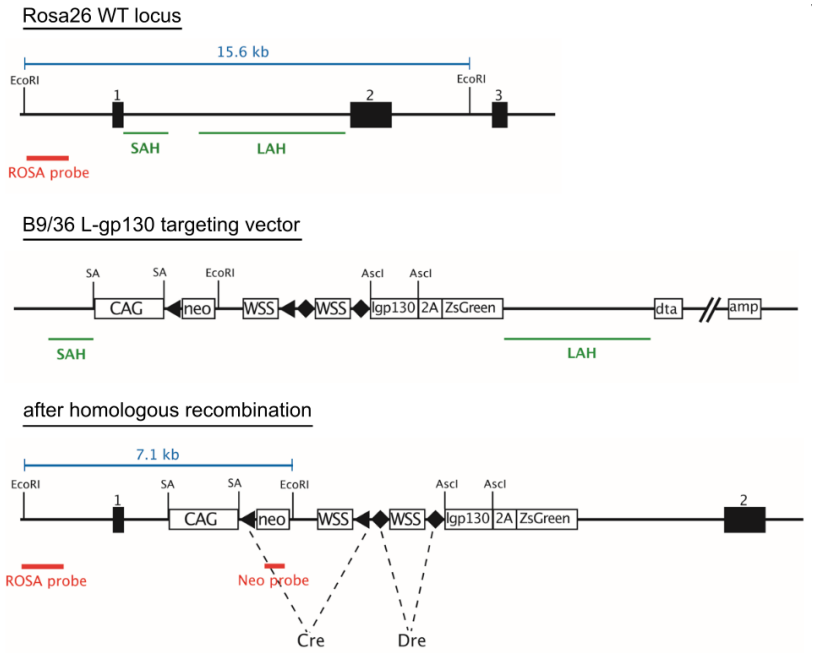

Figure 10: Generation of *R26 fl rx L-gp130* mice. The targeted locus for insertion of the floxed L-gp130-2A-ZsGreen cassette under control of the CAG promotor is depicted before and after homologous recombination. EcoRI sites within the targeted genomic region are indicated. Amp: ampicillin resistance gene, CAG: chicken-beta-actin promotor with CMV (cytomegalovirus)-IE enhancer, DTA: diphtheria toxin fragment A, LAH: long arm of homology, L-gp130: Leucine-zipper + glycoprotein130, loxP: locus of recombination by Cre, neo: neomycin resistance gene, rox: locus of recombination by Dre, SAH: short arm of homology, SV40: Simian Virus 40, WSS: Westphal Stop sequence, ZsGreen: Zoanthus sp. Green fluorescent protein. [Figure 7 was provided by F.-T. Wunderlich and M. Al-Maarri].

To test whether Cre-mediated L-gp130 activation resulted in activation of gp130 downstream signaling, *L-gp130*$^{fl/+}$ (*L-gp*) mice were bred and MEFs were isolated from WT, homozygous, and heterozygous *L-gp130* embryos at E13.5. Homozygous and heterozygous MEFs were then transduced with retrovirus encoding Cre recombinase (Cre-IRES-YFP) while WT MEFs transduced with retrovirus encoding the L-gp130 construct (L-gp130-IRES-GFP) served as a positive control and heterozygous L-gp130 MEFs as well as WT MEFs transduced with the empty vector control MIG (MSCV-IRES-GFP) served as positive controls, respectively. If transduction efficiency was less than 80 %, MEFs were sorted for further RNA and protein isolation. The procedure is depicted in **Figure 11**.

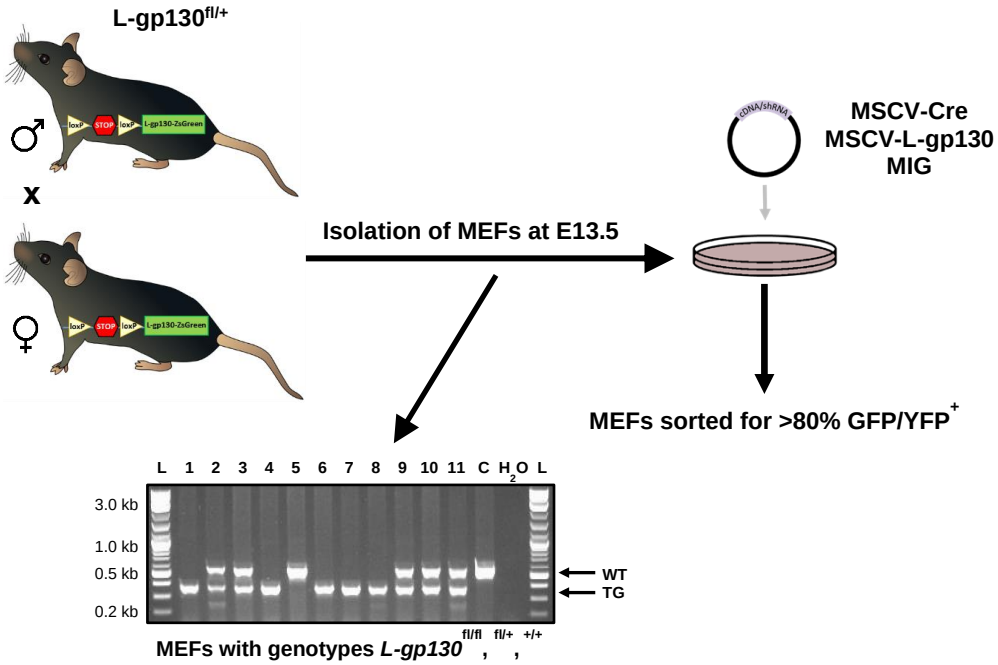

Figure 11: Overview of the experiment. Heterozygous L-gp130 mice were bred and MEFs isolated on E13.5. Genotyping revealed the existence of WT, homozygous, and heterozygous embryos. The WT band was at 570 bp, the transgene (TG) band was at 380 bp. MEFs were transduced with the depicted constructs and, when transduction efficiency was lower 80 %, sorted for GFP/YFP positivity. MEFs: murine embryonic fibroblasts, MIG: MSCV-IRES-GFP, GFP: green fluorescent protein, YFP: yellow fluorescent protein, WT: wildtype, TG: transgene, kb: kilo bases, L: ladder, C: homozygous control.

No dose effect was seen regarding L-gp130 expression from homozygous and heterozygous MEFs respectively. However, expression of L-gp130 seems to result in the suppression of endogenous gp130 transcript levels (**Figure 12A**). Additionally, on protein level, L-gp130 expression led to a slight activation of STAT3 (measured as phospo-STAT3; pSTAT3) in comparison to the negative control (**Figure 12B**). Thus, activation of the transgenic L-gp130 allele in MEFs generated from conditional L-gp130 knock-in mice caused gp130 downstream signaling activity.

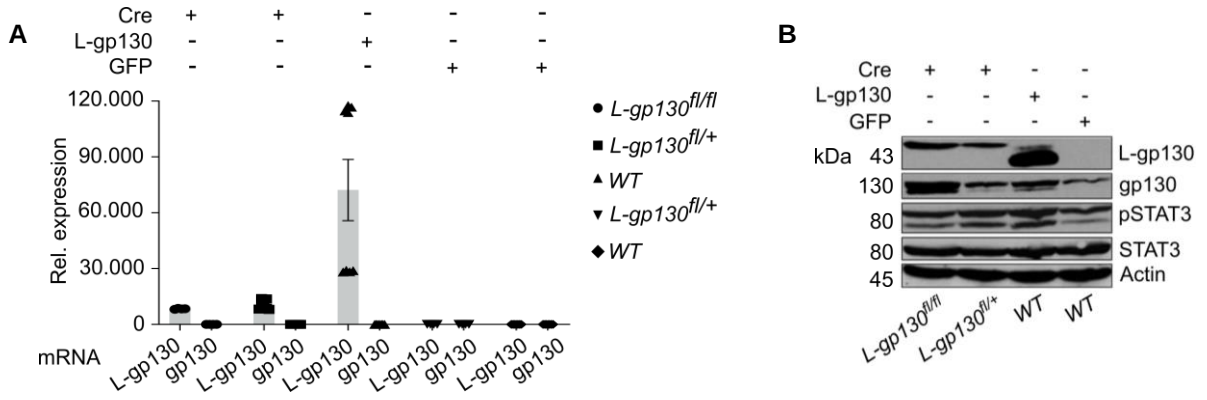

Figure 12: Expression of L-gp130 results in downstream activity. (A) MEFs of the indicated genotypes were transduced with the designated constructs and sorted for GFP/YFP positivity. Depicted is the mRNA expression for L-gp130 and gp130 relative to GAPDH. Shown are means ± SEM. (B) Immunoblot analysis of transduced and sorted MEFs to investigate JAK/STAT3 signaling on protein level. Activation of STAT3 by means of pSTAT3 is shown in MEFs expressing L-gp130 in comparison to control MEFs.

3.2 Gating strategy to define distinct B cell subsets by flow cytometry

For the investigation of consequences of constitutive gp130 activation in B cells, a specific flow cytometry panel was developed to define certain subsets of B cell differentiation. This panel was created based on a previous own study (Afshar-Sterle, Zotos et al. 2014) as well as on other studies focused on certain B cell subsets (Derudder, Cadera et al. 2009, Schmidt, McGinnes et al. 2012, Enders, Short et al. 2014). **Figure 13** depicts the designed gating strategy that was used throughout this study to identify definite B cell subsets using a healthy C57BL/6 mouse as an example. On the basis of this gating, augmentation of distinct B cell populations led to the characterization of different phenotypes upon malignant transformation hereinafter.

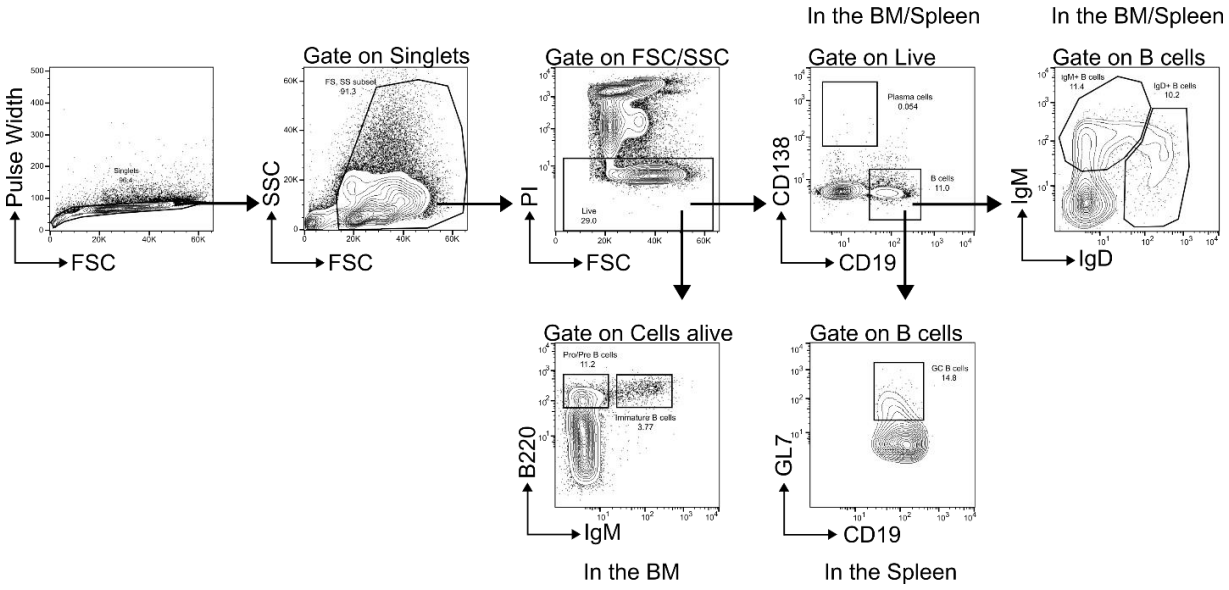

Figure 13: Flow cytometry gating strategy for the definition of distinct B cell subsets. First, doublets were excluded followed by exclusion of debris and red blood cells (RBC) by their cell size and granularity (FSC/SSC). Propidium iodide (PI) was further used to eliminate dead cells. Pro/Pre and immature B cells were defined by gating B220 against IgM. PCs were described as $CD138^{+}CD19^{-}$ while further gating on the $CD19^{+}$ B cell population defined GC B cells via GL7 staining and surface expression of immunoglobulins IgM and IgD revealed the maturity state of B cells. Previous gate is always indicated as is the organ of analysis.

3.3 Constant gp130 signaling promotes B cell differentiation in young *CD19;L-gp* mice

To examine how forced activation of gp130 downstream signaling pathways influences B cell differentiation and/or proliferation, the newly generated *L-gp130*$^{fl/+}$ strain was bred to *CD19Cre*$^{+/-}$ mice. *CD19Cre*$^{+/-}$*;L-gp130*$^{fl/+}$ (*CD19;L-gp*) compound mice and *L-gp130*$^{fl/+}$ (*L-gp*) controls were sacrificed at the age of six weeks and further analyzed. Gross physical examination at this early time point of life did not reveal any obvious pathology, and spleens did not show significant differences in weight between the two groups (**Figure 14A**). Moreover, histological investigations of spleens and BM displayed largely unaltered morphology and cellularity (**Figure 14B**) and absolute white blood cell (WBC) numbers were comparable between groups (**Figure 14C**). Flow cytometric analysis of the T cell and B cell compartments in BM, spleen, and peripheral blood (PB) of these young *CD19;L-gp* and age-matched *L-gp* control mice by means of CD3 and B220 surface staining, revealed no significant changes in T and B cell frequencies (**Figure 14D**). In *CD19;L-gp* mice, L-gp130 and subsequently ZsGreen are expressed upon the pro-B cell stage, where B cells start to express CD19 (Del Nagro, Otero et al. 2005) (see **Figure 9**). Hence, $CD19^{+}$ B cells in BM, spleen, and PB were analyzed for their ZsGreen positivity (**Figure 14E**). Gating on these $ZsGreen^{+}$ B cells and further examination of IgM and IgD surface staining showed a larger fraction of cells expressing IgD in *CD19;L-gp* mice in comparison to *L-gp* controls in all analyzed compartments (**Figure 14F**). This indicates that forced gp130 signaling already promotes B cell differentiation towards a mature stage in young mice. Immunoblot analysis of purified splenic B cells supported this notion by revealing L-gp130 expression and subsequent aberrant STAT3 activation in terms of phospho-STAT3 (pSTAT3) in B cells derived from *CD19;L-gp* mice (**Figure 14G**).

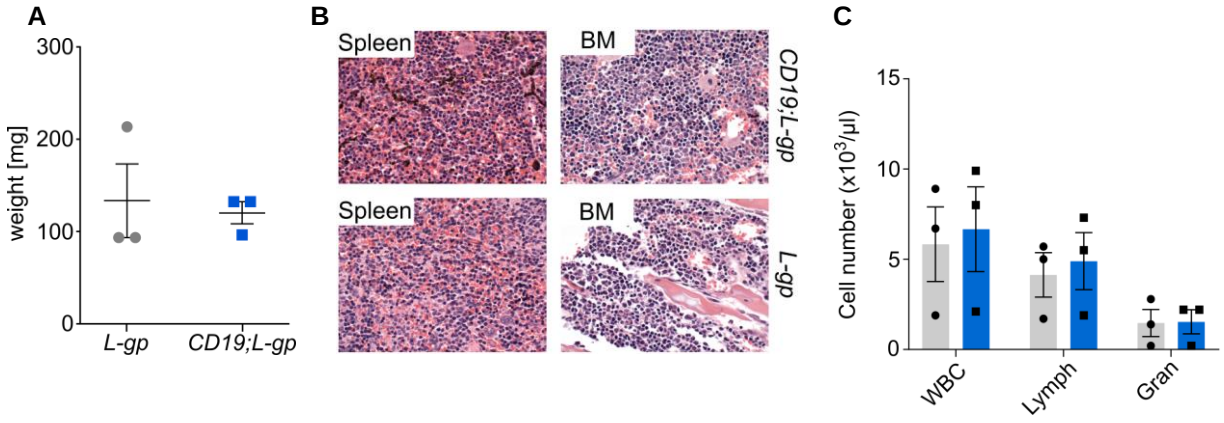

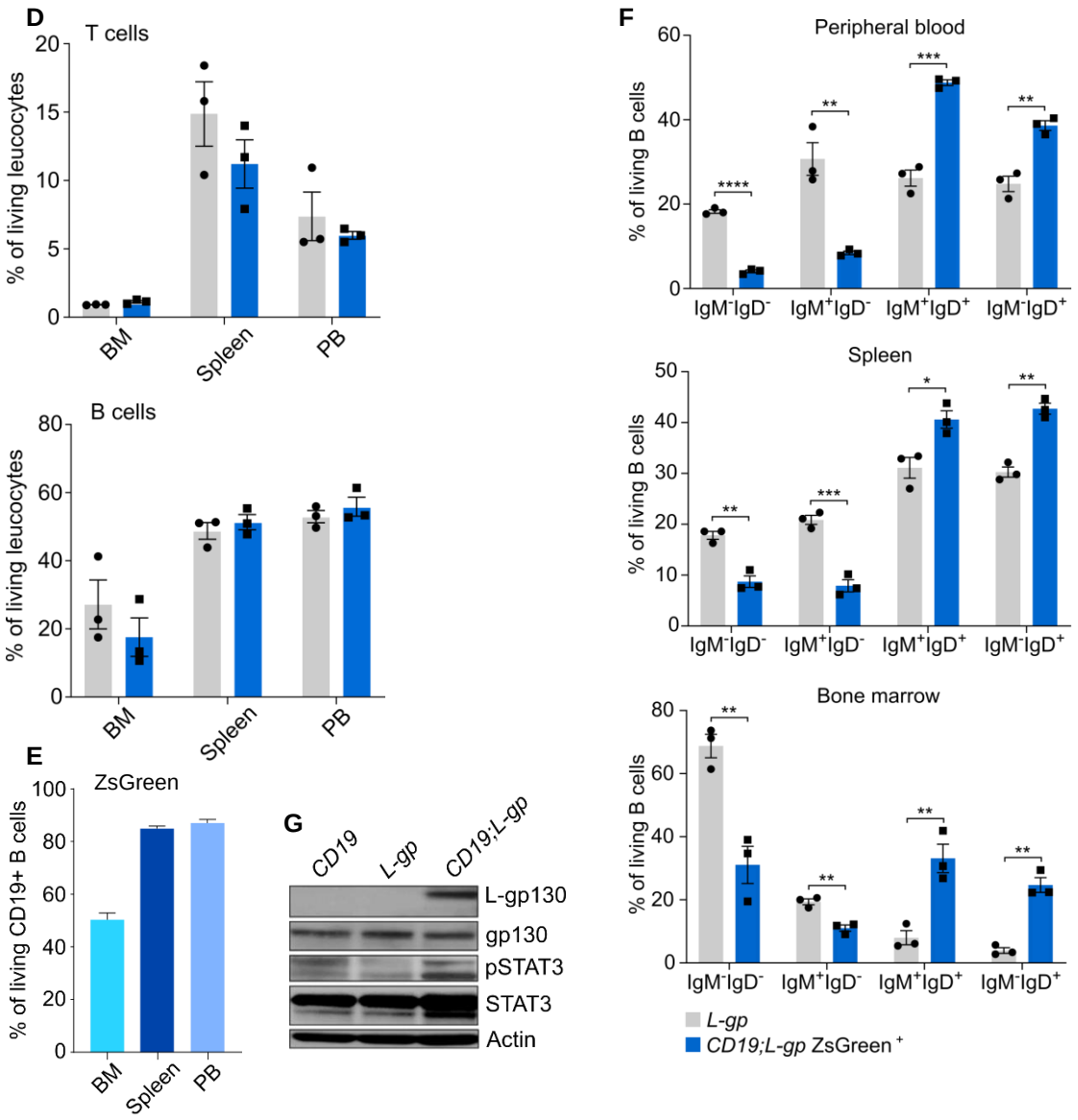

Figure 14: Forced gp130 signaling promotes B cell differentiation in young *CD19;L-gp* mice. Analyses depicted are from six weeks old *CD19;L-gp* mice and age-matched controls. Data shown are from one representative experiment with n = 3 animals per group. Shown are means ± SEM. (A) Spleen weight comparison of *CD19;L-gp* mice (blue) and *L-gp* controls (grey). (B) Histological analysis (H&E staining) of spleen and BM from one representative animal per group. Original magnification, x400. (C) Analysis of PB displaying WBC, lymphocyte (Lymph), and granulocyte (Gran) numbers. (D) T cell (upper panel) and B cell compartments (lower panel) in BM, spleen, and PB were identified by B220 and CD3 surface staining, respectively. (E) ZsGreen positivity of $CD19^+$ B cells in BM, spleen, and PB. (F) B cells in PB (upper panel), spleen (middle panel), and BM (lower panel) were analyzed for IgD^+ and IgM^+ surface expression. B cells in *CD19;L-gp* mice were $ZsGreen^+$, * $P < 0.05$, ** $P < 0.005$, *** $P < 0.0005$ and **** $P < 0.0001$ as determined by the Student's *t* test. (G) Immunoblot analysis of $CD19^+$ splenic B cells with the indicated antibodies. [Histology data from (B) was provided by K. Steiger and L. Quintanilla-Martinez].

Cγ1Cre$^{+/-}$*;L-gp130*$^{fl/+}$ (*Cγ1;L-gp*) as well as *Blimp1Cre*$^{+/-}$*;L-gp130*$^{fl/+}$ (*Blimp1;L-gp*) mice were also examined at the age of six weeks. Histological investigations of spleens and BM displayed unaltered morphology and cellularity in comparison to *L-gp* controls (**Figure 15A**) and also spleen size and weight were comparable between groups (**Figure 15B**). However, absolute WBC numbers differed substantially

with young *Blimp1;L-gp* mice already showing elevated levels when assessed in the PB at this early time point of analysis (**Figure 15C**). Mice of this genotype also presented with slight lymphadenopathy (**Figure 15C**). In flow cytometric analysis of *Cγ1;L-gp* mice, hardly any ZsGreen^{+} cells were seen and therefore gating on this population and subsequent further analysis was not possible. In *Blimp1;L-gp*, in contrast, a small ZsGreen^{+} population was seen. Gating on these cells, however, revealed the activation of gp130 signaling not only in the B lineage but also in T cells and granulocytes (data not shown).

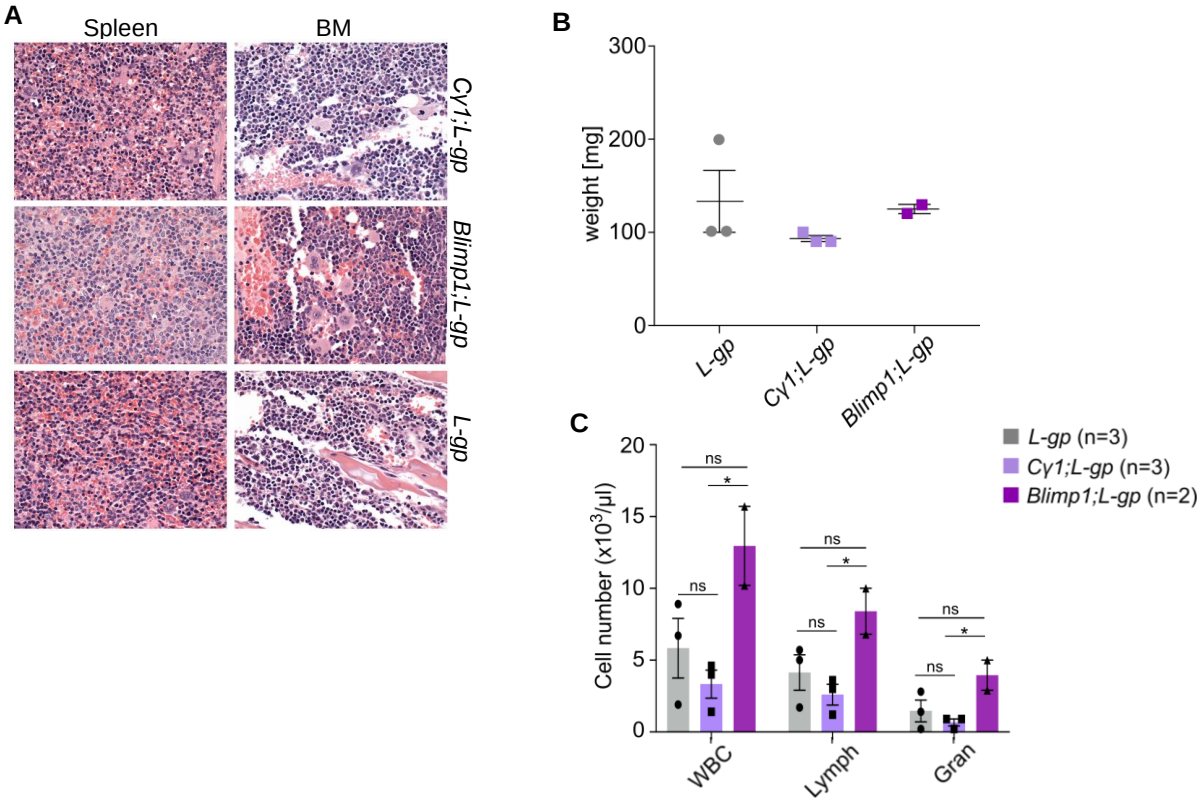

Figure 15: Forced gp130 signaling alters total WBC numbers in young mice. Analyses depicted are from six weeks old *Cγ1;L-gp* and *Blimp1;L-gp* mice compared to age-matched *L-gp* controls. Data shown is from one representative experiment with n = 2 – 3 animals per group. Shown are means ± SEM. (A) Histological analysis (H&E staining) of spleen and BM from one representative animal per group. Original magnification, x400. (B) Spleen weight comparison of *Cγ1;L-gp* and *Blimp1;L-gp* with *L-gp* controls revealing no significance as analyzed by the ANOVA test followed by the Tukey's test. (C) Analysis of PB displaying absolute numbers for WBC, lymphocytes (Lymph), and granulocytes (Gran) in the three cohorts. Significance was assessed by ANOVA testing followed by the Tukey's test. [Histology data from (A) was provided by K. Steiger and L. Quintanilla-Martinez].

3.4 Establishment of the Lgp-130 signature

Mining publicly available data for expression of STAT3 target genes during B cell development, the highest expression was found in plasmablasts and PCs in accordance with elevated STAT3 activity whereas STAT3 expression itself diminished during late B cell differentiation. IL-6/JAK/STAT3 signaling activity appeared to be highest in PCs as well as memory B cells (**Figure 16A**).

In order to investigate differences in the B cell compartment, a global gene expression analysis was performed on splenic B cells obtained from young *CD19;L-gp* and control mice via RNA-sequencing (RNASeq) followed by a principal component analysis (PCA). This approach revealed a different cluster of L-gp130 expressing B cells and control B cells (**Figure 16B, C**). A significant activation of IL-6/JAK/STAT3, PI3K/AKT/MTOR, WNT, MYC, as well as BCR and NF-kappaB signaling was seen in B cells form *CD19;L-gp* mice, being defined as the L-gp130 signature (**Figure 16D**, see methods section for further details). These results thus point to an activation of several pathways downstream of gp130 signaling in B cells of young *CD19;L-gp* mice associated with STAT3 and B cell proliferation as well as with differentiation and BCR signaling activity. Examining distinct stages during late B cell differentiation in humans, the described L-gp130 signature was found to be most prominent in GC B cells (**Figure 16E**). Isolated RNA samples were handed over to Rupert Öllinger at TranslaTUM for library preparation and RNASeq. Subsequent analysis of raw data was done in collaboration with Hans Carlo Maurer at Klinikum rechts der Isar (TUM), Department of Internal Medicine II.

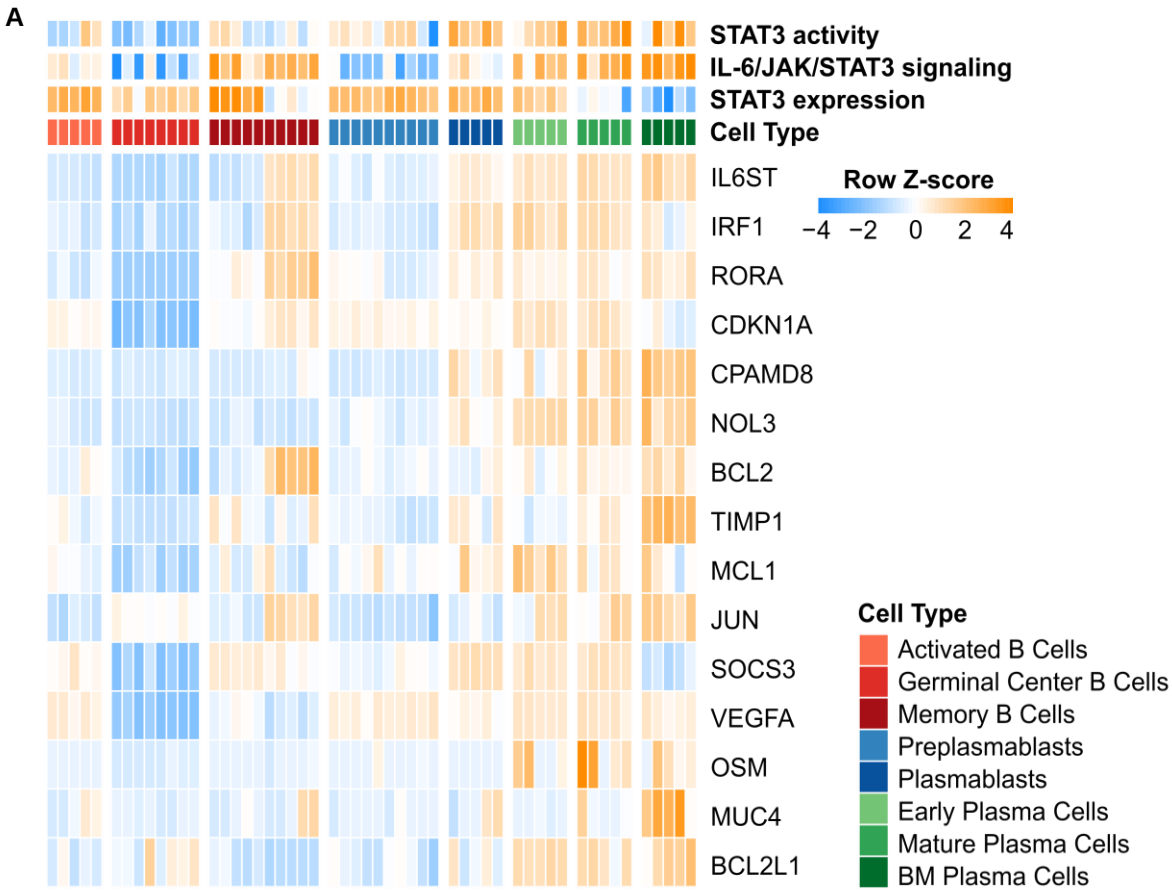

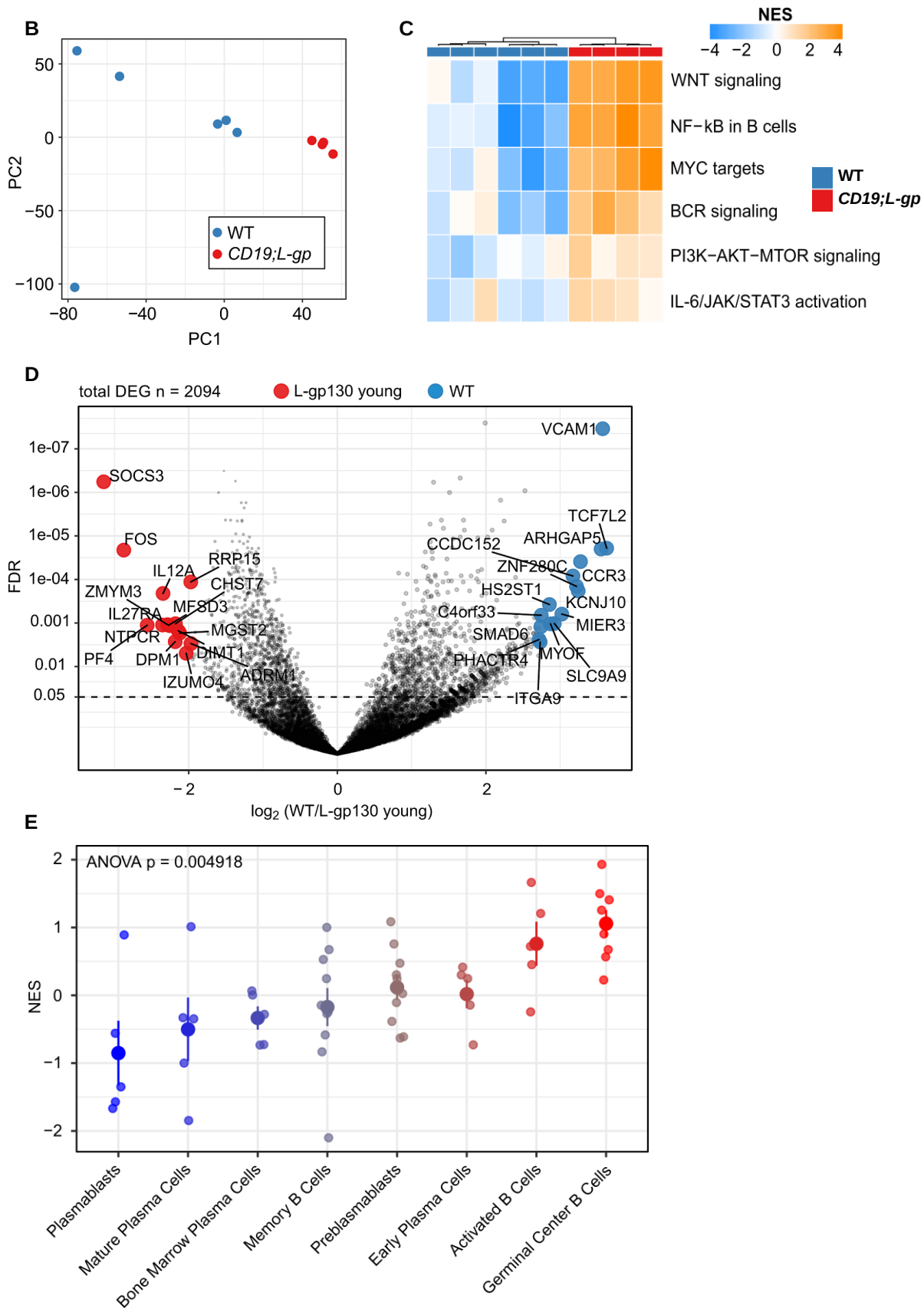
B
PC2
PC1
WT
CD19;L-gp
C
NES
WNT signaling
NF−kB in B cells
MYC targets
BCR signaling
PI3K−AKT−MTOR signaling
IL-6/JAK/STAT3 activation
WT
CD19;L-gp
D
total DEG n = 2094
L-gp130 young
WT
FDR
log2 (WT/L-gp130 young)
VCAM1
SOCS3
FOS
IL12A
RRP15
CHST7
ZMYM3
MFSD3
IL27RA
MGST2
NTPCR
PF4
DPM1
DIMT1
IZUMO4
ADRM1
TCF7L2
CCDC152
ARHGAP5
ZNF280C
CCR3
HS2ST1
KCNJ10
C4orf33
MIER3
SMAD6
MYOF
PHACTR4
SLC9A9
ITGA9
E
ANOVA p = 0.004918
NES
Plasmablasts
Mature Plasma Cells
Bone Marrow Plasma Cells
Memory B Cells
Preblasmablasts
Early Plasma Cells
Activated B Cells
Germinal Center B Cells

Figure 16: Expression and activity of STAT3 by hierarchical cluster analysis. (A) Heatmap illustrating the expression of STAT3 target genes among various stages of B cell development. The upper panel depicts the respective cell type as well as results for mere STAT3 expression (3rd row from top) as opposed to STAT3 activity and IL-6/JAK/STAT3 pathway activity (top and 2nd row from top, respectively) determined by ssGSEA. (B) Principal component analysis (PCA) of RNASeq gene expression profiles from $CD19^+$ splenocytes of young WT (blue) and *CD19;L-gp* (red) mice, respectively. (C) Volcano plot illustrating results from a differential gene expression analysis between $CD19^+$ splenocytes isolated from six weeks old WT and *CD19;L-gp* mice. The top 15 up- (blue) and downregulated (red) genes are labeled. Positive log_2 fold changes indicate higher levels in WT splenocytes. A total of 2094 differentially expressed genes (DEG) were identified at an FDR <= 0.05. (D) Heatmap depicting single sample gene set enrichment results as normalized enrichment scores (NES) for the indicated pathways and their distribution between $CD19^+$ splenocytes isolated from WT (blue) and *CD19;L-gp* (red) mice. These characteristics in young *CD19;L-gp* are defined as the Lgp130 signature. All pathways shown are differentially enriched at an FDR < 0.1. (E) ssGSEA results of the L-gp130 signature among various stages of B cell development in humans with highest enrichment results in activated B cells and GC B cells. [Data analysis was done by H.C. Maurer].

3.5 Activation of gp130 signaling in B cells leads to mature B cell malignancies

Having seen that B cell-specific activation of gp130/JAK/STAT3 signaling led to an increased percentage of mature IgD^+ B cells in young *CD19;L-gp* mice, an aging cohort of these mice was monitored for possible consequences of B cell-targeted constitutive gp130 signaling activity. *CD19;L-gp* showed deterioration of health with onset of a potential disease starting at 30 days of age with a medium survival of 151 days and were thus sacrificed. *$CD19Cre^{+/-}$* (*CD19*) as well as *L-gp* control mice did not develop signs of malignancy within the observed time frame (**Figure 17A**). The visible disease pattern comprised reduced activity, extended bellies due to mesenteric tumors with ascites (**Figure 17B**) occasionally accompanied by splenomegaly (**Figure 17C**), enlarged lymph nodes (LNs), and paralyzed hind limbs indicative of spinal affection. To investigate the cause of illness, *CD19;L-gp* mice underwent whole-body necropsy and extended flow cytometric analysis of the hematopoietic organs (gating strategies shown in **Figure 13**). B cell-specific activation of gp130 downstream signaling resulted in B cell malignancies with a penetrance of 100 %. Three different subtypes of $ZsGreen^+$ B cell disorders were identified in this cohort as defined by flow cytometry. The first subgroup was identified as a plasma cell (PC) disease characterized by the augmented presence of $CD19^-CD138^+$ cells. The second subtype represented $CD19^+$ B cell tumors characterized by strong expression of IgD and was thus termed mature B cell lymphoma (Mature). Only a minor portion of sick animals died from a third condition with accumulation of $B220^+IgM^+$ B cells and was therefore identified as a Pro-Pre/Immature phenotype (**Figure 17D, E**). Comparing survival of mice succumbing to either the PC or the Mature phenotype, no significant differences were seen with median survivals accounting to 151 days in both groups (**Figure 17F**). As already described in the analysis of MEFs heterozygous and homozygous for the L-gp130 allele (**Figure 11A, B**), a dose effect was again not observed in heterozygous (*$CD19;L\text{-}gp^{fl/+}$*) compared to homozygous (*$CD19;L\text{-}gp^{fl/fl}$*) mice as median survival did not significantly differ between both groups (151 days and 142 days, respectively, **Figure 17G**). Flow cytometric analysis revealed that mice homozygous for the L-gp130 allele also died from mesenteric tumors of the Mature and PC phenotypes (data not shown). Further testing of homozygous animals was not performed and all following data displayed in this study originates from analyses on mice heterozygous for the L-gp130 allele.

The results seen in flow cytometry on *CD19;L-gp* mice were confirmed by histological and IHC analyses, where the tumors arising could also be divided into three groups. Importantly, in tumors of all subtypes medium-sized tumor cells with abundant pale cytoplasm, eccentric nucleus, inconspicuous nucleolus, and nuclear pleomorphism were present. These cells showed $CD138^{+}$ staining thus identifying them as malignant PCs (**Figure 17H**). This indicated a possible continuum within the L-gp130-induced disease with malignant transformation occurring at various stages of B cell development. The transcription factor Pax5 is expressed in B cells from the pro- to the mature B cell stage but is absent in terminally differentiated PCs (Barberis, Widenhorn et al. 1990). IHC revealed strong Pax5 staining in the Pro-Pre/Immature and also in the Mature phenotype whereas tumors of the PC phenotype lacked expression of this transcription factor (**Figure 17H**). In line with results from flow cytometry (**Figure 17D**), staining for IgM was seen in the Pro-Pre/Immature phenotype but barely present in the Mature as well as PC phenotype (**Figure 17H**). Malignant PCs mainly located to the BM (average infiltration 29 %) and the mesenteric tumors (average infiltration 43 %) while the spleen was less infiltrated by PCs (average 2 %) (**Figure 17I**, upper panel). On the contrary, malignant mature B cells predominantly infiltrated spleen and BM (average 83 % and 79 %, respectively) and to a lesser extend located to the mesenteric tumors (average infiltration 43 %) (**Figure 17I**, lower panel). The existence of an M-protein in the serum is a characteristic in over 90 % of MM patients (International Myeloma Working 2003). Therefore, the serum of diseased mice underwent testing for presence of this feature. While 31.3 % of mice assigned to the PC group showed an M-protein, 55.3 % of animals with a Mature phenotype exhibited monoclonal gammopathy (**Figure 17J**). In accordance with clonality analysis of mesenteric nodal tumors by VDJ-PCR revealing that the majority were monoclonal (**Figure 17K**), analysis of Ig serum levels showed frequently elevated IgG levels in mice of both phenotypes (**Figure 17M**, lower panel). However, these differences were not statistically significant. Variances were also observed when performing RNASeq analysis for expression of Ig heavy constant gamma chains that encode for the IgG isotypes (**Figure 17L**, upper panel). In addition, pronounced changes were similarly seen for expression of the remaining heavy chains defining the IgA, IgD, and IgM isotypes (**Figure 17L,** upper panel). Light chain constant region gene expression revealed a shift toward higher κ and lower λ gene expression in the *CD19;L-gp* mice of both phenotypes in comparison to WT controls (**Figure 17L,** lower panel). Summarizing, activation of constitutive gp130 signaling very early during B cell development drives the establishment of mature B cell neoplasms and plasma cell disorders with a penetrance of 100 %.

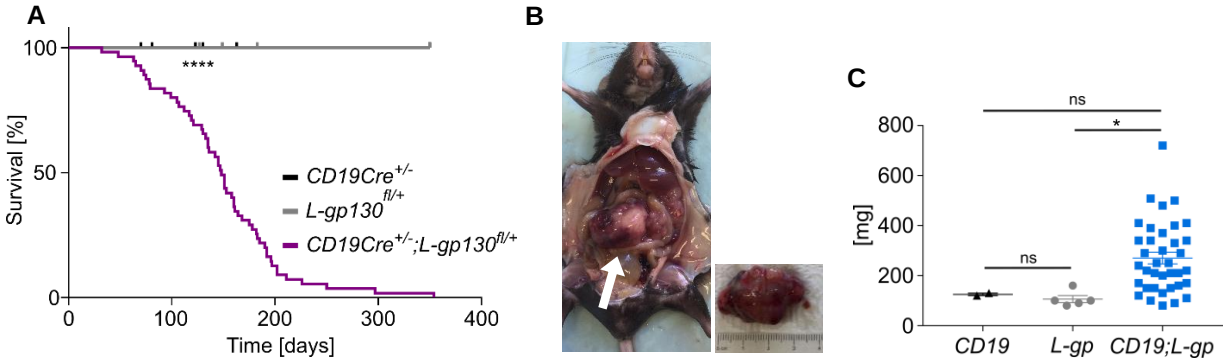

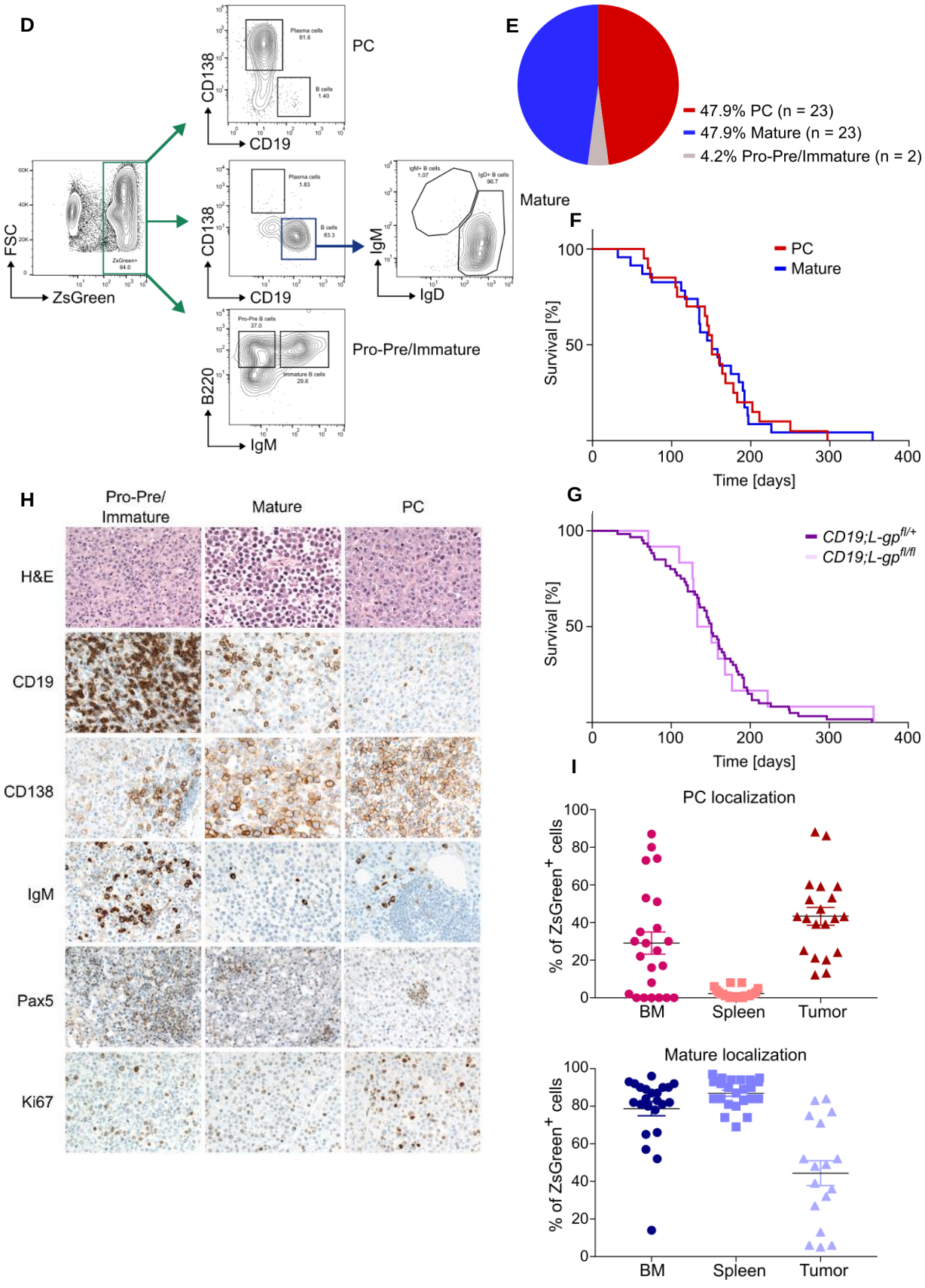
D
PC
CD138
CD19
Plasma cells
81.6
B cells
1.40
FSC
ZsGreen
ZsGreen+
84.0
Plasma cells
1.83
B cells
83.3
IgM
IgD
IgM+ B cells
1.07
IgD+ B cells
96.7
Mature
Pro-Pre B cells
37.0
Immature B cells
29.6
B220
Pro-Pre/Immature
E
47.9% PC (n = 23)
47.9% Mature (n = 23)
4.2% Pro-Pre/Immature (n = 2)
F
PC
Mature
Survival [%]
Time [days]
G
CD19;L-gp^fl/+
CD19;L-gp^fl/fl
Survival [%]
Time [days]
H
Pro-Pre/ Immature
Mature
PC
H&E
CD19
CD138
IgM
Pax5
Ki67
I
PC localization
% of ZsGreen+ cells
BM
Spleen
Tumor
Mature localization
% of ZsGreen+ cells
BM
Spleen
Tumor

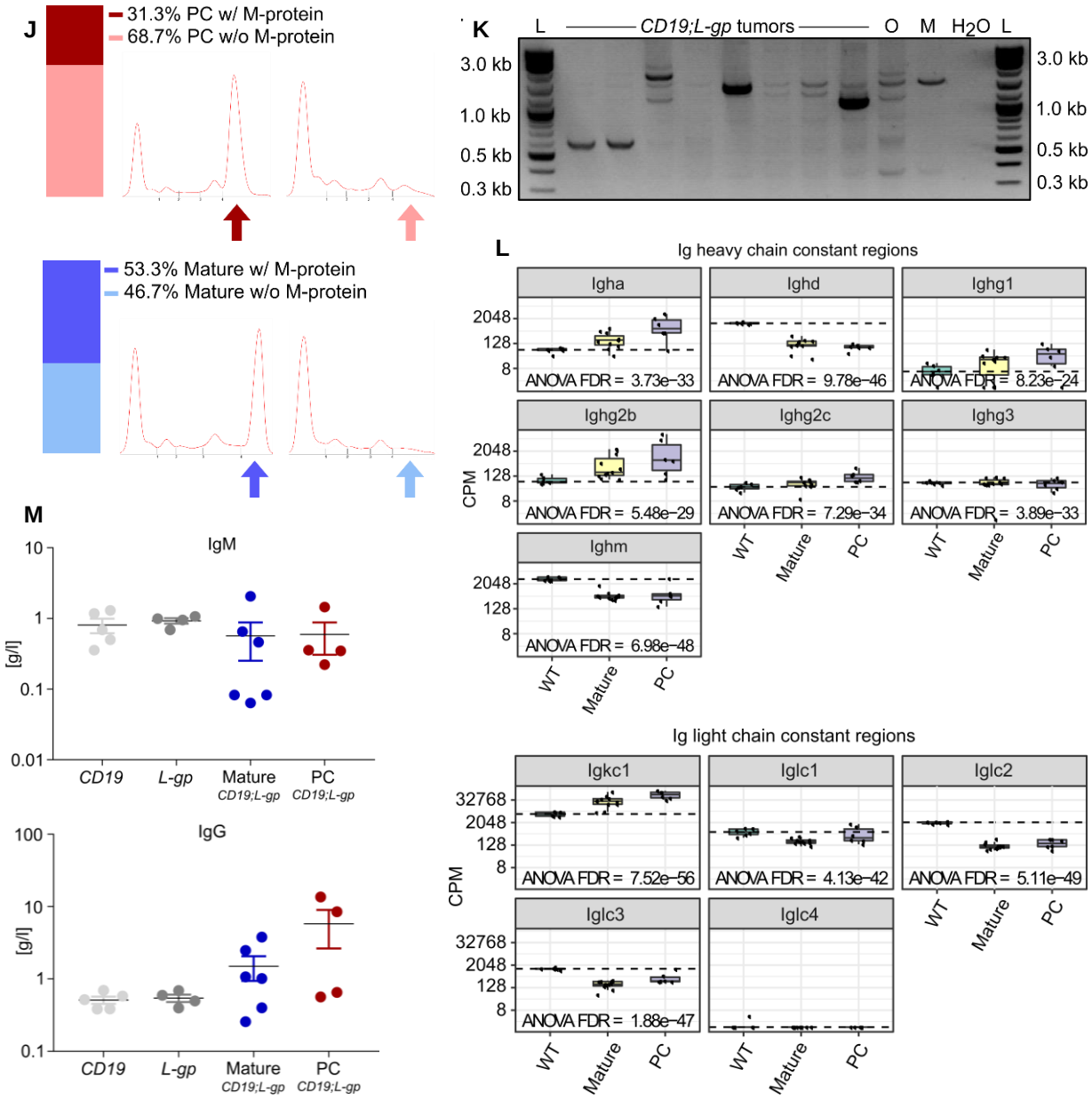

Figure 17: Activation of gp130 signaling in B cells results in B cell malignancies. (A) Kaplan-Meier curve showing survival of *CD19;L-gp* (n = 60) in comparison to *CD19* (n = 17) and *L-gp* (n = 18) controls. The median survival was 151 days. (****, P < 0.0001, Mantel-Cox test). (B) 77 % of diseased *CD19;L-gp* animals presented with mesenteric tumors. (C) A large proportion of diseased *CD19;L-gp* developed splenomegaly. Significance in comparison to controls was determined via the ANOVA test followed by the Tukey's test. (D) Flow cytometric gating strategy applied on tumors revealed three B cell phenotypes arising in *CD19;L-gp* mice. After exclusion of PI^+ dead cells, the gate was set for $ZsGreen^+$ cells to include all cells with activated JAK/STAT3 signaling. The first group was defined by $CD19^-CD138^+$ staining as a plasma cell (PC) phenotype, the second as a $CD19^+IgD^+$ mature B cell (Mature) phenotype, and the third group as a Pro-Pre/Immature $B220^+IgM^+$ phenotype. (E) Distribution of the spectrum of B cell malignancies in diseased *CD19;L-gp* as determined by flow cytometry. The majority of diseased mice accounted for the PC or Mature phenotype while two animals died of a Pro-Pre/Immature B cell phenotype. (F) Kaplan-Meier curve depicting survival comparison of mice of the PC and Mature phenotypes. No significant differences were seen with median survival accounting for 151 days for both phenotypes. (G) Kaplan-Meier curve depicting that median survival of heterozygous (*CD19;L-gp$^{fl/+}$*) and homozygous (*CD19;L-gp$^{fl/fl}$*) mice did not differ significantly. (H) Histological and IHC analyses of one representative mesenteric tumor of the Pro-Pre/Immature (left), Mature (middle), and PC (right) phenotype arising in *CD19;L-gp* mice. $CD138^+$ cells were present in all phenotypes. Original magnification, x400. (I) Extent of infiltration of tumor cells of the PC phenotype (upper panel) and Mature phenotype (lower panel) into BM, spleen, and mesenteric nodal tumor of diseased mice as assessed

by flow cytometry. 23 mice per phenotype were analyzed. (J) Serum protein electrophoresis from representative diseased *CD19;L-gp* mice of the PC phenotype (upper row) and the Mature phenotype (lower row). The arrows point towards the gamma fraction indicating whether the animals presented with (w/) or without (w/o) an M-protein at time point of analysis. A total of 31 mice was analyzed. (K) Clonality analysis from CD138$^+$ isolated tumor DNA of *CD19;L-gp* mice. Most tumors were monoclonal and only some represented an oligoclonal disease. O: oligoclonal control, M: monoclonal control, L: ladder. (L) RNASeq gene expression profiles of Ig heavy (upper panel) and light (lower panel) chain constant regions obtained from mesenteric nodal tumor material of *CD19;L-gp* of the Mature and PC phenotypes in comparison to CD19+ isolated WT splenocytes. CPM: counts per million, FDR: false discovery rate. Significance was evaluated by the ANOVA test with subsequent assessment of the FDR. (L) Ig levels, assessed by ELISA, from serum of sick *CD19;L-gp* mice of the Mature (n = 6) and PC (n = 4) phenotype in comparison to *CD19* (n = 5) and *L-gp* (n = 4) controls. Differences in IgM (upper panel) and IgG levels (lower panel) between groups were considered not significant as determined by the ANOVA test followed by the Tukey's test. Shown are means ± SEM. [Histology and IHC data from (H) were provided by K. Steiger and L. Quintanilla-Martinez, Serum electrophoresis from (J) was performed by M. Thaler, and Data analysis from (L) was done by H.C. Maurer].

3.6 Serial transplantability of the disease

Tumor cells from sick *CD19;L-gp* mice with a CD138$^+$ PC phenotype were serially transplanted into sublethally irradiated syngeneic recipients. The latency of disease onset in these animals was reduced to a median of 116 days (**Figure 18A**). Full necropsy of mice revealed the reestablishment of tumor formation seen in the donor mice with the existence of CD138$^+$ PCs (**Figure 18B**). Therefore, the disease from *CD19;L-gp* donor mice was serially transplantable with reproduction of the phenotype.

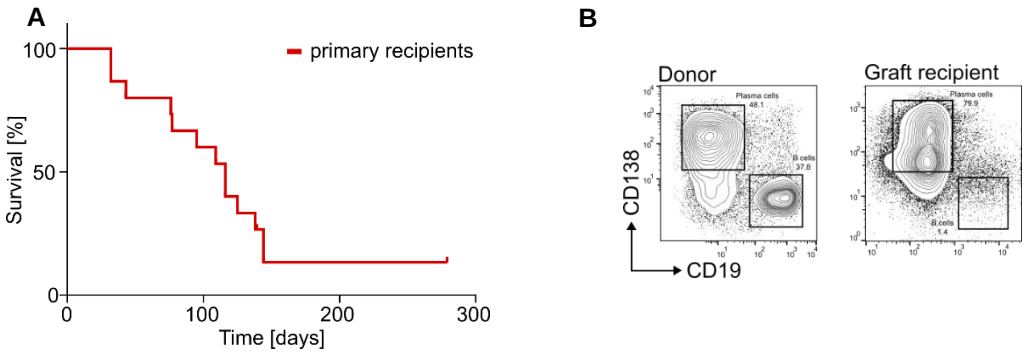

Figure 18: Serial transplantation of cells from *CD19;L-gp* tumors results in reestablishment of the disease. (A) Kaplan-Meier curve depicting survival of serially transplanted animals. The median survival was 116 days. (B) FACS plots showing the CD138$^+$ phenotype in donor and graft recipient. Results are representative for five independent experiments with n = 3 recipients per primary tumor.

3.7 Activation of gp130 during or post the GC reaction results in delayed tumor formation

Activating L-gp130 in B cells using *CD19Cre* led to the development of mature B cell lymphomas and PC neoplasms. As MM is thought to arise from malignantly transformed post-GC PCs (Hallek, Bergsagel et al. 1998), two additional Cre transgenic strains leading to gp130/JAK/STAT3 activation in late B cells were included in this study to identify the precise role of this pathway for B cell transformation. *Cγ1Cre* mice allow conditional gene activation within the GC (Casola, Cattoretti et al. 2006) and *PRDM1Cre* (herein referred to as *Blimp1Cre*) leads to signaling initiation when B cells leave the GC to differentiate

towards the PC stage (Kallies, Hasbold et al. 2007). As previously seen in *CD19;L-gp*, both *Cγ1Cre*$^{+/-}$*;L-gp130*$^{fl/+}$ (*Cγ1;L-gp*) as well as *Blimp1Cre*$^{+/-}$*;L-gp130*$^{fl/+}$ (*Blimp1;L-gp*) mice frequently developed expanded bellies as a result of mesenteric tumors with ascites and showed general signs of a consuming disease. The median survival for *Cγ1;L-gp* accounted to 629 days (**Figure 19A**), whereas *Blimp1;L-gp* died significantly earlier, showing a median survival of 309 days (**Figure 19B**). In addition to the PC and Mature phenotype identified in diseased *CD19;L-gp* mice, a third phenotype was seen in *Cγ1;L-gp* animals characterized by an accumulation of CD19^{+}GL7^{+} GC B cells. This subtype was thus termed GC (**Figure 19C**, right panel). **Figure 19E** depicts the distribution of the three different phenotypes within the *Cγ1;L-gp* cohort. Diseased *Blimp1;L-gp* mice presented with the PC and Mature phenotypes, affirming that B cell transformation occurred subsequent to the GC reaction upon activation of gp130/JAK/STAT3 signaling (**Figure 19D, F**). Histological and IHC analyses of tumors from diseased *Cγ1;L-gp* and *Blimp1;L-gp* mice with the PC phenotype revealed high infiltration of PCs with abundant pale cytoplasm, eccentric nucleus, inconspicuous nucleolus, nuclear pleomorphism, and positive CD138^{+} staining whereas the infiltration of these CD138^{+} PCs in tumors from *Cγ1;L-gp* mice with a GC phenotype was considerably less (**Figure 19G**). Several of the mice of both genotypes showed the existence of an M-protein in the serum indicating Ig production (**Figure 19H, I**). Consequently, significantly elevated IgG levels in *Cγ1;L-gp* mice were seen compared to *L-gp* controls whereas IgM levels were equal between groups (**Figure 19J**). These results confirm the development of terminally differentiated B cell cancers by oncogenic gp130 activation upon activation at the GC or post-GC stage of B cell development.

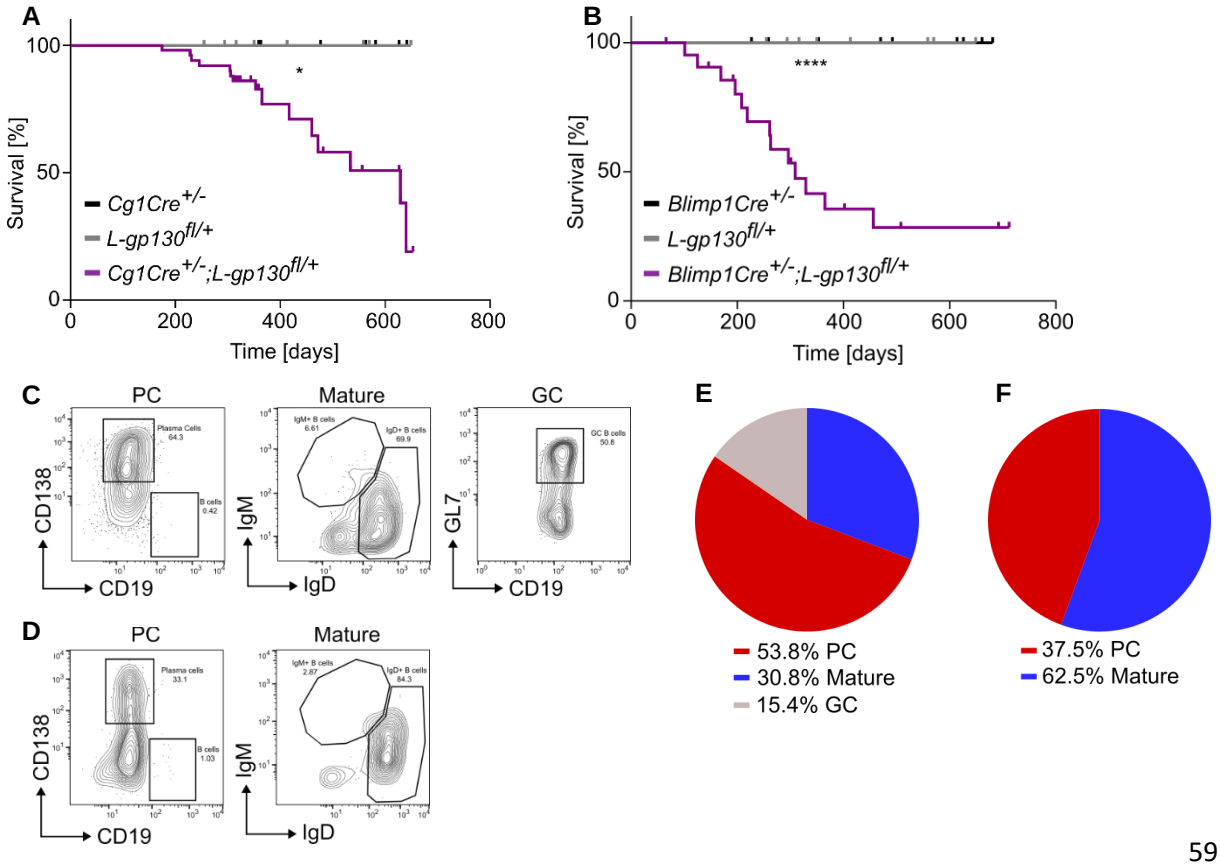

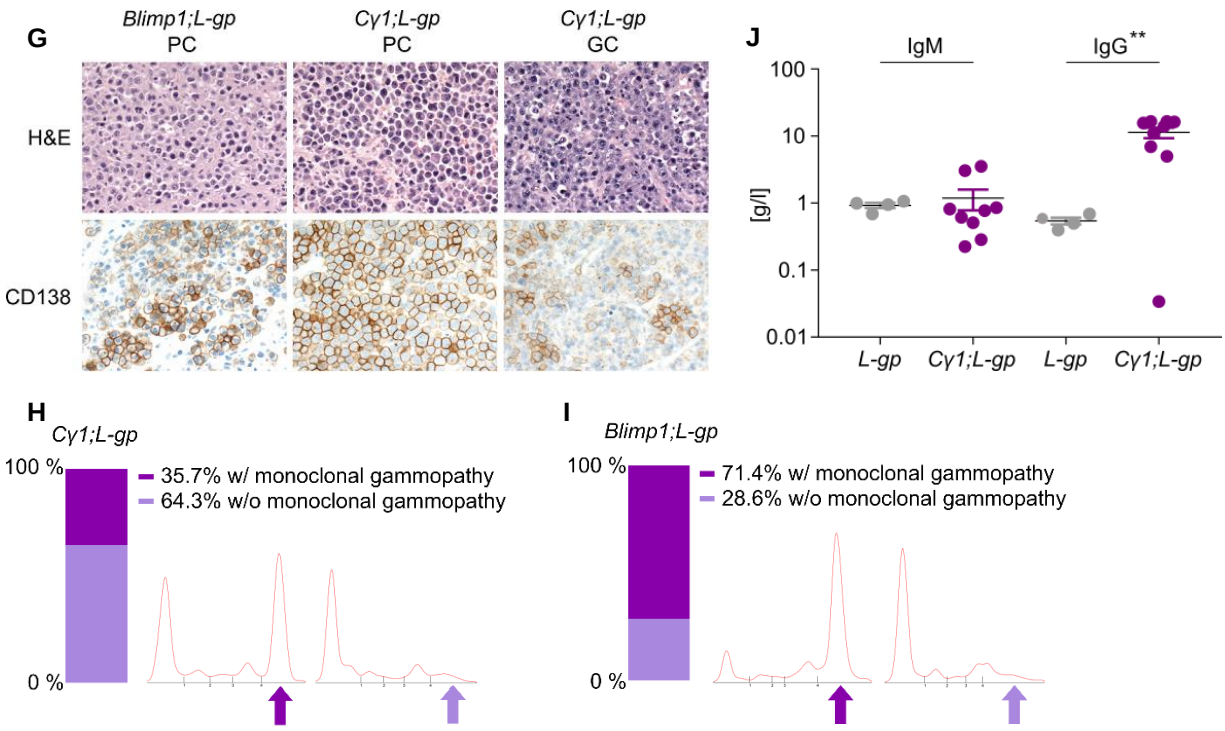

Figure 19: Gp130 activation during or post GC B cell differentiation results in lymphoma and plasmacytoma. (A) Kaplan-Meier curve showing survival of *Cγ1;L-gp* (n = 50) in comparison to *Cγ1* (n = 7) and *L-gp* (n = 12) controls. The median survival of *Cγ1;L-gp* compound mice was 629 days. Controls did not show any signs of malignancy during the observed time frame (*, P = 0.0109, Mantel-Cox test). (B) Kaplan-Meier curve showing survival of *Blimp1;L-gp* (n = 22) in comparison to *Blimp1* (n = 11) and *L-gp* (n = 12) controls. The median survival of *Blimp1;L-gp* mice was 309 days. Controls did not show any signs of disease during the observed time frame (****, P < 0.0001, Mantel-Cox test). (C) Flow cytometric analysis from tumors of diseased *Cγ1;L-gp* mice identified three phenotypes: $CD19^{-}CD138^{+}$ (PC, left), $CD19^{+}IgD^{+}$ mature B cell (Mature, middle), and $CD19^{+}GL7^{+}$ GC B cells (GC, right). Shown is the analysis of tumor material from one representative animal per phenotype. At least three mice per group were analyzed. (D) Flow cytometric analysis from diseased *Blimp1;L-gp* mice identified a $CD19^{-}CD138^{+}$ (PC, left) and a $CD19^{+}IgD^{+}$ (Mature, right) phenotype. Shown is the analysis of tumor material from one representative animal per phenotype. At least three mice per phenotype were analyzed. (E) Distribution of the three types of B cell malignancies in diseased *Cγ1;L-gp*. (F) Distribution of the two types of B cell malignancies in diseased *Blimp1;L-gp*. (G) Histological and IHC analysis of one representative tumor from *Blimp1;L-gp* (left) and *Cγ1;L-gp* (middle and right) mice. Tumors with the PC phenotype showed high infiltration of malignant cells positive for CD138 (left and middle). The GC phenotype displayed only minor infiltration of $CD138^{+}$ cells (right). Original magnification, x400. (H, I) Serum protein electrophoresis from representative diseased *Cg1;L-gp* and *Blimp1;L-gp* mice. The bars indicate the percentage of mice with (w/) or without (w/o) gammopathy. At least eight mice per genotype were analyzed. (J) Ig levels, assessed by ELISA, from serum of diseased *Cg1;L-gp* mice in comparison to *L-gp* controls. The outlier presenting with low IgG level did also not show evidence of monoclonal gammopathy as assessed by serum protein electrophoresis. Shown are means ± SEM. (** P = 0.0051, by the student's t test). [Histology and IHC data from (G) were provided by K. Steiger and L. Quintanilla-Martinez, Serum electrophoresis from (H, I) was performed by M. Thaler].

3.8 Immunization of *Cγ1;L-gp* mice leads to the formation of a GC but does not promote tumor development

The absent $ZsGreen^{+}$ population in young (chapter 3.3) as well as the late disease onset in aged *Cγ1;L-gp* mice (chapter 3.7) led to the assumption that B cells of these mice had only infrequently undergone the GC reaction. Intravenous (i.v.) sheep red blood cell (SRBC) injection has been shown to initiate a

GC reaction (Zhang, Tech et al. 2018). To induce mature B cells to enter the GC and therefore activate *Cγ1*-dependent gp130 signaling, *Cγ1;L-gp* mice were immunized i.v. with SRBCs and analyzed eleven days thereafter as the GC reaction usually peaks at around 10 – 12 days after immunization (Calame 2001). SRBC injection resulted in an increased $CD19^{+}GL7^{+}$ GC B cell population in the spleen of both, *Cγ1;L-gp* as well as *L-gp* control animals (**Figure 20A**). Nevertheless, an accumulation of $CD19^{+}CD138^{+}$ plasmablasts in the BM was only seen in immunized *Cγ1;L-gp* but not *L-gp* controls (**Figure 20B**). However, immunization of *Cγ1;L-gp* with SRBC did not promote immediate tumor development. These data together with the results presented in the previous section indicate that enforced gp130 downstream signaling activity in GC B cells is sufficient to cause malignant transformation but is not further amplified by SRBC immunization.

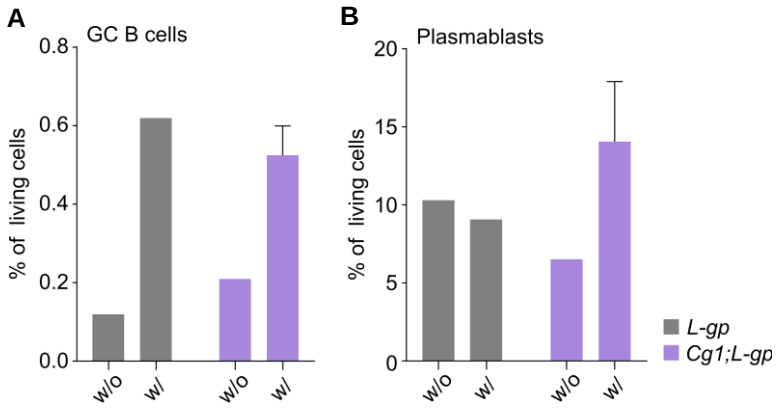

Figure 20: SRBC immunization promotes the formation of a GC reaction. (A) I.v. injection of SRBC leads to an accumulation of GC B cells in the spleen of *Cγ1;L-gp* and *L-gp* controls and (B) to an increased plasmablast population in *Cγ1;L-gp* mice in the BM. w/o: without, w/: with.

3.9 Activation of gp130 overcomes the lymphoma phenotype of B cell–targeted *Myc* by enforcing plasmacytic differentiation

Secondary translocations like deregulation of the oncogene *MYC* or loss of the tumor suppressor *TP53* promote disease progression in patients suffering from MM (Kuehl and Bergsagel 2002). To unravel whether additional secondary mutations would accelerate tumor development in *CD19;L-gp* mice, $p53^{-/-}$ *KO* mice were bred to $CD19Cre^{+/+}$;*L-gp130*$^{fl/fl}$ leading to $CD19Cre^{+/-}$;*L-gp130*$^{fl/-}$;$p53^{+/-}$ offspring. However, neither disease onset nor phenotype in the two triple transgenic animals that were analyzed differed substantially from what was seen in sick *CD19;L-gp*. Hence, in the present study a collaboration between *TP53* function and the gp130 pathway was not evident and therefore this breeding was not taken further (data not shown).

MYC aberrations not only play an important role in MM but also frequently occur in GC and post GC B cell lymphomas and are often associated with poor prognosis (Reddy, Zhang et al. 2017, Chapuy, Stewart et al. 2018). In healthy B cells, Myc expression triggers GC commitment. After suppression of Myc in the GC dark zone, an increase in Myc expression in the light zone selects B cells for re-entry into

the GC dark zone and further affinity maturation (Dominguez-Sola, Victora et al. 2012). This physiological regulation of Myc expression is largely abrogated in *Eμ-Myc* mice where *Myc* is under control of the Eμ immunoglobulin heavy chain enhancer leading to its expression targeted to the B cell lineage (Adams, Harris et al. 1985). To test the relevance of gp130 signaling for B cell differentiation in a scenario of Myc overexpression committed to B cells, triple transgenic mice of the *CD19Cre;L-gp130;Eμ-Myc* (*CD19;L-gp;Myc*) genotype were generated with *CD19;L-gp* and *Myc* serving as controls. Triple transgenic animals were not born at Mendelian frequency with only one out of 61 littermates (i.e. 1.6 % vs. 25 % expected) born alive, that had to be sacrificed at the age of 13 days when it had already reached the endpoints of the study (i.e. reduced activity, lymphadenopathy, expanded belly due to splenomegaly, **Figure 21A**). Flow cytometric analysis of PB, LN, and spleen showed accumulation of $CD19^+GL7^+$ GC B cells as well as $CD19^-CD138^+$ PCs within the $ZsGreen^+$ compartment (**Figure 21B**). Due to the very low number of triple transgenic animals fetal liver hematopoietic stem/progenitor cell (FL-HSPC) grafts from E13.5 embryos were generated. Genotyping revealed triple transgenic embryos at the expected Mendelian ratio. *CD19;L-gp;Myc* and control FL-HSPC were subsequently transplanted into lethally irradiated syngeneic recipient mice (**Figure 21C**). The median survival after transplantation was 20 days for *CD19;L-gp;Myc* recipients, whereas recipients of control grafts survived significantly longer (median survival for *CD19;L-gp* was at 265 days and for *Myc* 277 at days, respectively) (**Figure 21D**). Flow cytometric analysis of *CD19;L-gp;Myc* tumors showed an accumulation of $CD19^+GL7^+$ GC B cells as well as $CD19^-CD138^+$ PCs thus representing the same phenotype as previously seen in the single surviving triple transgenic mouse (**Figure 21B, E, F**). The phenotypes of control recipients, however, varied considerably. The *Myc* control group succumbed to an immature B cell disease characterized by $CD19^+$ B cells expressing IgM but not IgD on their surface, while missing mature B cell subsets including GC B cells and PCs (**Figure 21E, F**). In contrast, the *CD19;L*-gp control group developed a mature B cell disorder characterized by the accumulation of IgD^+ and the absence of IgM^+ B cells (**Figure 21E, F**). These flow cytometric results were confirmed by IHC staining of tumor material from *CD19;L-gp;Myc* as well as *CD19;L-gp* and *Myc* control mice. *CD19;L-gp;Myc* transplanted animals displayed intensive CD138 staining thereby lacking B220 expression whereas *CD19;L-gp* controls stained positive for the PC marker CD138 but also for the B cell marker B220 (**Figure 21G**). On the contrary, in *Myc* controls, $CD138^+$ staining was completely absent (**Figure 21G**). *CD19;L-gp;Myc* as well as *CD19;L-gp* transplanted mice showed only minor Myc and Pax5 staining in contrast to *Myc* controls (**Figure 21G**). Although dying significantly later, *Myc* graft recipients demonstrated higher expression of the proliferation marker Ki67 in tumor cells than did *CD19;L-gp;Myc* mice (**Figure 21G**).

In summary, the activation of gp130 downstream signaling solely in B cells dominantly progresses the pre-/immature B cell lymphoma phenotype characteristics of *Eμ-Myc* mice towards a mature B cell/plasma cell disorder. These data confirm a collaboration between activated gp130/JAK/STAT3 signaling and the oncogene *Myc* and further underline the role of gp130 signaling in plasmacytoma and myeloma pathogenesis.

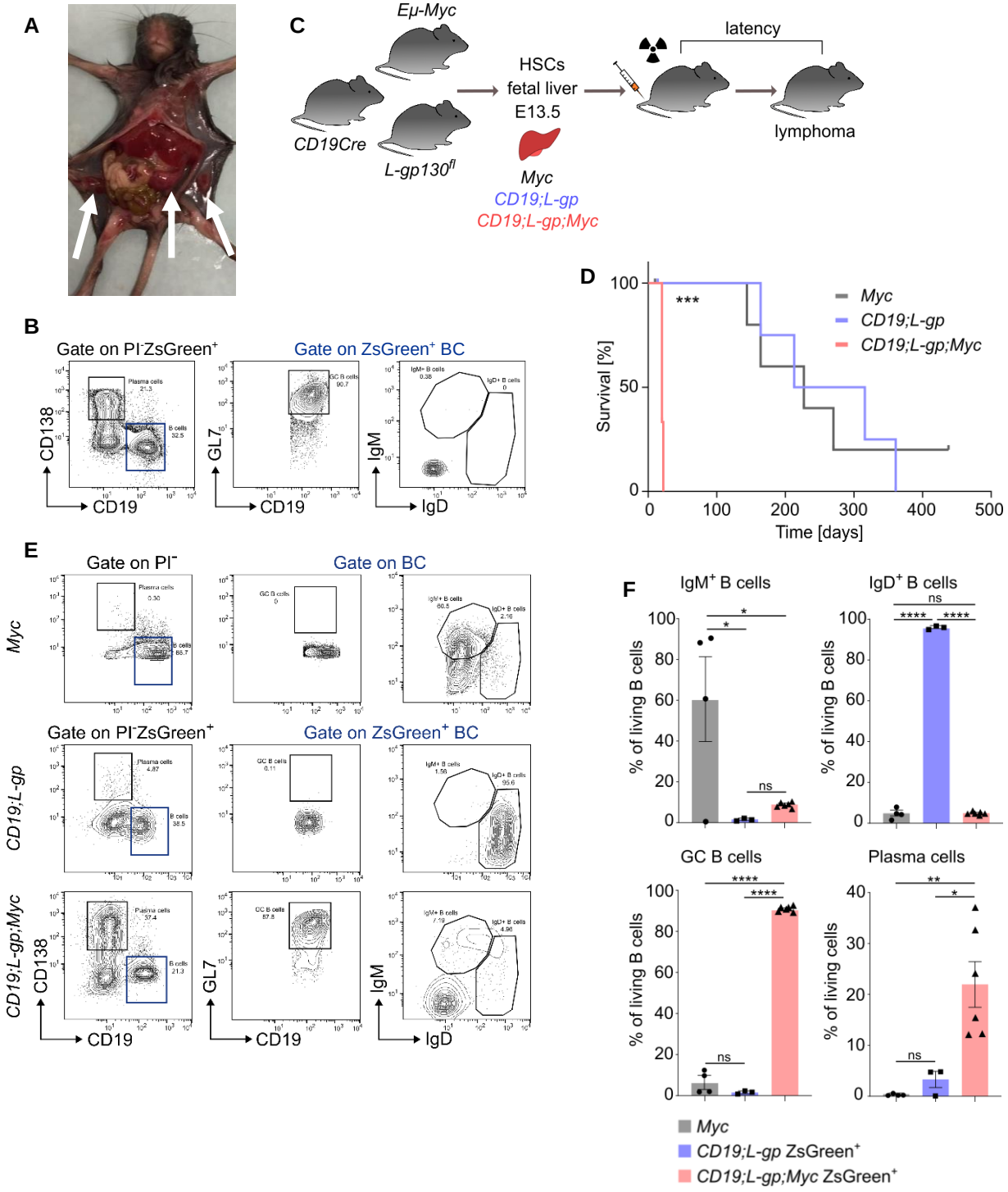
A
C
Eμ-Myc
CD19Cre
L-gp130fl
HSCs
fetal liver
E13.5
Myc
CD19;L-gp
CD19;L-gp;Myc
latency
lymphoma
B
Gate on PI-ZsGreen+
Gate on ZsGreen+ BC
CD138
CD19
GL7
IgM
IgD
D
Survival [%]
Time [days]
***
Myc
CD19;L-gp
CD19;L-gp;Myc
E
Gate on PI-
Gate on BC
Gate on PI-ZsGreen+
Gate on ZsGreen+ BC
F
IgM+ B cells
IgD+ B cells
GC B cells
Plasma cells
% of living B cells
% of living cells
ns
Myc
CD19;L-gp ZsGreen+
CD19;L-gp;Myc ZsGreen+

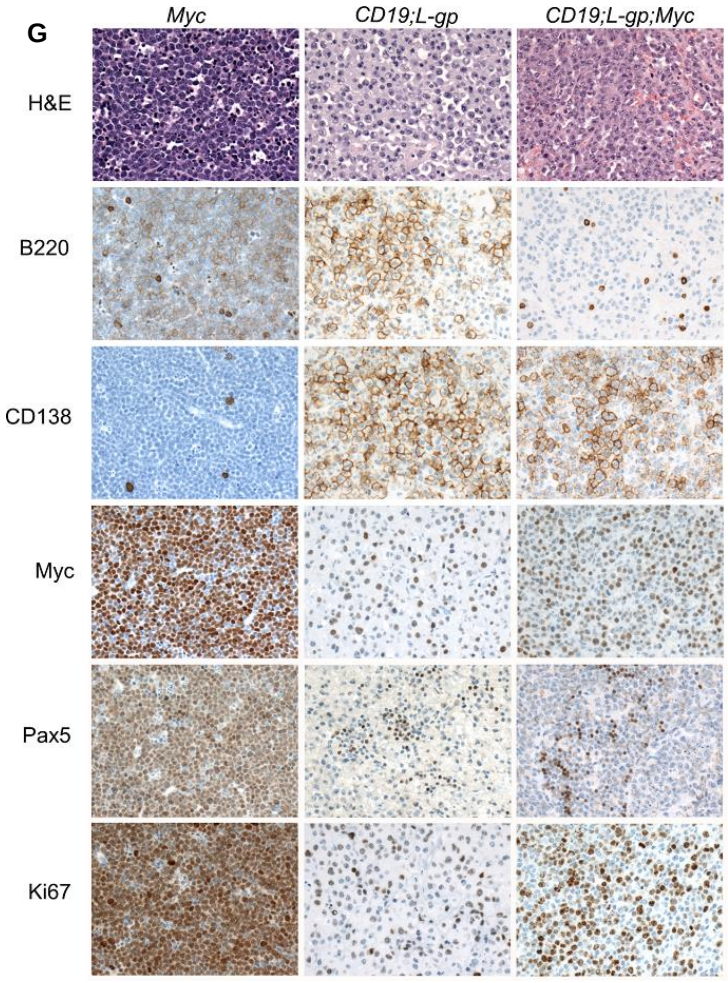

Figure 21: Activated gp130 collaborates with *Myc* to enforce plasmacytic differentiation. (A) The single *CD19;L-gp;Myc* animal presented with lymphadenopathy and splenomegaly as indicated by the white arrows. (B) Flow cytometric analysis of the spleen from the animal shown in (A). (C) Scheme of the *CD19;L-gp;Myc* FL-HSPC transplantation. FL-HSPC from triple transgenic *CD19;L-gp;Myc* embryos and from *CD19;L-gp* and *Myc* controls were isolated at day 13.5 of embryonic development. 1.2 x 10^6 FL-HSPC together with 0.2 x 10^6 Ly5.1 BM support cells were transplanted i.v. into lethally irradiated C57BL/6 recipients. Mice were sacrificed upon disease onset and whole body necropsy performed. The data shown are from one representative experiment from a group size of n = 6 animals each. (D) Kaplan-Meier curve revealing a significant shorter survival of mice transplanted with FL-HSPC from *CD19;L-gp;Myc* as compared to *CD19;L-gp* and *Myc* controls (n = 6 mice per group) (***, P = 0.003, Mantel-Cox test). (E) Flow cytometric analysis of tumors. Tumors from *CD19;L-gp;Myc* transplanted animals demonstrating a phenotype of a late B cell disease as stated in the text. At least three mice per genotype were analyzed. Shown are representative analyses. (F) Analysis of organ infiltration in *CD19;L-gp;Myc*, *CD19;L-gp,* and *Myc* transplanted animals by distinct B cell populations as assessed by flow cytometry. Data are shown as mean percentage ± SEM assessed from at least three mice per genotype. Asterisks indicate significant differences as determined by ANOVA testing followed by the Tukey's test. (G) Histology and IHC from tumor material of one representative animal per group showing substantial differences between cohorts. Original magnification, x400. [Histology and IHC data from (G) were provided by K. Steiger and L. Quintanilla-Martinez].

3.10 Conditional gp130 activation in hematopoietic stem/progenitor cells results in a highly aggressive B cell malignancy

The data presented heretofore indicated that activated constitutive gp130 signaling at either a very early stage of B cell development or towards final differentiation drives late B cell commitment and eventually leads to highly aggressive mature B cell lymphomas and PC tumors. However, JAK/STAT3 activation is also a recurrent event in other hematopoietic neoplasms, including chronic as well as acute leukemia and T/natural killer (NK) cell neoplasms ((Kucuk, Jiang et al. 2015) and reviewed in (Sansone and Bromberg 2012, Munoz, Dhillon et al. 2014)).

Therefore, to ultimately test the significance of constitutive gp130 activation for promoting mature B cell lymphoma and plasma cell disorders, genetic activation of the *L-gp130* transgene to hematopoietic stem cells and thus to the entire hematopoietic system was realized by using the transgenic *Vav1Cre* strain (Ogilvy, Elefanty et al. 1998, Ogilvy, Metcalf et al. 1999). *Vav1Cre$^{+/-}$;L-gp130$^{fl/+}$* (*Vav1;L-gp*) compound mice began to deteriorate in their general condition within the first two months of life and were sacrificed in compliance with the endpoints of the study. The median survival was 53 days (**Figure 22A**). Whole body necropsy displayed brittle bones, lymphadenopathy, and splenomegaly (**Figure 22B, C**), suspicious for an aggressive hematopoietic disorder. Examination of PB from diseased *Vav1;L-gp* mice revealed a significant increase in WBC numbers and platelets when compared to *Vav1* and *L-gp* controls (**Figure 22D, E**). All leucocyte subpopulations in the PB, LN, spleen, and BM of *Vav1;L-gp* mice were characterized by ZsGreen expression indicative of activation of gp130 signaling in the entire hematopoietic system (**Figure 22F**). However, no significant differences in the frequency of HSPC were seen in diseased mice in comparison to age-matched controls by means of Lin$^-$Sca1$^+$c-kit$^+$ (LSK) and Lin$^-$Sca1$^-$c-kit$^+$ (multipotent progenitors, MPP) compartments in the BM (**Figure 22G**). Flow cytometry analysis of LNs rather showed that the B cell compartment of these mice consisted of immature and Pro-Pre-B cells (**Figure 22H** and **22I** left) as well as mature IgD$^+$ B cells (**Figure 22H** and **22I** right). This finding was supported by histological and IHC analyses that revealed the presence of two different B cell subpopulations in the spleen and LNs of *Vav1;L-gp* mice. The first resembled morphologically an aggressive B cell malignancy while the second represented a CD138$^+$ plasma cell disorder that has already been seen before in the other *xCre;L-gp* breedings of this study (**Figure 22K**). IHC as well as flow cytometry showed scattered infiltration of T cells into LNs (**Figure 22J**), however, the main pathological feature was the massive accumulation of CD138$^+$ PCs and B220$^+$ Pax5$^+$ B cells (**Figure 22K**). The PC disorder in *Vav1;L-gp* mice was also underpinned by the presence of gammopathy in 100% of tested animals, however only to a moderate extent (**Figure 22L, M**). These findings were supported by results obtained from RNASeq analysis of Ig heavy chain constant regions (**Figure 22N**, upper panel). Assessment of light chain constant region gene expression revealed significantly lower λ gene profiles in *Vav1;L-gp* mice compared with WT controls (**Figure 22N**, lower panel). In accordance with the aggressive phenotype leading to an early disease onset in *Vav1;L-gp* mice, transcript analysis of splenocytes showed MAPK pathway signaling as well as strong activation of the pro-survival proteins

Bcl-XL and Bcl-2 besides the expression of the L-gp130 construct and excessive STAT3 activation by means of pSTAT3 (**Figure 22O**). The latter was also seen not only in the B cell (**Figure 22P,** upper row) but also the T cell compartment (**Figure 22P,** lower row) of diseased *Vav1;L-gp* mice by intracellular flow cytometric staining of splenocytes in comparison to age-matched *Vav1* control mice.

Thus, these results are consistent with a dominant gp130 downstream signaling mechanism that enforces the development of B cell cancers even when activated at the stage of HSPCs.

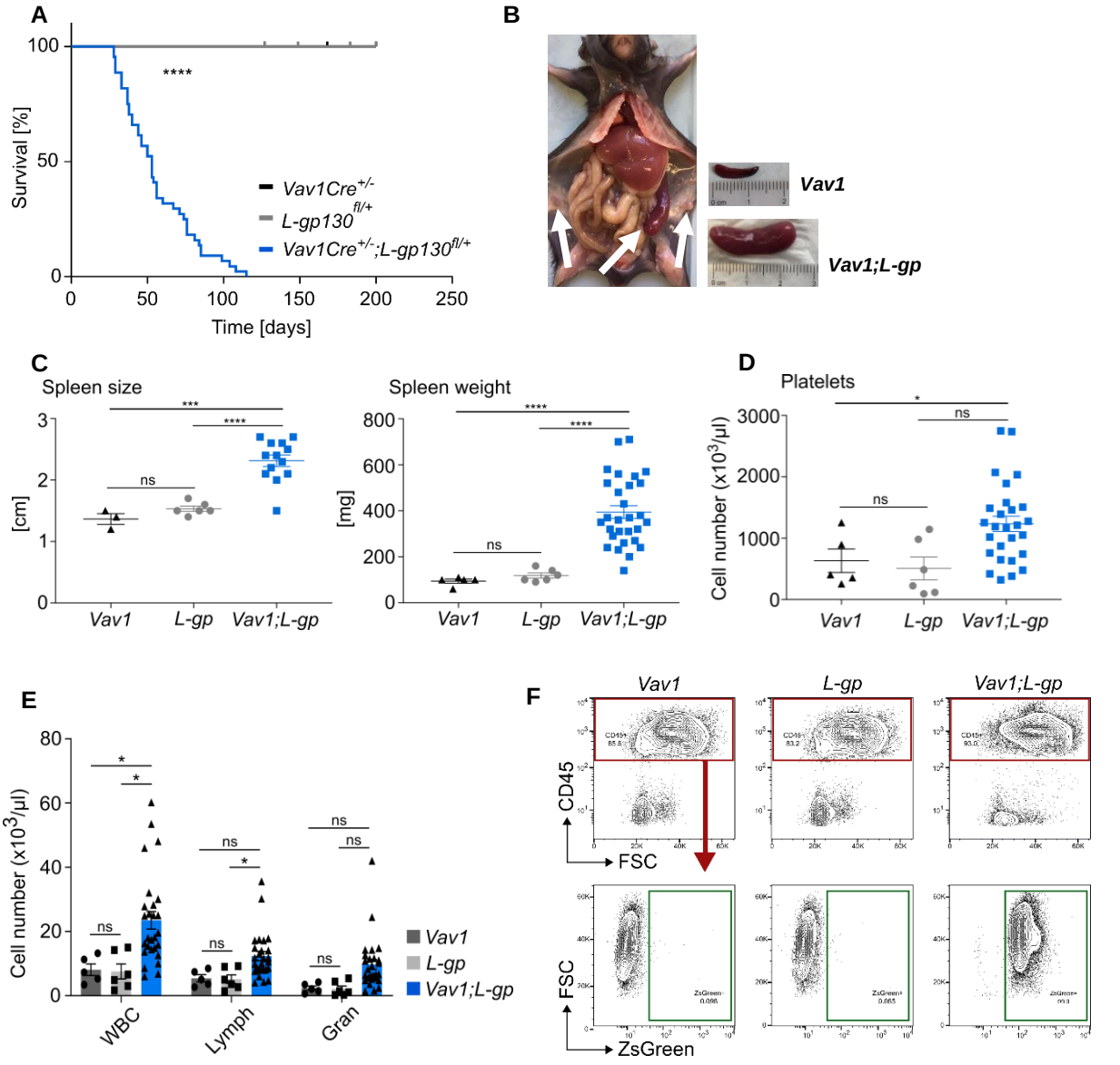

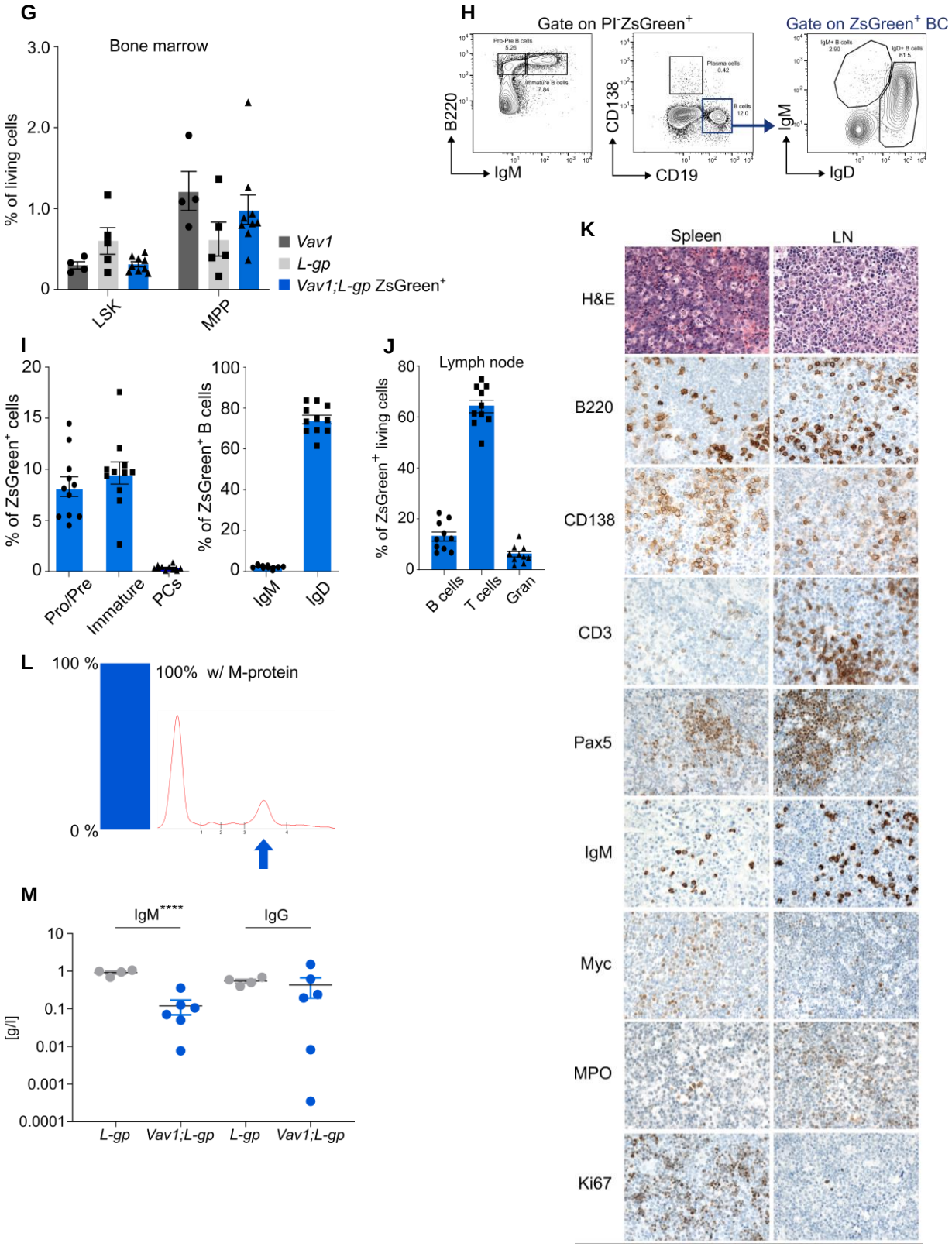
G
Bone marrow
% of living cells
3.0
2.0
1.0
0
LSK
MPP
Vav1
L-gp
Vav1;L-gp ZsGreen+
H
Gate on PI-ZsGreen+
Gate on ZsGreen+ BC
B220
IgM
CD138
CD19
IgM
IgD
I
% of ZsGreen+ cells
Pro/Pre
Immature
PCS
% of ZsGreen+ B cells
IgM
IgD
J
Lymph node
% of ZsGreen+ living cells
B cells
T cells
Gran
K
Spleen
LN
H&E
B220
CD138
CD3
Pax5
IgM
Myc
MPO
Ki67
L
100 %
0 %
100% w/ M-protein
M
IgM****
IgG
[g/l]
10
1
0.1
0.01
0.001
0.0001
L-gp
Vav1;L-gp
L-gp
Vav1;L-gp

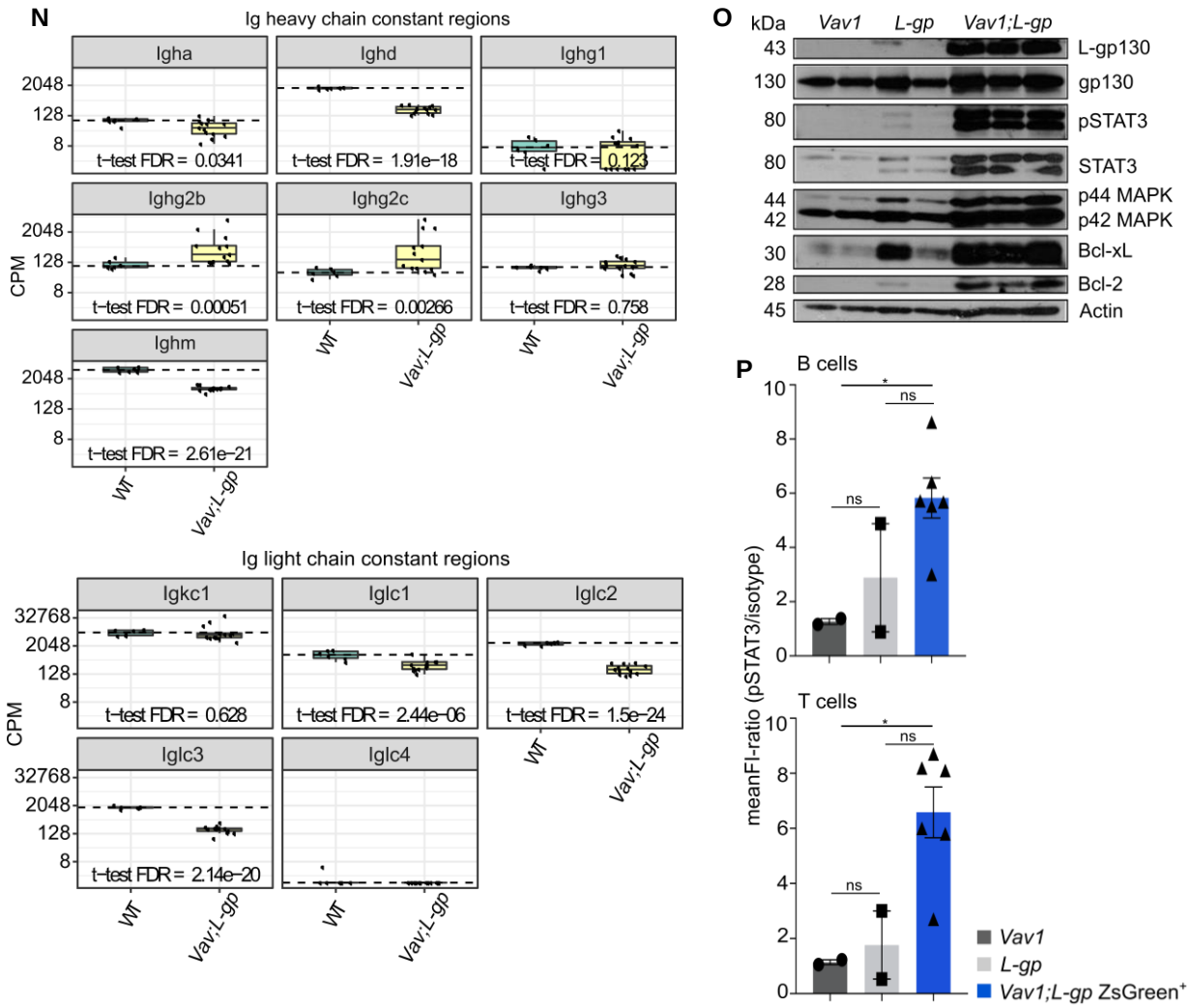

Figure 22: Conditional gp130 activation in hematopoietic stem/progenitor cells results in a highly aggressive B cell malignancy (A) Kaplan-Meier curve showing survival of *Vav1;L-gp* (n = 44) in comparison to *Vav1* (n = 26) and *L-gp* (n = 33) controls. *Vav1;L-gp* compound mice had a median survival of 53 days. Controls did not show any signs of malignancy within the observed time frame (****, P < 0.0001, Mantel-Cox test). (B) Diseased *Vav1;L-gp* animals presented with lymphadenopathy and splenomegaly as indicated by the white arrows. The spleen of an age-matched healthy *Vav1* mouse is shown for comparative reasons. (C) Spleen size (left) and weight (right) of diseased *Vav1;L-gp* in comparison to controls. Differences were significant as determined by ANOVA testing followed by the Tukey's test. (D) The majority of sick *Vav1;L-gp* animals showed thrombocytosis. (E) WBC analysis of PB in diseased *Vav1;L-gp* (n = 27) in comparison to normal *Vav1* (n = 5) and *L-gp* (n = 6) controls (*, P < 0.05, ANOVA test followed by Tukey's test). Shown are means ± SEM. (F) Flow cytometric analysis revealing genetic activation of L-gp130 expression in nearly all PI^-CD45^+ cells from diseased *Vav1;L-gp* as defined by ZsGreen positivity (right). In contrast, *Vav1* (left) and *L-gp* controls (middle) cells did not show a ZsGreen signal. Depicted is the BM of one representative animal per cohort. At least four mice were analyzed per cohort. (G) Flow cytometric analysis of BM from diseased *Vav1;L-gp* animals displaying no significant differences in the $Lin^-Sca1^+c\text{-}kit^-$ (LSK) as well as $Lin^-Sca1^-c\text{-}kit^-$ (MPP) compartments in comparison to age-matched control groups as assessed by the ANOVA test followed by the Tukey's test. Shown are means ± SEM of at least four mice per group. (H) Flow cytometric analysis of diseased *Vav1;L-gp* mice (n = 11 analyzed) for distinct B cell subsets. Cells were gated for $PI^-ZsGreen^+$ living cells. Shown is the LN sample of one representative animal. Pro-Pre- and immature B cells (left) were present while a small fraction of $CD138^+$ PCs was seen (middle). The $CD19^+$ B cell population was identified as a mature IgD^+ differentiation state (right). The previous gate is indicated. (I) Quantitative analysis of LN infiltration by the distinct B cell subsets as shown in H from n = 11 mice. Bars represent the mean percentage ± SEM. (J) T cells are the major leucocyte subpopulation of living ZsGreen+ cells in LNs from diseased *Vav1;L-gp* as determined by flow cytometry (n = 11). Shown are means ± SEM. (K) Histological and IHC analyses from spleen (left) and LN (right) of a representative diseased *Vav1;L-gp* mouse. H&E stainings revealed high infiltration of tumor cells into

both organs (upper row). Both, spleen and LN showed expression of B220 and CD138 as well as Pax5 and IgM. Infiltration of $CD3^+$ T cells was seen into the LN but not the spleen. Ki67 staining reveals a higher proliferation rate in the spleen as compared to the LN. Original magnification, x400. (L) Serum protein electrophoresis from one representative *Vav1;L-gp* animal indicative of moderate but significant monoclonal gammopathy. The arrow indicates the abnormal protein fraction. All tested animals presented with this feature (n = 15). (M) Ig levels, assessed by ELISA, from serum of diseased *Vav1;L-gp* mice (n = 6) in comparison to *L-gp* controls (n = 4). Shown are means ± SEM (****, P < 0.0001, student's *t* test). (N) RNASeq gene expression profiles of Ig heavy (upper panel) and light (lower panel) chain constant regions obtained from mesenteric nodal tumor material of *Vav1;L-gp* in comparison to CD19+ isolated WT splenocytes. CPM: counts per million, FDR: false discovery rate. Significance was evaluated by student's *t* test with subsequent assessment of the FDR. (O) Splenocytes from diseased *Vav1;L-gp* show expression of the L-gp130 protein and strong activation of gp130 downstream signaling cascades including anti-apoptotic pathways. (P) Intracellular flow cytometry for pSTAT3 expression in $ZsGreen^+$ B cells (upper panel) and T cells (lower panel) of sick *Vav1;L-gp* mice (n = 6) in comparison to *Vav1* and *L-gp* controls (n = 2 each). Significance was assessed by the ANOVA test followed by the Tukey's test. [Histology and IHC data from (K) were provided by K. Steiger and L. Quintanilla-Martinez, Serum electrophoresis from (L) was performed by M. Thaler and Data analysis from (N) was done by H.C. Maurer].

3.11 RNASeq of tumor material from diseased mice reveals clustering of genotypes

Independent of the time point of activation during hematopoietic and B cell differentiation, all x*Cre;L-gp* compound mice succumbed to tumors of B cell origin. When comparing tumor material from *Vav1;L-gp* and *CD19;L-gp* mice by RNASeq, an evident clustering of the two genotypes was seen (**Figure 23A**). Unlike *CD19;L-gp* tumors of the Mature phenotype, tumors of the PC phenotype showed strong activation of WNT, BCR, and NF-kappaB signaling and also expression of gp130 downstream targets (**Figure 23B**). *Vav1;L-gp* tumors, however, displayed activation of all the distinct downstream cascades activated by IL-6/gp130 signaling (**Figure 23B**). These analyses show that initiation of the same signaling axis at distinct time points of hematopoietic and B cell development leads to the activation of – at least partly – different gp130 downstream pathways and targets.

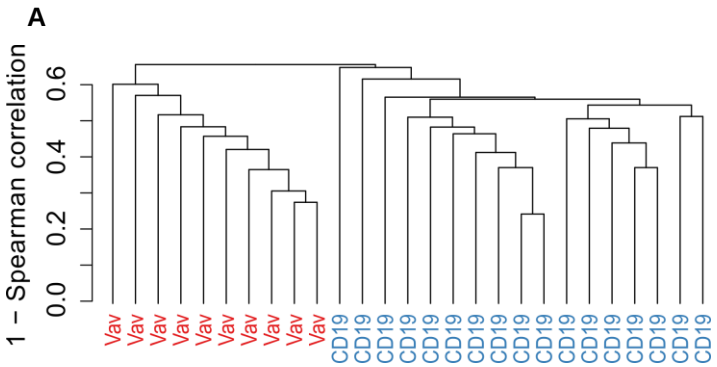

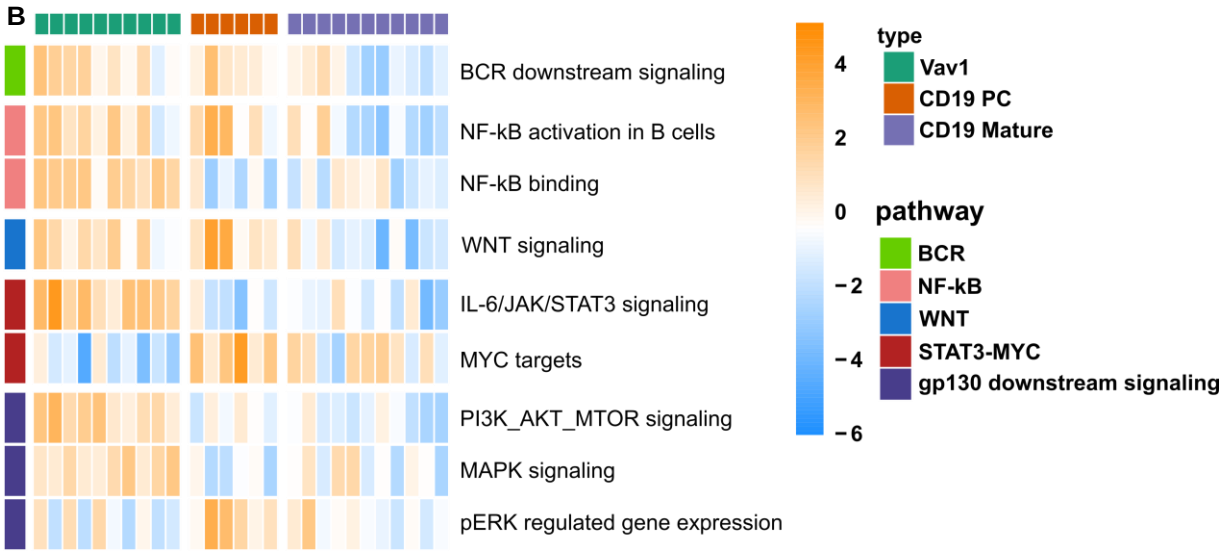

Figure 23: Transcriptional programs in murine lymphomagenesis. (A) Hierarchical clustering of RNASeq gene expression profiles obtained from *Vav1;L-gp* (red) and *CD19;L-gp* (blue) tumors reveals clear separation by genotype. Distance measure: 1- Spearman correlation, HC linkage: complete. (B) Heatmap depicting ssGSEA results as normalized enrichment scores (NES) for the indicated pathways and their distribution between lymphomas derived from the *Vav1;L-gp* (green) and *CD19;L-gp* mouse models (orange: PC phenotype, purple: Mature phenotype). All pathways shown are differentially enriched at an FDR < 0.1. [RNASeq was done by R Öllinger and subsequent data analysis was performed by HC Maurer].

3.12 The L-gp130 signature is represented during progression of human MM

Having seen that constitutive activation of gp130/JAK/STAT3 signaling results in mature B cell lymphomas and MM irrespective of its activation during hematopoietic and B cell development, publicly available gene expression datasets were interrogated for the in chapter 3.4 defined L-gp130 signature in diverse disease stages of human MM in comparison to MGUS and normal PCs. Among different progression stages of MM, the L-gp130 signature was most highly activated in patients suffering from relapsed MM while lowest activation was seen in normal PCs as depicted in **Figure 24**.

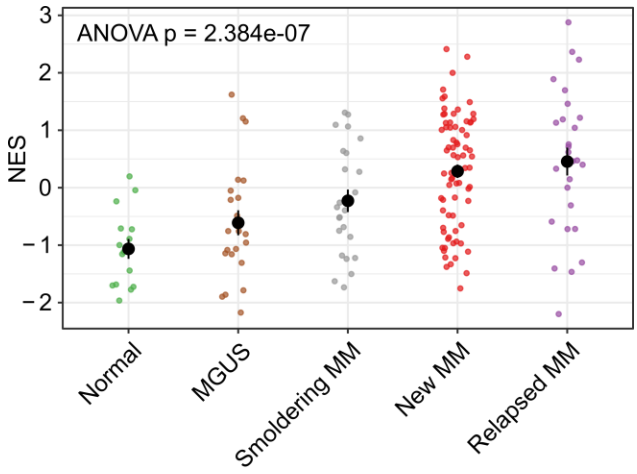

Figure 24: The L-gp130 signature during progression of MM. ssGSEA results of the previously defined L-gp130 signature among different progression stages of MM. The stages were earlier profiled by Keats et al. Enrichment results are positively correlated with disease progression. [Data was provided by HC Maurer].

4 Discussion

Although major advances in understanding its development and progression have been made, MM is still considered a disease with a short-limited survival, and most patients die from the malignancy. Nevertheless, research has significantly improved the life of MM patients with the introduction of 18 newly approved treatments within the past twelve years thereby increasing the median overall survival (OS) over three fold (Guang, McCann et al. 2018). Treatment options include (1) autologous stem cell transplantation (ASCT), (2) therapies targeting MM in the context of the BMM (e.g. proteasome inhibitors, IMiDs, histone deacetylase inhibitors), as well as (3) immunotherapy (e.g. monoclonal antibodies, checkpoint inhibitors and T-cell immunotherapy). However, most patients still succumb to MM as they eventually progress into a refractory disease (Guang, McCann et al. 2018). Therefore, a deeper understanding of this severe malignancy is still needed. The focus of this study thus was a signaling pathway that has been shown to play a prominent role as a driver in the development and progression of MM, namely the IL-6/gp130/JAK/STAT3 axis (Catlett-Falcone, Landowski et al. 1999). Even though this pathway has already been targeted by the development of several JAK inhibitors that revealed efficacy by inducing growth arrest and cell death (Pedranzini, Dechow et al. 2006, Monaghan, Khong et al. 2011, Scuto, Krejci et al. 2011), yet MM remains incurable for the vast majority of patients. The absence of good animal models of MM still impedes a full understanding of disease mechanisms and the successful translation into novel therapies for patients. Several mouse models of MM based on activation of the IL-6/IL-6R axis have already been designed (Dechow, Steidle et al. 2014, Paton-Hough, Chantry et al. 2015, Rossi, Botta et al. 2018), underscoring the importance of this pathway regarding proliferation as well as malignant transformation of late B cells. However, these models are restricted due to their late disease onset and/or low penetrance. Therefore, novel transgenic mouse models that conditionally activate gp130 signaling on a C57BL/6 background thus eliminating the role of the mutation in the INK4a/ARF locus that supports lymphomagenesis in MM models on a BALB/c background were introduced here (Zhang, DuBois et al. 2001).

In summary, activation of gp130 signaling by means of L-gp130 in a novel *in vivo* approach on the frequently used C57BL/6 background promoted B cell differentiation and eventually resulted in the development of $CD138^+$ tumors with characteristics of MM irrespective of its activation during hematopoietic and B cell differentiation.

4.1 Forced activation of gp130 signaling within the B cell compartment results in STAT3 activation, accumulation of mature B cell subsets, and malignant transformation

IL-6/IL-6R/gp130 signaling is crucial for normal B cell differentiation and function including the production of Ig by terminally differentiated PCs (Hirano, Yasukawa et al. 1986, Muraguchi, Hirano et al. 1988, Akira,

Taga et al. 1993, Kopf, Baumann et al. 1994, Kumanogoh, Marukawa et al. 1997, Silver and Hunter 2010, Schaper and Rose-John 2015). Already in six weeks old *CD19;L-gp* mice, STAT3 activation in $CD19^+$ B cells from splenocytes (Figure 14G) as well as an accumulation of mature B cell subsets in the $ZsGreen^+$ compartments was seen (Figure 14F). Subsequently, at an average of five months of age these mice showed the development of mainly late B cell lymphomas and plasma cell disorders while only two out of 48 analyzed mice presented with a Pro-/Pre-/Immature B cell phenotype in flow cytometric analysis (Figure 17D, E). This transformation in early B cell development might be due to additional mutations that by chance occurred in these two animals thus preventing further B cell differentiation. However, tumor material of this phenotype was limited to state this hypothesis in further analyses. Still, histology and IHC investigations revealed the presence of $CD138^+$ PCs with abundant pale cytoplasm, eccentric nucleus, inconspicuous nucleolus and nuclear pleomorphism also in this phenotype as well as in sick mice of the Mature and PC phenotypes (Figure 17H). CD138 (Syndecan-1) is a cell surface marker of malignant PCs that is expressed from the majority of MM cell lines as well as patient specimens (Wijdenes, Vooijs et al. 1996, Chilosi, Adami et al. 1999, Wei and Juneja 2003). It acts as a major regulator of the BMM that supports myeloma growth and metastasis (Ridley, Xiao et al. 1993) In the present study, all tumors showed strong infiltration of malignantly transformed PCs as a feature of MM in IHC analyses (Figure 17H). Assessing diseased *CD19;L-gp* mice of the PC and Mature phenotypes by flow cytometric analysis, infiltration of high amounts of malignant cells at multiple sites of the body was detected (Figure 17I). These characteristics clearly distinguish the present plasma cell disorder from solitary plasmacytomas where a localized accumulation of less than 10 % of neoplastic monoclonal PCs is seen (Durie and Salmon 1975, Knowling, Harwood et al. 1983, International Myeloma Working 2003), suggesting that the disease resembled MM. High amounts of monoclonal Ig or Ig fragments that can be measured in the serum as an M-protein spike are produced from these malignantly transformed PCs. Over 90 % of myeloma patients present with this characteristic at time point of diagnosis (International Myeloma Working 2003). In the here described animal model about one third (PC) and half (Mature) of the cohorts revealed the presence of monoclonal gammopathy (Figure 17J). Also in human MM it has been shown that some patients present with a non-secretory form of the disease and therefore do not show a detectable M-protein in their serum or urine. However, the subset of these patients is really small, only accounting to 3 – 5 % (Cavo, Galieni et al. 1985, Blade and Kyle 1999, Middela and Kanse 2009).

Serial transplantation of tumor cells from sick *CD19;L-gp* mice resulted in the establishment of secondary tumors with a significantly shorter survival time (Figure 18). A reestablishment of the primary disease was shown earlier by the group in a transduction-transplantation model of L-gp130 (Dechow, Steidle et al. 2014). However, there, activation of gp130 signaling was brought to the whole hematopoietic compartment on a BALB/c background that makes mice prone to developing plasma cell disorders upon adequate stimuli due to a mutation in the inhibitor of Cdk4/alternative reading frame (INK4a/ARF) locus leading to partial disability of the tumor suppressor protein $p16^{Ink4a}$ (Zhang, DuBois et al. 2001). In contrast, in *CD19;L-gp* mice described in this study, gp130 activation only took part in the B cell compartment and on the frequently used C57BL/6 background. This approach shows the importance of

the gp130/JAK/STAT3 axis for B cell differentiation and malignant transformation while eliminating the role of the mutation in the INK4a/ARF locus that supports lymphomagenesis (Zhang, DuBois et al. 2001).

4.2 *CD19;L-gp* show collaboration with the oncogene *Myc* but not with the tumor suppressor *Trp53*

The hypothesis to see a disease progression in *CD19;L-gp* mice when bred to the p53 KO strain originated from the knowledge that secondary translocations like loss of the tumor suppressor *TP53* promoted tumor development in MM patients (Kuehl and Bergsagel 2002). However, triple transgenic *CD19;L-gp;p53*$^{+/-}$ animals in the present study did not reveal a shorter survival than *CD19;L-gp* mice (data not shown). This finding can be explained by the fact that heterozygous p53 KO mice also only show tumorigenesis at very low numbers and with a long latency while mice carrying a homozygous deletion in the *TP53* gene are highly prone to malignancy (Donehower, Harvey et al. 1992). This is supported by two studies on samples of human MM patients which showed that a bi-allelic deletion of *TP53* had a significant impact on clinical outcomes in MM patients while hardly any or only moderate effects were seen for *TP53* single-lesion disease (Thanendrarajan, Tian et al. 2017, Walker, Mavrommatis et al. 2019). On the contrary, a study by Teoh and colleagues proposed a role for *TP53* as a haploinsufficient tumor suppressor underlining the importance of p53 baseline protein expression levels in MM. Mechanisms like promoter hypermethylation may thereby silence the remaining WT allele, leading to loss of heterozygosity (LOH) with a poor prognosis for patients. Moreover, abnormalities of the more extended p53 network, such as increased expression of the E3 ubiquitin-protein ligase Mdm2 and deregulation of other downstream targets, may be of clinical relevance (Teoh, Chung et al. 2014). In the present study no mechanistic examinations were performed. Therefore, conclusions cannot be made whether the remaining WT allele was silenced or still expressed p53 protein, even though the unaltered latency of *CD19;L-gp;p53*$^{+/-}$ animals in comparison to *CD19;L-gp* mice would suppose the latter. However, the very small cohort of only two animals analyzed does not allow to draw a conclusion regarding the significance of the survival time. Hence, extended mechanistic analysis of a larger cohort of triple transgenic mice is needed.

On the other hand, when combining the oncogene *Myc* in B cells with B cell specific L-gp130 activation *(CD19;L-gp)*, triple transgenic animals succumbed to a CD138^{+} PC disease within three weeks of age (Figure 21). This accelerated disease onset as well as the CD138^{+} phenotype was seen earlier in a transduction-transplantation model. There, FL-HSPC from *Eμ-Myc*$^{+/-}$ transgenic mice were transduced with the L-gp130 construct *in vitro* and subsequently transplanted into lethally irradiated recipients. Thereby *Myc* was overexpressed in B cells while gp130/JAK/STAT3 signaling was active in the whole hematopoietic compartment, leading to a shift from a pre-/immature B cell malignancy towards a CD138^{+} disease (Dechow, Steidle et al. 2014). In the present study, both, overexpression of *Myc* as well as constitutive activation of gp130 signaling were solely within the B cell lineage and abolished the pre-

/immature B cell phenotype of *Eμ-Myc*$^{+/-}$ transgenic mice leading to the development of a CD138^{+} disease of high penetrance and fast latency. This outcome is in line with the observation of a previous study where genetic alterations of *Myc* were found to be a secondary event in murine MM pathogenesis that accelerate but do not drive malignant transformation (Chesi, Robbiani et al. 2008). The novel transgenic model hereby shows the simplicity of introducing a second hit, important for malignant transformation, into the context of activated gp130/JAK/STAT3 signaling. Thereby is not only possible to study MM in depth but also to unravel other malignancies where this pathway is of major importance f.e. rheumatoid arthritis, cholangiocarcinoma, hepatocellular carcinomas, as well as breast and lung cancer (He, You et al. 2003, Niwa, Kanda et al. 2005, Isomoto, Mott et al. 2007, Ying, Li et al. 2010, Garbers, Heink et al. 2018)

4.3 Conditional gp130 activation during late B cell differentiation results in B cell tumors with a long latency

Knowing that MM is thought to arise from malignantly transformed post-GC PCs (Hallek, Bergsagel et al. 1998), the transgenic *L-gp130* strain was bred to *Cγ1Cre* as well as *Blimp1Cre* mice, thereby achieving constitutive gp130 signaling in B cells during the GC reaction and beyond. This approach would help to unravel the exact differentiation step at which malignant transformation occurs.

In addition to young *CD19;L-gp* mice described in chapter 3.3, *Blimp1;L-gp* as well as *Cγ1;L-gp* mice were also analyzed at the age of six weeks. While histological analysis of organs did not reveal evidence for malignant transformation (Figure 15A), WBC were already significantly elevated in *Blimp1;L-gp* in comparison to *Cγ1;L-gp* mice as well as *L-gp* controls (Figure 15C). In contrast to young *Cγ1;L-gp* mice, *Blimp1;L-gp* presented with a small ZsGreen^{+} population in all organs examined (data not shown). However, not only late B cells could be allocated to this population. This might be due to the fact that the transcription factor Blimp1 is not only expressed immediately after the B cells exit the GC reaction, but also plays a role in the terminal differentiation of other cell subsets (Xin, Nutt et al. 2011) and therefore gp130/JAK/STAT3 signaling in these mice is not exclusively restricted to late B cells. This finding could also explain why a much shorter median survival was observed in *Blimp1;L-gp* than in *Cγ1;L-gp* mice although activation of gp130/JAK/STAT3 signaling takes place later during B cell differentiation in the former (Figure 19A, B). However, even in *Blimp1;L-gp* the development of mature B cell diseases including plasma cell disorders was seen, again confirming the prominent role of this pathway for B cell development as well as malignant transformation (Figure 19D, F). In diseased *Cγ1;L-gp* mice an additional phenotype characterized by the accumulation of CD19^{+}GL7^{+} GC B cells was observed (Figure 19C, E). As genetic changes taking place during the GC reaction make DNA prone to damage, the GC displays a source for lymphoma development (Allen, Okada et al. 2007, Lenz and Staudt 2010). It is not surprising that the additional activation of gp130 signaling in the GC by means of *Cγ1Cre* would therefore lead to an increased proliferation and accumulation of GC B cells. Furthermore, several of *Cγ1;L-gp* mice

showed the presence of a characteristic M-protein in the serum as well as significantly elevated IgG levels (Figure 19H, J), both features of MM. As *Cγ1;L-gp* mice had such a long latency, the initiation of the GC reaction and therefore the activation of gp130 signaling was aimed to be triggered by i.v. injection of SRBC (Zhang, Tech et al. 2018). Thereby an increase of GC B cells in the spleen as well as of plasmablasts in the BM was achieved (Figure 20). The observation made in *Cγ1;L-gp* mice was in concordance with a study on immunized IL-6 deficient mice that presented with lower antigen-specific antibody titers and were impaired in the formation of a normal GC. Thus, in the absence of IL-6 and therefore impaired gp130 signaling, size and volume of GC B cells were severely diminished (Kopf, Herren et al. 1998). Although an increased GC and plasmablast reaction was noticed upon activation of gp130/JAK/STAT3 signaling in *Cγ1;L-gp* mice, accelerated malignant transformation did not take place. This also accounted for *Cγ1;L-gp* mice that underwent repeated immunization rounds and were monitored for a longer time (data not shown). Yet the number of immunized animals was very low, so it is difficult to draw a meaningful conclusion from these results.

4.4 Gp130 activation in hematopoietic stem/progenitor cells leads to a rapid and aggressive B cell malignancy

So far, this study was able to show that activation of gp130/JAK/STAT3 signaling by means of *L-gp130* at distinct stages of B cell differentiation led to the development of $CD138^+$ neoplasms. Besides its crucial role in B cells (Hirano, Yasukawa et al. 1986, Akira, Taga et al. 1993), IL-6/IL-6R/gp130 signaling is also important in regulating normal hematopoiesis (Bernad, Kopf et al. 1994, Yoshida, Taga et al. 1996, Peters, Schirmacher et al. 1997). Using the *Vav1Cre* strain, the intent was to unravel the influence of constitutive activation of gp130 signaling for malignant transformation by targeting this axis to the entire hematopoietic system (Ogilvy, Elefanty et al. 1998, Ogilvy, Metcalf et al. 1999). In contrast to the other *xCre;L-gp* models discussed in this study, *Vav1;L-gp* mice did not develop mesenteric tumors but presented with brittle bones, lymphadenopathy, and splenomegaly (Figure 22B, C) and showed a short latency of median 53 days (Figure 22A). The animals revealed strong expression of pSTAT3 (Figure 22O, P) as a downstream mediator of activated gp130 signaling. Persistent STAT3 activation is seen in a plethora of hematologic diseases, including myeloproliferative and lymphoproliferative disorders (Benekli, Baer et al. 2003), and IL-6/gp130/JAK/STAT3 activation displays a recurrent event also in chronic as well as acute leukemia (reviewed in (Sansone and Bromberg 2012, Munoz, Dhillon et al. 2014)). Hence the BM of diseased *Vav1;L-gp* mice was examined for variances in HSPC subsets, but no significant differences in the MPP or LSK compartments of these animals in comparison to age-matched controls were detected (Figure 22G). Instead, infiltration of malignant cells of the B cell lineage were also the cause of disease in those animals (Figure 22H, I, K). However, in contrast to *xCre;L-gp* described before, *Vav1;L-gp* mice presented with two populations of neoplastic B cells: the first resembled a $CD138^+$ plasma cell disorder as seen before in the other *xCre;L-gp* breedings of this study

whereas the second morphologically reminded of an aggressive early B cell malignancy similar to BL. Consistent with the latter, expression of early B cell markers Pax5 and IgM in infiltrated organs was seen (Figure 22K). These results from *Vav1;L-gp* mice are in some parts in contrast to mice homozygous for a knock-in mutation in gp130 (gp130$^{Y757F/Y757F}$) that showed gp130-dependent STAT1/3 hyperactivation in the hematopoietic system due to the inability of gp130 to bind to SOCS3 and SHP2 (Jenkins, Roberts et al. 2005). Just like the cohort presented here (Figure 22B, C, D), these transgenic mice demonstrated the occurrence of splenomegaly, lymphadenopathy, and thrombocytosis when compared to gp130$^{+/+}$ littermates. However, while in diseased *Vav1;L-gp* mice also significantly elevated total WBC counts were detected (Figure 22E), this characteristic was not seen by Jenkins and colleagues. Furthermore, their animals revealed expanded numbers of immature and committed hematopoietic progenitor cells in the BM and spleen, clearly contrasting the results on the examination of HSPCs in the current study (Figure 22G). Still, infiltration of immature and mature B cells was also seen. However, the presence of neoplastic early B cells and CD138^{+} PCs that were the cause of malignancy in *Vav1;L-gp* mice presented here (Figure 22H, I, K), was not mentioned by Jenkins and colleagues. Consistent with data from *Vav1;L-gp* mice (Figure 22O), gp130$^{Y757F/Y757F}$ animals also showed increased expression of pSTAT3 and the anti-apoptotic protein Bcl-XL confirming gp130 downstream signaling. Moreover, this group unraveled, that, when STAT3 activity was genetically reduced in *gp130*$^{Y757F/Y757F}$ mice, the onset of the hematopoietic phenotype was impeded, indicating that the level of STAT3 activation is crucial for gp130-controlled hematopoietic homeostasis *in vivo* (Jenkins, Roberts et al. 2005).

Taken together, the results presented here are consistent with a dominant gp130 downstream signaling mechanism that enforces the development of B cell cancers even when activated at the stage of HSPCs.

4.5 The L-gp130 signature in human MM

RNASeq and subsequent data analysis from B cells of young *CD19;L-gp* mice in comparison to age-matched controls revealed the L-gp130 signature, which is defined by the activation of IL-6/JAK/STAT3, PI3K/AKT/MTOR, WNT, MYC, as well as BCR and NF-kappaB signaling (Figure 16C). As all *CD19;L-gp* mice with aging developed B cell cancers, mainly of the Mature and PC phenotypes, it is not surprising that all signaling pathways found to be activated in young *CD19;L-gp* mice, are known to play an important role in human MM. An earlier study by Chesi et al. showed that progression from MGUS to MM was associated with activation of the MYC pathway by demonstrating that both, MYC expression and the MYC signature, were not present in normal PCs, hardly seen in MGUS but present in the majority of MM (Chesi, Robbiani et al. 2008). In the current study, MYC targets were already upregulated in young *CD19;L-gp* mice (Figure 16C) and still showed strong activation in diseased *CD19;L-gp* animals of both phenotypes while this pattern was not seen in sick *Vav1;L-gp* mice (Figure 23B). This finding supports the hypothesis that young *CD19;L-gp* mice are already prone to malignant transformation. Likewise, multiple studies revealed the frequent activation of the PI3K/AKT/MTOR pathway and its impact in the

development and progression of human MM (Hideshima, Nakamura et al. 2001, Pene, Claessens et al. 2002). Sustained overactivation of this pathway was seen in *Vav1;L-gp* tumors in the present study. However, in tumor material from *CD19;L-gp* mice of both phenotypes this axis was rather downregulated (Figure 23B), even though this cascade is also triggered by IL-6/gp130 signaling (Costa-Pereira 2014) and the BCR downstream pathway (Herman and Johnson 2012), that was also seen to be activated in this study (Figure 16C and 23B). The canonical WNT signaling pathway does not only play a major role in early development of B cells (Reya, O'Riordan et al. 2000, Ranheim, Kwan et al. 2005) and is moreover required for normal PC function (Yu, Quinn et al. 2008), its overexpression was also frequently found in MM patients (Derksen, Tjin et al. 2004) (reviewed in (van Andel, Kocemba et al. 2019)). The use of murine GEM models of MM, however, revealed diverging results. While some studies showed that downregulation of WNT signaling promoted tumor growth *in vivo* (Yaccoby, Ling et al. 2007, Edwards, Edwards et al. 2008, Qiang, Shaughnessy et al. 2008), others reported progression of the disease upon activation of this axis (Ashihara, Kawata et al. 2009, Dutta-Simmons, Zhang et al. 2009). This corresponds with outcomes of the current study where WNT signaling was found to be activated in tumors from *Vav1;L-gp* mice and *CD19;L-gp* mice of the PC phenotype but was downregulated in most tumors assessed from *CD19;L-gp* mice with a Mature phenotype (Figure 23B). Yet, a difference in the latency between *CD19;L-gp* animals of the Mature phenotype and the PC phenotype was not seen (Figure 17F). The importance and activation of NF-kappaB signaling in normal B cell development but also in MM patients was described in numerous studies (reviewed in (Keats, Fonseca et al. 2007)). Gene expression analysis in samples from MM patients as well as in MM cell lines revealed constitutive activation of the non-canonical NF-kappaB pathway in several investigations (Annunziata, Davis et al. 2007, Keats, Fonseca et al. 2007, Broyl, Hose et al. 2010). In line with this, activation of NF-kappaB signaling was also seen in the present study, predominantly in *Vav1;L-gp* tumors and *CD19;L-gp* tumors of the PC phenotype (Figure 23B).

Having seen that mice from all x*Cre;L-gp* breedings eventually succumbed to mainly plasma cell neoplasms, publicly available gene expression datasets were mined for the L-gp130 signature in normal human PCs and the diverse disease stages of human MM including MGUS. Thereby the L-gp130 signature was found to be most highly activated in patients suffering from relapsed MM whereas lowest activation was seen in normal PCs (Figure 24). This observation illustrates that the signature defined in the present study on basis of the novel transgenic mouse models is represented in the human disease.

4.6 Limitations of the novel transgenic mouse models of MM

There are several murine models currently used to mimic and study human MM, yet, all of them have their limitations and the ideal model, that would span all aspects of disease biology and genetic build, so far does not exist.

The 5TMM models closely resemble human disease based on the knowledge that interaction with the BMM is crucial for MM development, clonal selection, and genomic instability. The 5T33MM and 5T2MM models are the most characterized and widely used models of the 5TMM series. Upon transplantation of their BM into syngeneic mice, recipients develop the presence of a monoclonal protein and osteolytic bone disease (Radl, De Glopper et al. 1979, Radl, Croese et al. 1988, Radl 1989, Radl 1990, Vanderkerken, De Raeve et al. 1997). Even though malignant transformation occurs rapidly in the BM of recipient animals with an intact immune system, 5T2MM and 5T3MM mice all have myeloma cells derived from the same original donor mice and therefore fail to capture the variability of the human disease. Additionally, they are murine myeloma models in a murine BMM of the host and therefore do not provide insights on the critical interactions between malignant PCs with their own BMM (Manning, Berger et al. 1992, Vanderkerken, De Greef et al. 2000, Vanderkerken, Asosingh et al. 2003, Vlummens, De Veirman et al. 2019).

In the humanized mouse model (SCID-hu) the limitations of the 5TMM models are overcome by reproducing the human BMM when implanting human embryonic bone grafts in the flank of mice and subsequently seeding them with fresh primary human BM explanted cells or human MM cell lines. In this approach, human MM cells grow in an orthotopic full human environment, where BM stromal cells support their proliferation which triggers osteoclasts activity and the development of bone lesions also seen in MM patients (Rossi, Botta et al. 2018). Although high level of tumor engraftment is seen in SCID-hu mice, ethical concerns were raised over the use of human embryonic material in this model. Its major limitations rely on fetal bone chip availability and the fact that fetal BMM does not recapitulate adult BMM with MM being a cancer entity of mostly the elderly (Palumbo and Anderson 2011).

Previous attempts to mimic human MM in mice through overactivation of IL-6 signaling have only led to tumor formation in animals on a BALB/c background (Suematsu, Matsusaka et al. 1992, Dechow, Steidle et al. 2014). However, the BALB/c strain itself is prone to developing PC disorders upon adequate stimuli due to a mutation in the inhibitor of Cdk4/alternative reading frame (INK4a/ARF) locus leading to partial disability of the tumor suppressor protein $p16^{Ink4a}$ (Zhang, DuBois et al. 2001). In contrast, the models described in this study are on a C57BL/6 genetic background, yet, they also have their limitations. The diseases arising in the *xCre;L-gp130* mice were mostly of late B cell stages, however, while IHC analysis revealed the presence of $CD138^{+}$ PCs in virtually every single tumor, only about a half of all tumors analyzed in this study showed a PC phenotype in flow cytometric analyses. While malignant transformation of *CD19;L-gp* (Figure 17A) and *Vav1;L-gp* mice (Figure 22A) occurred fast, *Cg1;L-gp* and *Blimp1;L-gp* animals had a rather long latency (Figures 19A, B). Moreover, MM development could not be triggered in *Cg1;L-gp130* mice by immunization (Chapter 3.8) as it was shown earlier in the Vk*MYC model (Chesi, Robbiani et al. 2008). While other GEM models of MM (*Eμ-xbp-1s*, *Eμ c-Maf,* and Vk*MYC) predominantly develop intramedullary myeloma, where proliferation of clonal PCs is restricted to the BM like it is seen in the majority of MM patients, most of sick *xCre;L-gp* mice in this study showed presence of malignantly transformed cells also outside the BM, mainly in the gastro-intestinal tract. This

extra-medullary dissemination occurs with advanced stages of the disease only in around 6 % of MM patients affecting liver, CNS, kidneys, LNs, and the gastro-intestinal tract amongst others (Soutar, Lucraft et al. 2004, Blade, Fernandez de Larrea et al. 2011, Weinstock and Ghobrial 2013). Additionally, an M-Gradient, which is seen in over 90 % of MM patients at time point of diagnosis (International Myeloma Working 2003), was not consistently detected in the serum of all mice that were analyzed. This non-secretory form of MM was also reported in patients, yet it is a very rare phenomenon (Cavo, Galieni et al. 1985, Blade and Kyle 1999, Middela and Kanse 2009). Therefore, the here described models to some extent represent a minority of MM patients where malignantly transformed PCs are not mainly localized to the BM but to secondary lymphoid organs.

5 Summary

In summary, this study shows the importance of the IL-6/gp130/JAK/STAT3 axis for hematopoietic development as well as B cell differentiation *in vivo* by means of a novel transgenic mouse model on the frequently used C57BL/6 background. Thereby, activation of gp130 signaling targeted to distinct stages of B cell development as well as to the entire hematopoietic system resulted in mature B cell lymphoma and plasma cell neoplasms and was also sufficient to completely abolish activity of a B cell-targeted *Myc* transgene. Gp130 signaling thus provides a selective growth and differentiation advantage for mature B cells and directs lymphomagenesis towards terminally differentiated B cell cancers that are serially transplantable. With MM still being an incurable cancer entity and several mouse models trying to mimic the human disease show their limitations, the present work might lead to finding new ways for treating the disease, especially for the EMM type.

The models generated in this study can be used for testing novel therapeutic approaches targeting the IL-6/gp130/JAK/STAT3 axis in MM and also for investigating gp130 downstream signaling, as a key feature in cancer and many other diseases including autoimmune and inflammatory conditions, in basically any desired tissue. As shown here for *Trp53* and *Myc*, it is thereby easily possible to investigate the impact of certain gene expressions in the IL-6/gp130/JAK/STAT3 context by breeding x*Cre;L-gp* mice to respective transgenic strains.

6 References

Abremski, K. and R. Hoess (1984). "Bacteriophage P1 site-specific recombination. Purification and properties of the Cre recombinase protein." J Biol Chem **259**(3): 1509-1514.

Adams, J. (2004). "The proteasome: a suitable antineoplastic target." Nat Rev Cancer **4**(5): 349-360.

Adams, J. M., A. W. Harris, C. A. Pinkert, L. M. Corcoran, W. S. Alexander, S. Cory, R. D. Palmiter and R. L. Brinster (1985). "The c-myc oncogene driven by immunoglobulin enhancers induces lymphoid malignancy in transgenic mice." Nature **318**(6046): 533-538.

Afshar-Sterle, S., D. Zotos, N. J. Bernard, A. K. Scherger, L. Rodling, A. E. Alsop, J. Walker, F. Masson, G. T. Belz, L. M. Corcoran, L. A. O'Reilly, A. Strasser, M. J. Smyth, R. Johnstone, D. M. Tarlinton, S. L. Nutt and A. Kallies (2014). "Fas ligand-mediated immune surveillance by T cells is essential for the control of spontaneous B cell lymphomas." Nat Med **20**(3): 283-290.

Akira, S., T. Taga and T. Kishimoto (1993). "Interleukin-6 in biology and medicine." Adv Immunol **54**: 1-78.

Alizadeh, A. A., M. B. Eisen, R. E. Davis, C. Ma, I. S. Lossos, A. Rosenwald, J. C. Boldrick, H. Sabet, T. Tran, X. Yu, J. I. Powell, L. Yang, G. E. Marti, T. Moore, J. Hudson, Jr., L. Lu, D. B. Lewis, R. Tibshirani, G. Sherlock, W. C. Chan, T. C. Greiner, D. D. Weisenburger, J. O. Armitage, R. Warnke, R. Levy, W. Wilson, M. R. Grever, J. C. Byrd, D. Botstein, P. O. Brown and L. M. Staudt (2000). "Distinct types of diffuse large B-cell lymphoma identified by gene expression profiling." Nature **403**(6769): 503-511.

Allen, C. D., T. Okada and J. G. Cyster (2007). "Germinal-center organization and cellular dynamics." Immunity **27**(2): 190-202.

Alt, F. W., G. D. Yancopoulos, T. K. Blackwell, C. Wood, E. Thomas, M. Boss, R. Coffman, N. Rosenberg, S. Tonegawa and D. Baltimore (1984). "Ordered rearrangement of immunoglobulin heavy chain variable region segments." EMBO J **3**(6): 1209-1219.

Alvarez, M. J., F. Giorgi, and A. Califano (2014). Using viper, a package for Virtual Inference of Protein-activity by Enriched Regulon analysis. Bioconductor**:** 1-14.

Alvarez, M. J., Y. Shen, F. M. Giorgi, A. Lachmann, B. B. Ding, B. H. Ye and A. Califano (2016). "Functional characterization of somatic mutations in cancer using network-based inference of protein activity." Nat Genet **48**(8): 838-847.

Anastassiadis, K., J. Fu, C. Patsch, S. Hu, S. Weidlich, K. Duerschke, F. Buchholz, F. Edenhofer and A. F. Stewart (2009). "Dre recombinase, like Cre, is a highly efficient site-specific recombinase in E. coli, mammalian cells and mice." Dis Model Mech **2**(9-10): 508-515.

Annunziata, C. M., R. E. Davis, Y. Demchenko, W. Bellamy, A. Gabrea, F. Zhan, G. Lenz, I. Hanamura, G. Wright, W. Xiao, S. Dave, E. M. Hurt, B. Tan, H. Zhao, O. Stephens, M. Santra, D. R. Williams, L. Dang, B. Barlogie, J. D. Shaughnessy, Jr., W. M. Kuehl and L. M. Staudt (2007). "Frequent engagement of the classical and alternative NF-kappaB pathways by diverse genetic abnormalities in multiple myeloma." Cancer Cell **12**(2): 115-130.

Aref, S., T. Goda and M. El-Sherbiny (2003). "Syndecan-1 in multiple myeloma: relationship to conventional prognostic factors." Hematology **8**(4): 221-228.

Ashihara, E., E. Kawata, Y. Nakagawa, C. Shimazaski, J. Kuroda, K. Taniguchi, H. Uchiyama, R. Tanaka, A. Yokota, M. Takeuchi, Y. Kamitsuji, T. Inaba, M. Taniwaki, S. Kimura and T. Maekawa (2009). "beta-catenin small interfering RNA successfully suppressed progression of multiple myeloma in a mouse model." Clin Cancer Res **15**(8): 2731-2738.

Asosingh, K., J. Radl, I. Van Riet, B. Van Camp and K. Vanderkerken (2000). "The 5TMM series: a useful in vivo mouse model of human multiple myeloma." Hematol J **1**(5): 351-356.

Ataie-Kachoie, P., M. H. Pourgholami and D. L. Morris (2013). "Inhibition of the IL-6 signaling pathway: a strategy to combat chronic inflammatory diseases and cancer." Cytokine Growth Factor Rev **24**(2): 163-173.

Ataie-Kachoie, P., M. H. Pourgholami, D. R. Richardson and D. L. Morris (2014). "Gene of the month: Interleukin 6 (IL-6)." J Clin Pathol **67**(11): 932-937.

Auernhammer, C. J., C. Bousquet and S. Melmed (1999). "Autoregulation of pituitary corticotroph SOCS-3 expression: characterization of the murine SOCS-3 promoter." Proc Natl Acad Sci U S A **96**(12): 6964-6969.

Baltimore, D. (1970). "RNA-dependent DNA polymerase in virions of RNA tumour viruses." Nature **226**(5252): 1209-1211.

Barberis, A., K. Widenhorn, L. Vitelli and M. Busslinger (1990). "A novel B-cell lineage-specific transcription factor present at early but not late stages of differentiation." Genes Dev **4**(5): 849-859.

Bataille, R., M. Jourdan, X. G. Zhang and B. Klein (1989). "Serum levels of interleukin 6, a potent myeloma cell growth factor, as a reflect of disease severity in plasma cell dyscrasias." J Clin Invest **84**(6): 2008-2011.

Bazan, J. F. (1990). "Structural design and molecular evolution of a cytokine receptor superfamily." Proc Natl Acad Sci U S A **87**(18): 6934-6938.

Becker, S., B. Groner and C. W. Muller (1998). "Three-dimensional structure of the Stat3beta homodimer bound to DNA." Nature **394**(6689): 145-151.

Belgardt, B. F., A. Husch, E. Rother, M. B. Ernst, F. T. Wunderlich, B. Hampel, T. Klockener, D. Alessi, P. Kloppenburg and J. C. Bruning (2008). "PDK1 deficiency in POMC-expressing cells reveals FOXO1-dependent and -independent pathways in control of energy homeostasis and stress response." Cell Metab **7**(4): 291-301.

Bende, R. J., F. van Maldegem and C. J. van Noesel (2009). "Chronic inflammatory disease, lymphoid tissue neogenesis and extranodal marginal zone B-cell lymphomas." Haematologica **94**(8): 1109-1123.

Benekli, M., M. R. Baer, H. Baumann and M. Wetzler (2003). "Signal transducer and activator of transcription proteins in leukemias." Blood **101**(8): 2940-2954.

Berek, C., A. Berger and M. Apel (1991). "Maturation of the immune response in germinal centers." Cell **67**(6): 1121-1129.

Bernad, A., M. Kopf, R. Kulbacki, N. Weich, G. Koehler and J. C. Gutierrez-Ramos (1994). "Interleukin-6 is required in vivo for the regulation of stem cells and committed progenitors of the hematopoietic system." Immunity **1**(9): 725-731.

Blade, J., C. Fernandez de Larrea, L. Rosinol, M. T. Cibeira, R. Jimenez and R. Powles (2011). "Soft-tissue plasmacytomas in multiple myeloma: incidence, mechanisms of extramedullary spread, and treatment approach." J Clin Oncol **29**(28): 3805-3812.

Blade, J. and R. A. Kyle (1999). "Nonsecretory myeloma, immunoglobulin D myeloma, and plasma cell leukemia." Hematol Oncol Clin North Am **13**(6): 1259-1272.

Botta, C., M. T. Di Martino, D. Ciliberto, M. Cuce, P. Correale, M. Rossi, P. Tagliaferri and P. Tassone (2016). "A gene expression inflammatory signature specifically predicts multiple myeloma evolution and patients survival." Blood Cancer J **6**(12): e511.

Boulanger, M. J., D. C. Chow, E. E. Brevnova and K. C. Garcia (2003). "Hexameric structure and assembly of the interleukin-6/IL-6 alpha-receptor/gp130 complex." Science **300**(5628): 2101-2104.

Bradford, M. M. (1976). "A rapid and sensitive method for the quantitation of microgram quantities of protein utilizing the principle of protein-dye binding." Anal Biochem **72**: 248-254.

Brighton, T. A., A. Khot, S. J. Harrison, D. Ghez, B. M. Weiss, A. Kirsch, H. Magen, M. Gironella, A. Oriol, M. Streetly, B. Kranenburg, X. Qin, R. Bandekar, P. Hu, M. Guilfoyle, M. Qi, S. Nemat and H. Goldschmidt (2019). "Randomized, Double-Blind, Placebo-Controlled, Multicenter Study of Siltuximab in High-Risk Smoldering Multiple Myeloma." Clin Cancer Res **25**(13): 3772-3775.

Bromberg, J. and J. E. Darnell, Jr. (2000). "The role of STATs in transcriptional control and their impact on cellular function." Oncogene **19**(21): 2468-2473.

Broyl, A., D. Hose, H. Lokhorst, Y. de Knegt, J. Peeters, A. Jauch, U. Bertsch, A. Buijs, M. Stevens-Kroef, H. B. Beverloo, E. Vellenga, S. Zweegman, M. J. Kersten, B. van der Holt, L. el Jarari, G. Mulligan, H. Goldschmidt, M. van Duin and P. Sonneveld (2010). "Gene expression profiling for molecular classification of multiple myeloma in newly diagnosed patients." Blood **116**(14): 2543-2553.

Brudno, J. N. and J. N. Kochenderfer (2016). "Toxicities of chimeric antigen receptor T cells: recognition and management." Blood **127**(26): 3321-3330.

Buettner, R., L. B. Mora and R. Jove (2002). "Activated STAT signaling in human tumors provides novel molecular targets for therapeutic intervention." Clin Cancer Res **8**(4): 945-954.

Busslinger, M. (2004). "Transcriptional control of early B cell development." Annu Rev Immunol **22**: 55-79.

Bustin, S. A. and R. Mueller (2005). "Real-time reverse transcription PCR (qRT-PCR) and its potential use in clinical diagnosis." Clin Sci (Lond) **109**(4): 365-379.

Calame, K. L. (2001). "Plasma cells: finding new light at the end of B cell development." Nat Immunol **2**(12): 1103-1108.

Caligaris-Cappio, F., L. Bergui, M. G. Gregoretti, G. Gaidano, M. Gaboli, M. Schena, A. Z. Zallone and P. C. Marchisio (1991). "'Role of bone marrow stromal cells in the growth of human multiple myeloma." Blood **77**(12): 2688-2693.

Caron, G., S. Le Gallou, T. Lamy, K. Tarte and T. Fest (2009). "CXCR4 expression functionally discriminates centroblasts versus centrocytes within human germinal center B cells." J Immunol **182**(12): 7595-7602.

Carrasco, D. R., K. Sukhdeo, M. Protopopova, R. Sinha, M. Enos, D. E. Carrasco, M. Zheng, M. Mani, J. Henderson, G. S. Pinkus, N. Munshi, J. Horner, E. V. Ivanova, A. Protopopov, K. C. Anderson, G. Tonon and R. A. DePinho (2007). "The differentiation and stress response factor XBP-1 drives multiple myeloma pathogenesis." Cancer Cell **11**(4): 349-360.

Casola, S., G. Cattoretti, N. Uyttersprot, S. B. Koralov, J. Seagal, Z. Hao, A. Waisman, A. Egert, D. Ghitza and K. Rajewsky (2006). "Tracking germinal center B cells expressing germ-line immunoglobulin gamma1 transcripts by conditional gene targeting." Proc Natl Acad Sci U S A **103**(19): 7396-7401.

Catlett-Falcone, R., T. H. Landowski, M. M. Oshiro, J. Turkson, A. Levitzki, R. Savino, G. Ciliberto, L. Moscinski, J. L. Fernandez-Luna, G. Nunez, W. S. Dalton and R. Jove (1999). "Constitutive activation of

Stat3 signaling confers resistance to apoptosis in human U266 myeloma cells." Immunity **10**(1): 105-115.

Cattoretti, G., C. C. Chang, K. Cechova, J. Zhang, B. H. Ye, B. Falini, D. C. Louie, K. Offit, R. S. Chaganti and R. Dalla-Favera (1995). "BCL-6 protein is expressed in germinal-center B cells." Blood **86**(1): 45-53.

Cavo, M., P. Galieni, M. Gobbi, L. Baldrati, L. Leardini, M. Baccarani and S. Tura (1985). "Nonsecretory multiple myeloma. Presenting findings, clinical course and prognosis." Acta Haematol **74**(1): 27-30.

Chapuy, B., C. Stewart, A. J. Dunford, J. Kim, A. Kamburov, R. A. Redd, M. S. Lawrence, M. G. M. Roemer, A. J. Li, M. Ziepert, A. M. Staiger, J. A. Wala, M. D. Ducar, I. Leshchiner, E. Rheinbay, A. Taylor-Weiner, C. A. Coughlin, J. M. Hess, C. S. Pedamallu, D. Livitz, D. Rosebrock, M. Rosenberg, A. A. Tracy, H. Horn, P. van Hummelen, A. L. Feldman, B. K. Link, A. J. Novak, J. R. Cerhan, T. M. Habermann, R. Siebert, A. Rosenwald, A. R. Thorner, M. L. Meyerson, T. R. Golub, R. Beroukhim, G. G. Wulf, G. Ott, S. J. Rodig, S. Monti, D. S. Neuberg, M. Loeffler, M. Pfreundschuh, L. Trumper, G. Getz and M. A. Shipp (2018). "Molecular subtypes of diffuse large B cell lymphoma are associated with distinct pathogenic mechanisms and outcomes." Nature Medicine **24**(5): 679-+.

Chauveau, D. and G. Choukroun (1996). "Bence Jones proteinuria and myeloma kidney." Nephrol Dial Transplant **11**(3): 413-415.

Chen, W. and G. K. Khurana Hershey (2007). "Signal transducer and activator of transcription signals in allergic disease." J Allergy Clin Immunol **119**(3): 529-541; quiz 542-523.

Chen, X., U. Vinkemeier, Y. Zhao, D. Jeruzalmi, J. E. Darnell, Jr. and J. Kuriyan (1998). "Crystal structure of a tyrosine phosphorylated STAT-1 dimer bound to DNA." Cell **93**(5): 827-839.

Chesi, M., P. L. Bergsagel, O. O. Shonukan, M. L. Martelli, L. A. Brents, T. Chen, E. Schrock, T. Ried and W. M. Kuehl (1998). "Frequent dysregulation of the c-maf proto-oncogene at 16q23 by translocation to an Ig locus in multiple myeloma." Blood **91**(12): 4457-4463.

Chesi, M., G. M. Matthews, V. M. Garbitt, S. E. Palmer, J. Shortt, M. Lefebure, A. K. Stewart, R. W. Johnstone and P. L. Bergsagel (2012). "Drug response in a genetically engineered mouse model of multiple myeloma is predictive of clinical efficacy." Blood **120**(2): 376-385.

Chesi, M., D. F. Robbiani, M. Sebag, W. J. Chng, M. Affer, R. Tiedemann, R. Valdez, S. E. Palmer, S. S. Haas, A. K. Stewart, R. Fonseca, R. Kremer, G. Cattoretti and P. L. Bergsagel (2008). "AID-dependent activation of a MYC transgene induces multiple myeloma in a conditional mouse model of post-germinal center malignancies." Cancer Cell **13**(2): 167-180.

Chilosi, M., F. Adami, M. Lestani, L. Montagna, L. Cimarosto, G. Semenzato, G. Pizzolo and F. Menestrina (1999). "CD138/syndecan-1: a useful immunohistochemical marker of normal and neoplastic plasma cells on routine trephine bone marrow biopsies." Mod Pathol **12**(12): 1101-1106.

Cobaleda, C., A. Schebesta, A. Delogu and M. Busslinger (2007). "Pax5: the guardian of B cell identity and function." Nat Immunol **8**(5): 463-470.

Coffin, J. M. (1992). Structure and Classification of retroviruses. Plenum Press, New York.

Costa-Pereira, A. P. (2014). "Regulation of IL-6-type cytokine responses by MAPKs." Biochem Soc Trans **42**(1): 59-62.

Dalby, B., S. Cates, A. Harris, E. C. Ohki, M. L. Tilkins, P. J. Price and V. C. Ciccarone (2004). "Advanced transfection with Lipofectamine 2000 reagent: primary neurons, siRNA, and high-throughput applications." Methods **33**(2): 95-103.

Darnell, J. E., Jr. (1997). "STATs and gene regulation." Science **277**(5332): 1630-1635.

Davis, H. E., J. R. Morgan and M. L. Yarmush (2002). "Polybrene increases retrovirus gene transfer efficiency by enhancing receptor-independent virus adsorption on target cell membranes." Biophys Chem **97**(2-3): 159-172.

de Boer, J., A. Williams, G. Skavdis, N. Harker, M. Coles, M. Tolaini, T. Norton, K. Williams, K. Roderick, A. J. Potocnik and D. Kioussis (2003). "Transgenic mice with hematopoietic and lymphoid specific expression of Cre." Eur J Immunol **33**(2): 314-325.

de Oliveira, M. B., V. L. Fook-Alves, A. I. P. Eugenio, R. C. Fernando, L. F. G. Sanson, M. F. de Carvalho, W. M. T. Braga, F. E. Davies and G. W. B. Colleoni (2017). "Anti-myeloma effects of ruxolitinib combined with bortezomib and lenalidomide: A rationale for JAK/STAT pathway inhibition in myeloma patients." Cancer Lett **403**: 206-215.

Dechow, T., S. Steidle, K. S. Gotze, M. Rudelius, K. Behnke, K. Pechloff, S. Kratzat, L. Bullinger, F. Fend, V. Soberon, N. Mitova, Z. Li, M. Thaler, J. Bauer, E. Pietschmann, C. Albers, R. Grundler, M. Schmidt-Supprian, J. Ruland, C. Peschel, J. Duyster, S. Rose-John, F. Bassermann and U. Keller (2014). "GP130 activation induces myeloma and collaborates with MYC." J Clin Invest **124**(12): 5263-5274.

Del Nagro, C. J., D. C. Otero, A. N. Anzelon, S. A. Omori, R. V. Kolla and R. C. Rickert (2005). "CD19 function in central and peripheral B-cell development." Immunol Res **31**(2): 119-131.

Derksen, P. W., E. Tjin, H. P. Meijer, M. D. Klok, H. D. MacGillavry, M. H. van Oers, H. M. Lokhorst, A. C. Bloem, H. Clevers, R. Nusse, R. van der Neut, M. Spaargaren and S. T. Pals (2004). "Illegitimate WNT signaling promotes proliferation of multiple myeloma cells." Proc Natl Acad Sci U S A **101**(16): 6122-6127.

Derudder, E., E. J. Cadera, J. C. Vahl, J. Wang, C. J. Fox, S. Zha, G. van Loo, M. Pasparakis, M. S. Schlissel, M. Schmidt-Supprian and K. Rajewsky (2009). "Development of immunoglobulin lambda-chain-positive B cells, but not editing of immunoglobulin kappa-chain, depends on NF-kappaB signals." Nat Immunol **10**(6): 647-654.

Dimopoulos, M. A. and G. Hamilos (2002). "Solitary bone plasmacytoma and extramedullary plasmacytoma." Curr Treat Options Oncol **3**(3): 255-259.

Dimopoulos, M. A., L. A. Moulopoulos, A. Maniatis and R. Alexanian (2000). "Solitary plasmacytoma of bone and asymptomatic multiple myeloma." Blood **96**(6): 2037-2044.

Dominguez-Sola, D., G. D. Victora, C. Y. Ying, R. T. Phan, M. Saito, M. C. Nussenzweig and R. Dalla-Favera (2012). "The proto-oncogene MYC is required for selection in the germinal center and cyclic reentry." Nature Immunology **13**(11): 1083-1091.

Donehower, L. A., M. Harvey, B. L. Slagle, M. J. McArthur, C. A. Montgomery, Jr., J. S. Butel and A. Bradley (1992). "Mice deficient for p53 are developmentally normal but susceptible to spontaneous tumours." Nature **356**(6366): 215-221.

Dorshkind, K. (2002). "Multilineage development from adult bone marrow cells." Nat Immunol **3**(4): 311-313.

Drappatz, J. and T. Batchelor (2004). "Neurologic complications of plasma cell disorders." Clin Lymphoma **5**(3): 163-171.

Durie, B. G. and S. E. Salmon (1975). "A clinical staging system for multiple myeloma. Correlation of measured myeloma cell mass with presenting clinical features, response to treatment, and survival." Cancer **36**(3): 842-854.

Dutta-Simmons, J., Y. Zhang, G. Gorgun, M. Gatt, M. Mani, T. Hideshima, K. Takada, N. E. Carlson, D. E. Carrasco, Y. T. Tai, N. Raje, A. G. Letai, K. C. Anderson and D. R. Carrasco (2009). "Aurora kinase A is a target of Wnt/beta-catenin involved in multiple myeloma disease progression." Blood **114**(13): 2699-2708.

Edwards, C. M., J. R. Edwards, S. T. Lwin, J. Esparza, B. O. Oyajobi, B. McCluskey, S. Munoz, B. Grubbs and G. R. Mundy (2008). "Increasing Wnt signaling in the bone marrow microenvironment inhibits the development of myeloma bone disease and reduces tumor burden in bone in vivo." Blood **111**(5): 2833-2842.

Ehlers, M., J. Grotzinger, F. D. deHon, J. Mullberg, J. P. Brakenhoff, J. Liu, A. Wollmer and S. Rose-John (1994). "Identification of two novel regions of human IL-6 responsible for receptor binding and signal transduction." J Immunol **153**(4): 1744-1753.

Enders, A., A. Short, L. A. Miosge, H. Bergmann, Y. Sontani, E. M. Bertram, B. Whittle, B. Balakishnan, K. Yoshida, G. Sjollema, M. A. Field, T. D. Andrews, H. Hagiwara and C. C. Goodnow (2014). "Zinc-finger protein ZFP318 is essential for expression of IgD, the alternatively spliced Igh product made by mature B lymphocytes." Proc Natl Acad Sci U S A **111**(12): 4513-4518.

Engelhardt, M., E. Terpos, M. Kleber, F. Gay, R. Wasch, G. Morgan, M. Cavo, N. van de Donk, A. Beilhack, B. Bruno, H. E. Johnsen, R. Hajek, C. Driessen, H. Ludwig, M. Beksac, M. Boccadoro, C. Straka, S. Brighen, M. Gramatzki, A. Larocca, H. Lokhorst, V. Magarotto, F. Morabito, M. A. Dimopoulos, H. Einsele, P. Sonneveld, A. Palumbo and N. European Myeloma (2014). "European Myeloma Network recommendations on the evaluation and treatment of newly diagnosed patients with multiple myeloma." Haematologica **99**(2): 232-242.

Engvall, E. and P. Perlmann (1971). "Enzyme-linked immunosorbent assay (ELISA). Quantitative assay of immunoglobulin G." Immunochemistry **8**(9): 871-874.

Feng, X., L. Zhang, C. Acharya, G. An, K. Wen, L. Qiu, N. C. Munshi, Y. T. Tai and K. C. Anderson (2017). "Targeting CD38 Suppresses Induction and Function of T Regulatory Cells to Mitigate Immunosuppression in Multiple Myeloma." Clin Cancer Res **23**(15): 4290-4300.

Fonseca, R., B. Barlogie, R. Bataille, C. Bastard, P. L. Bergsagel, M. Chesi, F. E. Davies, J. Drach, P. R. Greipp, I. R. Kirsch, W. M. Kuehl, J. M. Hernandez, S. Minvielle, L. M. Pilarski, J. D. Shaughnessy, Jr., A. K. Stewart and H. Avet-Loiseau (2004). "Genetics and cytogenetics of multiple myeloma: a workshop report." Cancer Res **64**(4): 1546-1558.

Fonseca, R., P. L. Bergsagel, J. Drach, J. Shaughnessy, N. Gutierrez, A. K. Stewart, G. Morgan, B. Van Ness, M. Chesi, S. Minvielle, A. Neri, B. Barlogie, W. M. Kuehl, P. Liebisch, F. Davies, S. Chen-Kiang, B. G. Durie, R. Carrasco, O. Sezer, T. Reiman, L. Pilarski, H. Avet-Loiseau and G. International Myeloma Working (2009). "International Myeloma Working Group molecular classification of multiple myeloma: spotlight review." Leukemia **23**(12): 2210-2221.

Fonseca, R., E. A. Blood, M. M. Oken, R. A. Kyle, G. W. Dewald, R. J. Bailey, S. A. Van Wier, K. J. Henderson, J. D. Hoyer, D. Harrington, N. E. Kay, B. Van Ness and P. R. Greipp (2002). "Myeloma and the t(11;14)(q13;q32); evidence for a biologically defined unique subset of patients." Blood **99**(10): 3735-3741.

Frassanito, M. A., A. Cusmai, G. Iodice and F. Dammacco (2001). "Autocrine interleukin-6 production and highly malignant multiple myeloma: relation with resistance to drug-induced apoptosis." Blood **97**(2): 483-489.

Fuxa, M. and M. Busslinger (2007). "Reporter gene insertions reveal a strictly B lymphoid-specific expression pattern of Pax5 in support of its B cell identity function." J Immunol **178**(12): 8222-8228.

Galson, D. L., R. Silbermann and G. D. Roodman (2012). "Mechanisms of multiple myeloma bone disease." Bonekey Rep **1**: 135.

Garbers, C., S. Heink, T. Korn and S. Rose-John (2018). "Interleukin-6: designing specific therapeutics for a complex cytokine." Nat Rev Drug Discov **17**(6): 395-412.

Gearing, D. P., M. R. Comeau, D. J. Friend, S. D. Gimpel, C. J. Thut, J. McGourty, K. K. Brasher, J. A. King, S. Gillis, B. Mosley and et al. (1992). "The IL-6 signal transducer, gp130: an oncostatin M receptor and affinity converter for the LIF receptor." Science **255**(5050): 1434-1437.

George, E. D. and R. Sadovsky (1999). "Multiple myeloma: recognition and management." Am Fam Physician **59**(7): 1885-1894.

Georgopoulos, K. (2002). "Haematopoietic cell-fate decisions, chromatin regulation and ikaros." Nat Rev Immunol **2**(3): 162-174.

Ghermezi, M., T. M. Spektor and J. R. Berenson (2019). "The role of JAK inhibitors in multiple myeloma." Clin Adv Hematol Oncol **17**(9): 500-505.

Giles, A. J., T. P. Bender and K. S. Ravichandran (2009). "The adaptor protein Shc plays a key role during early B cell development." J Immunol **183**(9): 5468-5476.

Guang, M. H. Z., A. McCann, G. Bianchi, L. Zhang, P. Dowling, D. Bazou, P. O'Gorman and K. C. Anderson (2018). "Overcoming multiple myeloma drug resistance in the era of cancer 'omics'." Leuk Lymphoma **59**(3): 542-561.

Gutnik, S. H. and B. R. Bacon (1985). "Endoscopic appearance of gastric myeloma." Gastrointest Endosc **31**(4): 263-265.

Hallek, M., P. L. Bergsagel and K. C. Anderson (1998). "Multiple myeloma: increasing evidence for a multistep transformation process." Blood **91**(1): 3-21.

Han, H., J. W. Cho, S. Lee, A. Yun, H. Kim, D. Bae, S. Yang, C. Y. Kim, M. Lee, E. Kim, S. Lee, B. Kang, D. Jeong, Y. Kim, H. N. Jeon, H. Jung, S. Nam, M. Chung, J. H. Kim and I. Lee (2018). "TRRUST v2: an expanded reference database of human and mouse transcriptional regulatory interactions." Nucleic Acids Res **46**(D1): D380-D386.

He, B., L. You, K. Uematsu, K. Zang, Z. Xu, A. Y. Lee, J. F. Costello, F. McCormick and D. M. Jablons (2003). "SOCS-3 is frequently silenced by hypermethylation and suppresses cell growth in human lung cancer." Proc Natl Acad Sci U S A **100**(24): 14133-14138.

Heinrich, P. C., I. Behrmann, S. Haan, H. M. Hermanns, G. Muller-Newen and F. Schaper (2003). "Principles of interleukin (IL)-6-type cytokine signalling and its regulation." Biochem J **374**(Pt 1): 1-20.

Heinrich, P. C., I. Behrmann, G. Muller-Newen, F. Schaper and L. Graeve (1998). "Interleukin-6-type cytokine signalling through the gp130/Jak/STAT pathway." Biochem J **334 (Pt 2)**: 297-314.

Heinrich, P. C., J. V. Castell and T. Andus (1990). "Interleukin-6 and the acute phase response." Biochem J **265**(3): 621-636.

Herman, S. E. and A. J. Johnson (2012). "Molecular pathways: targeting phosphoinositide 3-kinase p110-delta in chronic lymphocytic leukemia." Clin Cancer Res **18**(15): 4013-4018.

Hibi, M., M. Murakami, M. Saito, T. Hirano, T. Taga and T. Kishimoto (1990). "Molecular cloning and expression of an IL-6 signal transducer, gp130." Cell **63**(6): 1149-1157.

Hideshima, T. and K. C. Anderson (2002). "Molecular mechanisms of novel therapeutic approaches for multiple myeloma." Nat Rev Cancer **2**(12): 927-937.

Hideshima, T., N. Nakamura, D. Chauhan and K. C. Anderson (2001). "Biologic sequelae of interleukin-6 induced PI3-K/Akt signaling in multiple myeloma." Oncogene **20**(42): 5991-6000.

Hirano, T. (1992). "The biology of interleukin-6." Chem Immunol **51**: 153-180.

Hirano, T. (1994). The Cytokine Handbook. London, Academic Press.

Hirano, T., K. Yasukawa, H. Harada, T. Taga, Y. Watanabe, T. Matsuda, S. Kashiwamura, K. Nakajima, K. Koyama, A. Iwamatsu, S. Tsunasawa, F. Sakiyama, H. Matsui, Y. Takahara, T. Taniguchi and T. Kishimoto (1986). "Complementary-DNA for a Novel Human Interleukin (Bsf-2) That Induces Lymphocytes-B to Produce Immunoglobulin." Nature **324**(6092): 73-76.

Hirano, T. a. K., T. (1990). Handbook of Experimental Pharmacology. Berlin, Springer-Verlag.

Hunter, C. A. and S. A. Jones (2015). "IL-6 as a keystone cytokine in health and disease." Nat Immunol **16**(5): 448-457.

Ihle, J. N. (2001). "The Stat family in cytokine signaling." Curr Opin Cell Biol **13**(2): 211-217.

International Myeloma Working, G. (2003). "Criteria for the classification of monoclonal gammopathies, multiple myeloma and related disorders: a report of the International Myeloma Working Group." Br J Haematol **121**(5): 749-757.

Ip, N. Y., S. H. Nye, T. G. Boulton, S. Davis, T. Taga, Y. Li, S. J. Birren, K. Yasukawa, T. Kishimoto, D. J. Anderson and et al. (1992). "CNTF and LIF act on neuronal cells via shared signaling pathways that involve the IL-6 signal transducing receptor component gp130." Cell **69**(7): 1121-1132.

Isomoto, H., J. L. Mott, S. Kobayashi, N. W. Werneburg, S. F. Bronk, S. Haan and G. J. Gores (2007). "Sustained IL-6/STAT-3 signaling in cholangiocarcinoma cells due to SOCS-3 epigenetic silencing." Gastroenterology **132**(1): 384-396.

Istvanffy, R., M. Kroger, C. Eckl, S. Gitzelmann, B. Vilne, F. Bock, S. Graf, M. Schiemann, U. B. Keller, C. Peschel and R. A. Oostendorp (2011). "Stromal pleiotrophin regulates repopulation behavior of hematopoietic stem cells." Blood **118**(10): 2712-2722.

Jacks, T., L. Remington, B. O. Williams, E. M. Schmitt, S. Halachmi, R. T. Bronson and R. A. Weinberg (1994). "Tumor spectrum analysis in p53-mutant mice." Curr Biol **4**(1): 1-7.

Jacob, J. and G. Kelsoe (1992). "In situ studies of the primary immune response to (4-hydroxy-3-nitrophenyl)acetyl. II. A common clonal origin for periarteriolar lymphoid sheath-associated foci and germinal centers." J Exp Med **176**(3): 679-687.

Jacob, J., G. Kelsoe, K. Rajewsky and U. Weiss (1991). "Intraclonal generation of antibody mutants in germinal centres." Nature **354**(6352): 389-392.

Jelinek, T. and R. Hajek (2016). "Monoclonal antibodies - A new era in the treatment of multiple myeloma." Blood Rev **30**(2): 101-110.

Jenkins, B. J., A. W. Roberts, M. Najdovska, D. Grail and M. Ernst (2005). "The threshold of gp130-dependent STAT3 signaling is critical for normal regulation of hematopoiesis." Blood **105**(9): 3512-3520.

Jiang, H., W. Zhang, P. Shang, H. Zhang, W. Fu, F. Ye, T. Zeng, H. Huang, X. Zhang, W. Sun, D. Man-Yuen Sze, Q. Yi and J. Hou (2014). "Transfection of chimeric anti-CD138 gene enhances natural killer cell activation and killing of multiple myeloma cells." Mol Oncol **8**(2): 297-310.

Jones, S. A., S. Horiuchi, N. Topley, N. Yamamoto and G. M. Fuller (2001). "The soluble interleukin 6 receptor: mechanisms of production and implications in disease." FASEB J **15**(1): 43-58.

Jourdan, M., A. Caraux, G. Caron, N. Robert, G. Fiol, T. Reme, K. Bollore, J. P. Vendrell, S. Le Gallou, F. Mourcin, J. De Vos, A. Kassambara, C. Duperray, D. Hose, T. Fest, K. Tarte and B. Klein (2011). "Characterization of a transitional preplasmablast population in the process of human B cell to plasma cell differentiation." J Immunol **187**(8): 3931-3941.

Jourdan, M., A. Caraux, J. De Vos, G. Fiol, M. Larroque, C. Cognot, C. Bret, C. Duperray, D. Hose and B. Klein (2009). "An in vitro model of differentiation of memory B cells into plasmablasts and plasma cells including detailed phenotypic and molecular characterization." Blood **114**(25): 5173-5181.

Jourdan, M., M. Cren, N. Robert, K. Bollore, T. Fest, C. Duperray, F. Guilloton, D. Hose, K. Tarte and B. Klein (2014). "IL-6 supports the generation of human long-lived plasma cells in combination with either APRIL or stromal cell-soluble factors." Leukemia **28**(8): 1647-1656.

Jozefczuk, J., K. Drews and J. Adjaye (2012). "Preparation of mouse embryonic fibroblast cells suitable for culturing human embryonic and induced pluripotent stem cells." J Vis Exp(64).

Jung, D., C. Giallourakis, R. Mostoslavsky and F. W. Alt (2006). "Mechanism and control of V(D)J recombination at the immunoglobulin heavy chain locus." Annu Rev Immunol **24**: 541-570.

Kallies, A., J. Hasbold, K. Fairfax, C. Pridans, D. Emslie, B. S. McKenzie, A. M. Lew, L. M. Corcoran, P. D. Hodgkin, D. M. Tarlinton and S. L. Nutt (2007). "Initiation of plasma-cell differentiation is independent of the transcription factor Blimp-1." Immunity **26**(5): 555-566.

Karasuyama, H., A. Rolink, Y. Shinkai, F. Young, F. W. Alt and F. Melchers (1994). "The expression of Vpre-B/lambda 5 surrogate light chain in early bone marrow precursor B cells of normal and B cell-deficient mutant mice." Cell **77**(1): 133-143.

Kawano, M., T. Hirano, T. Matsuda, T. Taga, Y. Horii, K. Iwato, H. Asaoku, B. Tang, O. Tanabe, H. Tanaka and et al. (1988). "Autocrine generation and requirement of BSF-2/IL-6 for human multiple myelomas." Nature **332**(6159): 83-85.

Keats, J. J., R. Fonseca, M. Chesi, R. Schop, A. Baker, W. J. Chng, S. Van Wier, R. Tiedemann, C. X. Shi, M. Sebag, E. Braggio, T. Henry, Y. X. Zhu, H. Fogle, T. Price-Troska, G. Ahmann, C. Mancini, L. A. Brents, S. Kumar, P. Greipp, A. Dispenzieri, B. Bryant, G. Mulligan, L. Bruhn, M. Barrett, R. Valdez, J. Trent, A. K. Stewart, J. Carpten and P. L. Bergsagel (2007). "Promiscuous mutations activate the noncanonical NF-kappaB pathway in multiple myeloma." Cancer Cell **12**(2): 131-144.

Kilciksiz, S., O. Karakoyun-Celik, F. Y. Agaoglu and A. Haydaroglu (2012). "A review for solitary plasmacytoma of bone and extramedullary plasmacytoma." ScientificWorldJournal **2012**: 895765.

Kisseleva, T., S. Bhattacharya, J. Braunstein and C. W. Schindler (2002). "Signaling through the JAK/STAT pathway, recent advances and future challenges." Gene **285**(1-2): 1-24.

Klein, B., X. G. Zhang, Z. Y. Lu and R. Bataille (1995). "Interleukin-6 in human multiple myeloma." Blood **85**(4): 863-872.

Klein, U. and R. Dalla-Favera (2008). "Germinal centres: role in B-cell physiology and malignancy." Nat Rev Immunol **8**(1): 22-33.

Klein, U., Y. Tu, G. A. Stolovitzky, J. L. Keller, J. Haddad, Jr., V. Miljkovic, G. Cattoretti, A. Califano and R. Dalla-Favera (2003). "Transcriptional analysis of the B cell germinal center reaction." Proc Natl Acad Sci U S A **100**(5): 2639-2644.

Knowling, M. A., A. R. Harwood and D. E. Bergsagel (1983). "Comparison of extramedullary plasmacytomas with solitary and multiple plasma cell tumors of bone." J Clin Oncol **1**(4): 255-262.

Kolde, R. (2015). pheatmap: Pretty Heatmaps. https://CRAN.R-project.org/package=pheatmap, *R package version*. **1.0.8**.

Kondo, M. (2010). "Lymphoid and myeloid lineage commitment in multipotent hematopoietic progenitors." Immunol Rev **238**(1): 37-46.

Kopf, M., H. Baumann, G. Freer, M. Freudenberg, M. Lamers, T. Kishimoto, R. Zinkernagel, H. Bluethmann and G. Kohler (1994). "Impaired immune and acute-phase responses in interleukin-6-deficient mice." Nature **368**(6469): 339-342.

Kopf, M., S. Herren, M. V. Wiles, M. B. Pepys and M. H. Kosco-Vilbois (1998). "Interleukin 6 influences germinal center development and antibody production via a contribution of C3 complement component." J Exp Med **188**(10): 1895-1906.

Korde, N., S. Y. Kristinsson and O. Landgren (2011). "Monoclonal gammopathy of undetermined significance (MGUS) and smoldering multiple myeloma (SMM): novel biological insights and development of early treatment strategies." Blood **117**(21): 5573-5581.

Kucuk, C., B. Jiang, X. Z. Hu, W. Y. Zhang, J. K. C. Chan, W. M. Xiao, N. Lack, C. Alkan, J. C. Williams, K. N. Avery, P. Kavak, A. Scuto, E. Sen, P. Gaulard, L. Staudt, J. Iqbal, W. W. Zhang, A. Cornish, Q. Gong, Q. P. Yang, H. Sun, F. d'Amore, S. Leppa, W. P. Liu, K. Fu, L. de Leval, T. McKeithan and W. C. Chan (2015). "Activating mutations of STAT5B and STAT3 in lymphomas derived from gamma delta-T or NK cells." Nature Communications **6**.

Kuehl, W. M. and P. L. Bergsagel (2002). "Multiple myeloma: evolving genetic events and host interactions." Nat Rev Cancer **2**(3): 175-187.

Kumanogoh, A., S. Marukawa, T. Kumanogoh, H. Hirota, K. Yoshida, I. S. Lee, T. Yasui, K. Yoshida, T. Taga and T. Kishimoto (1997). "Impairment of antigen-specific antibody production in transgenic mice expressing a dominant-negative form of gp130." Proceedings of the National Academy of Sciences of the United States of America **94**(6): 2478-2482.

Kumar, S., R. Fonseca, R. P. Ketterling, A. Dispenzieri, M. Q. Lacy, M. A. Gertz, S. R. Hayman, F. K. Buadi, D. Dingli, R. A. Knudson, A. Greenberg, S. J. Russell, S. R. Zeldenrust, J. A. Lust, R. A. Kyle, L. Bergsagel and S. V. Rajkumar (2012). "Trisomies in multiple myeloma: impact on survival in patients with high-risk cytogenetics." Blood **119**(9): 2100-2105.

Kumar, S. K., S. V. Rajkumar, A. Dispenzieri, M. Q. Lacy, S. R. Hayman, F. K. Buadi, S. R. Zeldenrust, D. Dingli, S. J. Russell, J. A. Lust, P. R. Greipp, R. A. Kyle and M. A. Gertz (2008). "Improved survival in multiple myeloma and the impact of novel therapies." Blood **111**(5): 2516-2520.

Kyle, R. A. and P. A. Greipp (1988). "Plasma cell dyscrasias: current status." Crit Rev Oncol Hematol **8**(2): 93-152.

Kyle, R. A. and S. V. Rajkumar (2004). "Multiple myeloma." N Engl J Med **351**(18): 1860-1873.

Kyle, R. A. and S. V. Rajkumar (2006). "Monoclonal gammopathy of undetermined significance." Br J Haematol **134**(6): 573-589.

Kyrtsonis, M. C., G. Dedoussis, C. Zervas, V. Perifanis, C. Baxevanis, M. Stamatelou and A. Maniatis (1996). "Soluble interleukin-6 receptor (sIL-6R), a new prognostic factor in multiple myeloma." Br J Haematol **93**(2): 398-400.

Lakso, M., B. Sauer, B. Mosinger, Jr., E. J. Lee, R. W. Manning, S. H. Yu, K. L. Mulder and H. Westphal (1992). "Targeted oncogene activation by site-specific recombination in transgenic mice." Proc Natl Acad Sci U S A **89**(14): 6232-6236.

LeBien, T. W. (2000). "Fates of human B-cell precursors." Blood **96**(1): 9-23.

Lee, H. C., K. Patel, P. Kongtim, S. Parmar, P. Lin, M.H. Qazilbash, S. Thomas and E.E. Manasanch (2016). Multiple Myeloma and Other Plasma Cell Dyscrasias. The MD Anderson Manual of Medical Oncology. H. M. a. W. Kantarjian, R.A., Cenveo® Publisher Services.

Lee, S. Y., I. A. Buhimschi, A. T. Dulay, U. A. Ali, G. Zhao, S. S. Abdel-Razeq, M. O. Bahtiyar, S. F. Thung, E. F. Funai and C. S. Buhimschi (2011). "IL-6 trans-signaling system in intra-amniotic inflammation, preterm birth, and preterm premature rupture of the membranes." J Immunol **186**(5): 3226-3236.

Lenz, G. and L. M. Staudt (2010). "Aggressive lymphomas." N Engl J Med **362**(15): 1417-1429.

Leonard, W. J. and J. J. O'Shea (1998). "Jaks and STATs: biological implications." Annu Rev Immunol **16**: 293-322.

Levy, D. E. and C. K. Lee (2002). "What does Stat3 do?" J Clin Invest **109**(9): 1143-1148.

Liberzon, A., C. Birger, H. Thorvaldsdottir, M. Ghandi, J. P. Mesirov and P. Tamayo (2015). "The Molecular Signatures Database (MSigDB) hallmark gene set collection." Cell Syst **1**(6): 417-425.

Liefeld, T., Q. Gao, M. A. Chapman, G. Tonon, D. Auclair, M. Reich, and T. R. Golub (2008). "The Multiple Myeloma Genomics Portal." Blood **112**(11): 5115-5115.

Lin, Y., K. Wong and K. Calame (1997). "Repression of c-myc transcription by Blimp-1, an inducer of terminal B cell differentiation." Science **276**(5312): 596-599.

Liu, J., B. Modrell, A. Aruffo, J. S. Marken, T. Taga, K. Yasukawa, M. Murakami, T. Kishimoto and M. Shoyab (1992). "Interleukin-6 signal transducer gp130 mediates oncostatin M signaling." J Biol Chem **267**(24): 16763-16766.

Loder, F., B. Mutschler, R. J. Ray, C. J. Paige, P. Sideras, R. Torres, M. C. Lamers and R. Carsetti (1999). "B cell development in the spleen takes place in discrete steps and is determined by the quality of B cell receptor-derived signals." J Exp Med **190**(1): 75-89.

Lonial, S., M. Dimopoulos, A. Palumbo, D. White, S. Grosicki, I. Spicka, A. Walter-Croneck, P. Moreau, M. V. Mateos, H. Magen, A. Belch, D. Reece, M. Beksac, A. Spencer, H. Oakervee, R. Z. Orlowski, M. Taniwaki, C. Rollig, H. Einsele, K. L. Wu, A. Singhal, J. San-Miguel, M. Matsumoto, J. Katz, E. Bleickardt, V. Poulart, K. C. Anderson, P. Richardson and E.-. Investigators (2015). "Elotuzumab Therapy for Relapsed or Refractory Multiple Myeloma." N Engl J Med **373**(7): 621-631.

Lonial, S., B. M. Weiss, S. Z. Usmani, S. Singhal, A. Chari, N. J. Bahlis, A. Belch, A. Krishnan, R. A. Vescio, M. V. Mateos, A. Mazumder, R. Z. Orlowski, H. J. Sutherland, J. Blade, E. C. Scott, A. Oriol, J. Berdeja, M. Gharibo, D. A. Stevens, R. LeBlanc, M. Sebag, N. Callander, A. Jakubowiak, D. White, J. de la Rubia, P. G. Richardson, S. Lisby, H. Feng, C. M. Uhlar, I. Khan, T. Ahmadi and P. M. Voorhees (2016). "Daratumumab monotherapy in patients with treatment-refractory multiple myeloma (SIRIUS): an open-label, randomised, phase 2 trial." Lancet **387**(10027): 1551-1560.

Lossos, I. S., A. A. Alizadeh, M. B. Eisen, W. C. Chan, P. O. Brown, D. Botstein, L. M. Staudt and R. Levy (2000). "Ongoing immunoglobulin somatic mutation in germinal center B cell-like but not in activated B cell-like diffuse large cell lymphomas." Proc Natl Acad Sci U S A **97**(18): 10209-10213.

Ludwig, H., D. M. Nachbaur, E. Fritz, M. Krainer and H. Huber (1991). "Interleukin-6 is a prognostic factor in multiple myeloma." Blood **77**(12): 2794-2795.

Lust, J. A., K. A. Donovan, M. P. Kline, P. R. Greipp, R. A. Kyle and N. J. Maihle (1992). "Isolation of an mRNA encoding a soluble form of the human interleukin-6 receptor." Cytokine **4**(2): 96-100.

MacLennan, I. C. (1994). "Germinal centers." Annu Rev Immunol **12**: 117-139.

Macosko, E. Z., A. Basu, R. Satija, J. Nemesh, K. Shekhar, M. Goldman, I. Tirosh, A. R. Bialas, N. Kamitaki, E. M. Martersteck, J. J. Trombetta, D. A. Weitz, J. R. Sanes, A. K. Shalek, A. Regev and S. A. McCarroll (2015). "Highly Parallel Genome-wide Expression Profiling of Individual Cells Using Nanoliter Droplets." Cell **161**(5): 1202-1214.

Manning, L. S., J. D. Berger, H. L. O'Donoghue, G. N. Sheridan, P. G. Claringbold and J. H. Turner (1992). "A model of multiple myeloma: culture of 5T33 murine myeloma cells and evaluation of tumorigenicity in the C57BL/KaLwRij mouse." Br J Cancer **66**(6): 1088-1093.

Mateos, M. V., M. A. Dimopoulos, M. Cavo, K. Suzuki, A. Jakubowiak, S. Knop, C. Doyen, P. Lucio, Z. Nagy, P. Kaplan, L. Pour, M. Cook, S. Grosicki, A. Crepaldi, A. M. Liberati, P. Campbell, T. Shelekhova, S. S. Yoon, G. Iosava, T. Fujisaki, M. Garg, C. Chiu, J. Wang, R. Carson, W. Crist, W. Deraedt, H. Nguyen, M. Qi, J. San-Miguel and A. T. Investigators (2018). "Daratumumab plus Bortezomib, Melphalan, and Prednisone for Untreated Myeloma." N Engl J Med **378**(6): 518-528.

Matsui, W., Q. Wang, J. P. Barber, S. Brennan, B. D. Smith, I. Borrello, I. McNiece, L. Lin, R. F. Ambinder, C. Peacock, D. N. Watkins, C. A. Huff and R. J. Jones (2008). "Clonogenic multiple myeloma progenitors, stem cell properties, and drug resistance." Cancer Res **68**(1): 190-197.

McGann, L. E. and M. L. Walterson (1987). "Cryoprotection by dimethyl sulfoxide and dimethyl sulfone." Cryobiology **24**(1): 11-16.

Michels, T. C. and K. E. Petersen (2017). "Multiple Myeloma: Diagnosis and Treatment." Am Fam Physician **95**(6): 373-383.

Middela, S. and P. Kanse (2009). "Nonsecretory multiple myeloma." Indian J Orthop **43**(4): 408-411.

Miller, D. G., M. A. Adam and A. D. Miller (1990). "Gene transfer by retrovirus vectors occurs only in cells that are actively replicating at the time of infection." Mol Cell Biol **10**(8): 4239-4242.

Mitsiades, N., C. S. Mitsiades, V. Poulaki, D. Chauhan, G. Fanourakis, X. Gu, C. Bailey, M. Joseph, T. A. Libermann, S. P. Treon, N. C. Munshi, P. G. Richardson, T. Hideshima and K. C. Anderson (2002). "Molecular sequelae of proteasome inhibition in human multiple myeloma cells." Proc Natl Acad Sci U S A **99**(22): 14374-14379.

Monaghan, K. A., T. Khong, C. J. Burns and A. Spencer (2011). "The novel JAK inhibitor CYT387 suppresses multiple signalling pathways, prevents proliferation and induces apoptosis in phenotypically diverse myeloma cells." Leukemia **25**(12): 1891-1899.

Morgan, G. J., B. A. Walker and F. E. Davies (2012). "The genetic architecture of multiple myeloma." Nat Rev Cancer **12**(5): 335-348.

Morito, N., K. Yoh, A. Maeda, T. Nakano, A. Fujita, M. Kusakabe, M. Hamada, T. Kudo, K. Yamagata and S. Takahashi (2011). "A novel transgenic mouse model of the human multiple myeloma chromosomal translocation t(14;16)(q32;q23)." Cancer Res **71**(2): 339-348.

Mullberg, J., H. Schooltink, T. Stoyan, M. Gunther, L. Graeve, G. Buse, A. Mackiewicz, P. C. Heinrich and S. Rose-John (1993). "The soluble interleukin-6 receptor is generated by shedding." Eur J Immunol **23**(2): 473-480.

Mullis, K. B. and F. A. Faloona (1987). "Specific synthesis of DNA in vitro via a polymerase-catalyzed chain reaction." Methods Enzymol **155**: 335-350.

Munoz, J., N. Dhillon, F. Janku, S. S. Watowich and D. S. Hong (2014). "STAT3 inhibitors: finding a home in lymphoma and leukemia." Oncologist **19**(5): 536-544.

Munshi, N. C. (1997). "Immunoregulatory mechanisms in multiple myeloma." Hematol Oncol Clin North Am **11**(1): 51-69.

Munshi, N. C., T. Hideshima, D. Carrasco, M. Shammas, D. Auclair, F. Davies, N. Mitsiades, C. Mitsiades, R. S. Kim, C. Li, S. V. Rajkumar, R. Fonseca, L. Bergsagel, D. Chauhan and K. C. Anderson (2004). "Identification of genes modulated in multiple myeloma using genetically identical twin samples." Blood **103**(5): 1799-1806.

Muraguchi, A., T. Hirano, B. Tang, T. Matsuda, Y. Horii, K. Nakajima and T. Kishimoto (1988). "The Essential Role of B-Cell Stimulatory Factor-Ii (Bsf-2/Il-6) for the Terminal Differentiation of B-Cells." Journal of Experimental Medicine **167**(2): 332-344.

Muramatsu, M., K. Kinoshita, S. Fagarasan, S. Yamada, Y. Shinkai and T. Honjo (2000). "Class switch recombination and hypermutation require activation-induced cytidine deaminase (AID), a potential RNA editing enzyme." Cell **102**(5): 553-563.

Nagy, A. (2000). "Cre recombinase: the universal reagent for genome tailoring." Genesis **26**(2): 99-109.

Nagy, A., L. Mar and G. Watts (2009). "Creation and use of a cre recombinase transgenic database." Methods Mol Biol **530**: 365-378.

Namen, A. E., S. Lupton, K. Hjerrild, J. Wignall, D. Y. Mochizuki, A. Schmierer, B. Mosley, C. J. March, D. Urdal and S. Gillis (1988). "Stimulation of B-cell progenitors by cloned murine interleukin-7." Nature **333**(6173): 571-573.

Naymagon, L. and M. Abdul-Hay (2016). "Novel agents in the treatment of multiple myeloma: a review about the future." J Hematol Oncol **9**(1): 52.

Neuberger, M. S., A. Lanoue, M. R. Ehrenstein, F. D. Batista, J. E. Sale and G. T. Williams (1999). "Antibody diversification and selection in the mature B-cell compartment." Cold Spring Harb Symp Quant Biol **64**: 211-216.

Nishihara, M., H. Ogura, N. Ueda, M. Tsuruoka, C. Kitabayashi, F. Tsuji, H. Aono, K. Ishihara, E. Huseby, U. A. Betz, M. Murakami and T. Hirano (2007). "IL-6-gp130-STAT3 in T cells directs the development of IL-17+ Th with a minimum effect on that of Treg in the steady state." Int Immunol **19**(6): 695-702.

Niwa, Y., H. Kanda, Y. Shikauchi, A. Saiura, K. Matsubara, T. Kitagawa, J. Yamamoto, T. Kubo and H. Yoshikawa (2005). "Methylation silencing of SOCS-3 promotes cell growth and migration by enhancing JAK/STAT and FAK signalings in human hepatocellular carcinoma." Oncogene **24**(42): 6406-6417.

Noguchi, M., H. Yi, H. M. Rosenblatt, A. H. Filipovich, S. Adelstein, W. S. Modi, O. W. McBride and W. J. Leonard (1993). "Interleukin-2 receptor gamma chain mutation results in X-linked severe combined immunodeficiency in humans." Cell **73**(1): 147-157.

Novick, D., H. Engelmann, D. Wallach and M. Rubinstein (1989). "Soluble cytokine receptors are present in normal human urine." J Exp Med **170**(4): 1409-1414.

Nussenzweig, A. and M. C. Nussenzweig (2010). "Origin of chromosomal translocations in lymphoid cancer." Cell **141**(1): 27-38.

Nutt, S. L., P. D. Hodgkin, D. M. Tarlinton and L. M. Corcoran (2015). "The generation of antibody-secreting plasma cells." Nat Rev Immunol **15**(3): 160-171.

O'Shea, E. K., R. Rutkowski, W. F. Stafford, 3rd and P. S. Kim (1989). "Preferential heterodimer formation by isolated leucine zippers from fos and jun." Science **245**(4918): 646-648.

Oettinger, M. A., D. G. Schatz, C. Gorka and D. Baltimore (1990). "RAG-1 and RAG-2, adjacent genes that synergistically activate V(D)J recombination." Science **248**(4962): 1517-1523.

Ogilvy, S., A. G. Elefanty, J. Visvader, M. L. Bath, A. W. Harris and J. M. Adams (1998). "Transcriptional regulation of vav, a gene expressed throughout the hematopoietic compartment." Blood **91**(2): 419-430.

Ogilvy, S., D. Metcalf, L. Gibson, M. L. Bath, A. W. Harris and J. M. Adams (1999). "Promoter elements of vav drive transgene expression in vivo throughout the hematopoietic compartment." Blood **94**(6): 1855-1863.

Ohinata, Y., B. Payer, D. O'Carroll, K. Ancelin, Y. Ono, M. Sano, S. C. Barton, T. Obukhanych, M. Nussenzweig, A. Tarakhovsky, M. Saitou and M. A. Surani (2005). "Blimp1 is a critical determinant of the germ cell lineage in mice." Nature **436**(7048): 207-213.

Orfao, A., A. Ruiz-Arguelles, F. Lacombe, K. Ault, G. Basso and M. Danova (1995). "Flow cytometry: its applications in hematology." Haematologica **80**(1): 69-81.

Orlowski, R. Z., L. Gercheva, C. Williams, H. Sutherland, T. Robak, T. Masszi, V. Goranova-Marinova, M. A. Dimopoulos, J. D. Cavenagh, I. Spicka, A. Maiolino, A. Suvorov, J. Blade, O. Samoylova, T. A. Puchalski, M. Reddy, R. Bandekar, H. van de Velde, H. Xie and J. F. Rossi (2015). "A phase 2, randomized, double-blind, placebo-controlled study of siltuximab (anti-IL-6 mAb) and bortezomib versus bortezomib alone in patients with relapsed or refractory multiple myeloma." Am J Hematol **90**(1): 42-49.

Palumbo, A. and K. Anderson (2011). "Multiple myeloma." N Engl J Med **364**(11): 1046-1060.

Parekh, S., C. Ziegenhain, B. Vieth, W. Enard and I. Hellmann (2016). "The impact of amplification on differential expression analyses by RNA-seq." Sci Rep **6**: 25533.

Park, S. J., T. Nakagawa, H. Kitamura, T. Atsumi, H. Kamon, S. Sawa, D. Kamimura, N. Ueda, Y. Iwakura, K. Ishihara, M. Murakami and T. Hirano (2004). "IL-6 regulates in vivo dendritic cell differentiation through STAT3 activation." J Immunol **173**(6): 3844-3854.

Paton-Hough, J., A. D. Chantry and M. A. Lawson (2015). "A review of current murine models of multiple myeloma used to assess the efficacy of therapeutic agents on tumour growth and bone disease." Bone **77**: 57-68.

Paul, B., B. Lipe, E. M. Ocio and S. Z. Usmani (2019). "Induction Therapy for Newly Diagnosed Multiple Myeloma." Am Soc Clin Oncol Educ Book **39**: e176-e186.

Pavri, R. and M. C. Nussenzweig (2011). "AID targeting in antibody diversity." Adv Immunol **110**: 1-26.
Pedranzini, L., T. Dechow, M. Berishaj, R. Comenzo, P. Zhou, J. Azare, W. Bornmann and J. Bromberg (2006). "Pyridone 6, a pan-Janus-activated kinase inhibitor, induces growth inhibition of multiple myeloma cells." Cancer Res **66**(19): 9714-9721.

Pelliniemi, T. T., K. Irjala, K. Mattila, K. Pulkki, A. Rajamaki, A. Tienhaara, M. Laakso and R. Lahtinen (1995). "Immunoreactive interleukin-6 and acute phase proteins as prognostic factors in multiple myeloma. Finnish Leukemia Group." Blood **85**(3): 765-771.

Pene, F., Y. E. Claessens, O. Muller, F. Viguie, P. Mayeux, F. Dreyfus, C. Lacombe and D. Bouscary (2002). "Role of the phosphatidylinositol 3-kinase/Akt and mTOR/P70S6-kinase pathways in the proliferation and apoptosis in multiple myeloma." Oncogene **21**(43): 6587-6597.

Pennica, D., K. J. Shaw, T. A. Swanson, M. W. Moore, D. L. Shelton, K. A. Zioncheck, A. Rosenthal, T. Taga, N. F. Paoni and W. I. Wood (1995). "Cardiotrophin-1. Biological activities and binding to the leukemia inhibitory factor receptor/gp130 signaling complex." J Biol Chem **270**(18): 10915-10922.

Peters, M., P. Schirmacher, J. Goldschmitt, M. Odenthal, C. Peschel, E. Fattori, G. Ciliberto, H. P. Dienes, K. H. Meyer zum Buschenfelde and S. Rose-John (1997). "Extramedullary expansion of hematopoietic progenitor cells in interleukin (IL)-6-sIL-6R double transgenic mice." J Exp Med **185**(4): 755-766.

Pieper, K., B. Grimbacher and H. Eibel (2013). "B-cell biology and development." J Allergy Clin Immunol **131**(4): 959-971.

Pillai, S. and D. Baltimore (1987). "Formation of disulphide-linked mu 2 omega 2 tetramers in pre-B cells by the 18K omega-immunoglobulin light chain." Nature **329**(6135): 172-174.

Potter, M. (1986). "Plasmacytomas in mice." Semin Oncol **13**(3): 275-281.

Prieyl, J. A. and T. W. LeBien (1996). "Interleukin 7 independent development of human B cells." Proc Natl Acad Sci U S A **93**(19): 10348-10353.

Puel, A., S. F. Ziegler, R. H. Buckley and W. J. Leonard (1998). "Defective IL7R expression in T(-)B(+)NK(+) severe combined immunodeficiency." Nat Genet **20**(4): 394-397.

Qiang, Y. W., J. D. Shaughnessy, Jr. and S. Yaccoby (2008). "Wnt3a signaling within bone inhibits multiple myeloma bone disease and tumor growth." Blood **112**(2): 374-382.

Quach, H., D. Ritchie, A. K. Stewart, P. Neeson, S. Harrison, M. J. Smyth and H. M. Prince (2010). "Mechanism of action of immunomodulatory drugs (IMiDS) in multiple myeloma." Leukemia **24**(1): 22-32.

R-Core-Team (2016). R: A Language and Environment for Statistical Computing. R Foundation for Statistical Computing, Vienna, Austria.

Radl, J. (1990). "Age-related monoclonal gammapathies: clinical lessons from the aging C57BL mouse." Immunol Today **11**(7): 234-236.

Radl, J., J. W. Croese, C. Zurcher, M. H. Van den Enden-Vieveen and A. M. de Leeuw (1988). "Animal model of human disease. Multiple myeloma." Am J Pathol **132**(3): 593-597.

Radl, J., E. D. De Glopper, H. R. Schuit and C. Zurcher (1979). "Idiopathic paraproteinemia. II. Transplantation of the paraprotein-producing clone from old to young C57BL/KaLwRij mice." J Immunol **122**(2): 609-613.

Radl, J., M.H.M. van den Enden-Vieveen, C. Zurcher, P.J.M. Roholl and E. Blauw (1989). "Morbus Waldenstrom-like lymphoma in the aging C57BL/KaLwRij mouse." Radl J and van Camp B (eds) Monoclonal Gammapathies - Clinical significance and basic mechanisms **Vol. 12**(Topics in Aging Research in Europe, Eurage, Rijswijk): 232-238.

Rajkumar, S. V., M. A. Dimopoulos, A. Palumbo, J. Blade, G. Merlini, M. V. Mateos, S. Kumar, J. Hillengass, E. Kastritis, P. Richardson, O. Landgren, B. Paiva, A. Dispenzieri, B. Weiss, X. LeLeu, S. Zweegman, S. Lonial, L. Rosinol, E. Zamagni, S. Jagannath, O. Sezer, S. Y. Kristinsson, J. Caers, S. Z. Usmani, J. J. Lahuerta, H. E. Johnsen, M. Beksac, M. Cavo, H. Goldschmidt, E. Terpos, R. A. Kyle, K. C. Anderson, B. G. Durie and J. F. Miguel (2014). "International Myeloma Working Group updated criteria for the diagnosis of multiple myeloma." Lancet Oncol **15**(12): e538-548.

Rajkumar, S. V. and S. Kumar (2016). "Multiple Myeloma: Diagnosis and Treatment." Mayo Clin Proc **91**(1): 101-119.

Ranheim, E. A., H. C. Kwan, T. Reya, Y. K. Wang, I. L. Weissman and U. Francke (2005). "Frizzled 9 knock-out mice have abnormal B-cell development." Blood **105**(6): 2487-2494.

Reddy, A., J. Zhang, N. S. Davis, A. B. Moffitt, C. L. Love, A. Waldrop, S. Leppa, A. Pasanen, L. Meriranta, M. L. Karjalainen-Lindsberg, P. Norgaard, M. Pedersen, A. O. Gang, E. Hogdall, T. B. Heavican, W. Lone, J. Iqbal, Q. Qin, G. J. Li, S. Y. Kim, J. Healy, K. L. Richards, Y. Fedoriw, L. Bernal-Mizrachi, J. L. Koff, A. D. Staton, C. R. Flowers, O. Paltiel, N. Goldschmidt, M. Calaminici, A. Clear, J. Gribben, E. Nguyen, M. B. Czader, S. L. Ondrejka, A. Collie, E. D. Hsi, E. Tse, R. K. H. Au-Yeung, Y. L. Kwong, G. Srivastava, W. W. L. Choi, A. M. Evens, M. Pilichowska, M. Sengar, N. Reddy, S. Y. Li, A. Chadburn, L. I. Gordon, E. S. Jaffe, S. Levy, R. Rempel, T. Tzeng, L. E. Happ, T. Dave, D. Rajagopalan, J. Datta, D. B. Dunson and S. S. Dave (2017). "Genetic and Functional Drivers of Diffuse Large B Cell Lymphoma." Cell **171**(2): 481-+.

Reijmers, R. M., R. W. Groen, H. Rozemuller, A. Kuil, A. de Haan-Kramer, T. Csikos, A. C. Martens, M. Spaargaren and S. T. Pals (2010). "Targeting EXT1 reveals a crucial role for heparan sulfate in the growth of multiple myeloma." Blood **115**(3): 601-604.

Reimold, A. M., N. N. Iwakoshi, J. Manis, P. Vallabhajosyula, E. Szomolanyi-Tsuda, E. M. Gravallese, D. Friend, M. J. Grusby, F. Alt and L. H. Glimcher (2001). "Plasma cell differentiation requires the transcription factor XBP-1." Nature **412**(6844): 300-307.

Remy, I., I. A. Wilson and S. W. Michnick (1999). "Erythropoietin receptor activation by a ligand-induced conformation change." Science **283**(5404): 990-993.

Reya, T., M. O'Riordan, R. Okamura, E. Devaney, K. Willert, R. Nusse and R. Grosschedl (2000). "Wnt signaling regulates B lymphocyte proliferation through a LEF-1 dependent mechanism." Immunity **13**(1): 15-24.

Richmond, A. and Y. Su (2008). "Mouse xenograft models vs GEM models for human cancer therapeutics." Dis Model Mech **1**(2-3): 78-82.

Rickert, R. C. (2013). "New insights into pre-BCR and BCR signalling with relevance to B cell malignancies." Nat Rev Immunol **13**(8): 578-591.

Rickert, R. C., J. Roes and K. Rajewsky (1997). "B lymphocyte-specific, Cre-mediated mutagenesis in mice." Nucleic Acids Res **25**(6): 1317-1318.

Ridley, R. C., H. Xiao, H. Hata, J. Woodliff, J. Epstein and R. D. Sanderson (1993). "Expression of syndecan regulates human myeloma plasma cell adhesion to type I collagen." Blood **81**(3): 767-774.

Ritchie, M. E., B. Phipson, D. Wu, Y. Hu, C. W. Law, W. Shi and G. K. Smyth (2015). "limma powers differential expression analyses for RNA-sequencing and microarray studies." Nucleic Acids Res **43**(7): e47.

Robinson, M. D., D. J. McCarthy and G. K. Smyth (2010). "edgeR: a Bioconductor package for differential expression analysis of digital gene expression data." Bioinformatics **26**(1): 139-140.

Rodriguez-Otero, P., B. Paiva, M. Engelhardt, F. Prosper and J. F. San Miguel (2017). "Is immunotherapy here to stay in multiple myeloma?" Haematologica **102**(3): 423-432.

Rollig, C., S. Knop and M. Bornhauser (2015). "Multiple myeloma." Lancet **385**(9983): 2197-2208.
Roodman, G. D. (2004). "Mechanisms of bone metastasis." N Engl J Med **350**(16): 1655-1664.

Rosean, T. R., V. S. Tompkins, G. Tricot, C. J. Holman, A. K. Olivier, F. Zhan and S. Janz (2014). "Preclinical validation of interleukin 6 as a therapeutic target in multiple myeloma." Immunol Res **59**(1-3): 188-202.

Rossi, M., C. Botta, M. Arbitrio, R. D. Grembiale, P. Tagliaferri and P. Tassone (2018). "Mouse models of multiple myeloma: technologic platforms and perspectives." Oncotarget **9**(28): 20119-20133.
Samitas, K., J. Lotvall and A. Bossios (2010). "B cells: from early development to regulating allergic diseases." Arch Immunol Ther Exp (Warsz) **58**(3): 209-225.

Sansone, P. and J. Bromberg (2012). "Targeting the interleukin-6/Jak/stat pathway in human malignancies." J Clin Oncol **30**(9): 1005-1014.

Sauer, B. and N. Henderson (1988). "Site-specific DNA recombination in mammalian cells by the Cre recombinase of bacteriophage P1." Proc Natl Acad Sci U S A **85**(14): 5166-5170.

Schaper, F. and S. Rose-John (2015). "Interleukin-6: Biology, signaling and strategies of blockade." Cytokine & Growth Factor Reviews **26**(5): 475-487.

Schatz, D. G., M. A. Oettinger and D. Baltimore (1989). "The V(D)J recombination activating gene, RAG-1." Cell **59**(6): 1035-1048.

Schmidt, M. R., L. W. McGinnes, S. A. Kenward, K. N. Willems, R. T. Woodland and T. G. Morrison (2012). "Long-term and memory immune responses in mice against Newcastle disease virus-like particles containing respiratory syncytial virus glycoprotein ectodomains." J Virol **86**(21): 11654-11662.

Schneeberger, C., P. Speiser, F. Kury and R. Zeillinger (1995). "Quantitative detection of reverse transcriptase-PCR products by means of a novel and sensitive DNA stain." PCR Methods Appl **4**(4): 234-238.

Schwab, G., C. B. Siegall, L. A. Aarden, L. M. Neckers and R. P. Nordan (1991). "Characterization of an interleukin-6-mediated autocrine growth loop in the human multiple myeloma cell line, U266." Blood **77**(3): 587-593.

Scuto, A., P. Krejci, L. Popplewell, J. Wu, Y. Wang, M. Kujawski, C. Kowolik, H. Xin, L. Chen, Y. Wang, L. Kretzner, H. Yu, W. R. Wilcox, Y. Yen, S. Forman and R. Jove (2011). "The novel JAK inhibitor AZD1480 blocks STAT3 and FGFR3 signaling, resulting in suppression of human myeloma cell growth and survival." Leukemia **25**(3): 538-550.

Sehgal, P. B., Grienger, G., and Tosato, G. (1989). "Regulation of the acute phase and immune responses: interleukin-6." Ann N Y Acad Sci **557**: 1-583.

Shaffer, A. L., 3rd, R. M. Young and L. M. Staudt (2012). "Pathogenesis of human B cell lymphomas." Annu Rev Immunol **30**: 565-610.

Shaffer, A. L., A. Rosenwald, E. M. Hurt, J. M. Giltnane, L. T. Lam, O. K. Pickeral and L. M. Staudt (2001). "Signatures of the immune response." Immunity **15**(3): 375-385.

Shapiro-Shelef, M. and K. Calame (2004). "Plasma cell differentiation and multiple myeloma." Curr Opin Immunol **16**(2): 226-234.

Shapiro-Shelef, M. and K. Calame (2005). "Regulation of plasma-cell development." Nat Rev Immunol **5**(3): 230-242.

Shapiro-Shelef, M., K. I. Lin, L. J. McHeyzer-Williams, J. Liao, M. G. McHeyzer-Williams and K. Calame (2003). "Blimp-1 is required for the formation of immunoglobulin secreting plasma cells and pre-plasma memory B cells." Immunity **19**(4): 607-620.

Shapiro-Shelef, M., K. I. Lin, D. Savitsky, J. Liao and K. Calame (2005). "Blimp-1 is required for maintenance of long-lived plasma cells in the bone marrow." J Exp Med **202**(11): 1471-1476.
Shen, F. W., Y. Saga, G. Litman, G. Freeman, J. S. Tung, H. Cantor and E. A. Boyse (1985). "Cloning of Ly-5 cDNA." Proc Natl Acad Sci U S A **82**(21): 7360-7363.

Shimshek, D. R., J. Kim, M. R. Hubner, D. J. Spergel, F. Buchholz, E. Casanova, A. F. Stewart, P. H. Seeburg and R. Sprengel (2002). "Codon-improved Cre recombinase (iCre) expression in the mouse." Genesis **32**(1): 19-26.

Shuai, K., C. M. Horvath, L. H. Huang, S. A. Qureshi, D. Cowburn and J. E. Darnell, Jr. (1994). "Interferon activation of the transcription factor Stat91 involves dimerization through SH2-phosphotyrosyl peptide interactions." Cell **76**(5): 821-828.

Silver, J. S. and C. A. Hunter (2010). "gp130 at the nexus of inflammation, autoimmunity, and cancer." Journal of Leukocyte Biology **88**(6): 1145-1156.

Smith, B. J. (1984). SDS Polyacrylamide Gel Electrophoresis of Proteins.

Sobol, U. and P. Stiff (2014). "Neurologic aspects of plasma cell disorders." Handb Clin Neurol **120**: 1083-1099.

Soutar, R., H. Lucraft, G. Jackson, A. Reece, J. Bird, E. Low, D. Samson, U. K. M. F. Guidelines Working Group of the, H. British Committee for Standards in and H. British Society for (2004). "Guidelines on the diagnosis and management of solitary plasmacytoma of bone and solitary extramedullary plasmacytoma." Br J Haematol **124**(6): 717-726.

Spiegelman, S., K. F. Watson and D. L. Kacian (1971). "Synthesis of DNA complements of natural RNAs: a general approach." Proc Natl Acad Sci U S A **68**(11): 2843-2845.

Sternberg, N. and D. Hamilton (1981). "Bacteriophage P1 site-specific recombination. I. Recombination between loxP sites." J Mol Biol **150**(4): 467-486.

Sternberg, N., D. Hamilton and R. Hoess (1981). "Bacteriophage P1 site-specific recombination. II. Recombination between loxP and the bacterial chromosome." J Mol Biol **150**(4): 487-507.

Stuhlmann-Laeisz, C., S. Lang, A. Chalaris, P. Krzysztof, S. Enge, J. Eichler, U. Klingmuller, M. Samuel, M. Ernst, S. Rose-John and J. Scheller (2006). "Forced dimerization of gp130 leads to constitutive STAT3 activation, cytokine-independent growth, and blockade of differentiation of embryonic stem cells." Mol Biol Cell **17**(7): 2986-2995.

Subramanian, A., P. Tamayo, V. K. Mootha, S. Mukherjee, B. L. Ebert, M. A. Gillette, A. Paulovich, S. L. Pomeroy, T. R. Golub, E. S. Lander and J. P. Mesirov (2005). "Gene set enrichment analysis: a knowledge-based approach for interpreting genome-wide expression profiles." Proc Natl Acad Sci U S A **102**(43): 15545-15550.

Suck, G., M. Odendahl, P. Nowakowska, C. Seidl, W. S. Wels, H. G. Klingemann and T. Tonn (2016). "NK-92: an 'off-the-shelf therapeutic' for adoptive natural killer cell-based cancer immunotherapy." Cancer Immunol Immunother **65**(4): 485-492.

Suematsu, S., T. Matsuda, K. Aozasa, S. Akira, N. Nakano, S. Ohno, J. Miyazaki, K. Yamamura, T. Hirano and T. Kishimoto (1989). "Igg1 Plasmacytosis in Interleukin-6 Transgenic Mice." Proceedings of the National Academy of Sciences of the United States of America **86**(19): 7547-7551.

Suematsu, S., T. Matsusaka, T. Matsuda, S. Ohno, J. Miyazaki, K. Yamamura, T. Hirano and T. Kishimoto (1992). "Generation of plasmacytomas with the chromosomal translocation t(12;15) in interleukin 6 transgenic mice." Proc Natl Acad Sci U S A **89**(1): 232-235.

Swerdlow, S. H., E. Campo and N. L. Harris (2017). WHO Classification of Tumors of Haematopoietic and Lymphoid Tissues, World Health Organization.

Sze, D. M., K. M. Toellner, C. Garcia de Vinuesa, D. R. Taylor and I. C. MacLennan (2000). "Intrinsic constraint on plasmablast growth and extrinsic limits of plasma cell survival." J Exp Med **192**(6): 813-821.

Szeberenyi, J. (2013). "Problem-solving test: conditional gene targeting using the Cre/loxP recombination system." Biochem Mol Biol Educ **41**(6): 445-449.

Taga, T., M. Hibi, Y. Hirata, K. Yamasaki, K. Yasukawa, T. Matsuda, T. Hirano and T. Kishimoto (1989). "Interleukin-6 triggers the association of its receptor with a possible signal transducer, gp130." Cell **58**(3): 573-581.

Tai, Y. T. and K. C. Anderson (2015). "Targeting B-cell maturation antigen in multiple myeloma." Immunotherapy **7**(11): 1187-1199.

Tarlinton, D. M. and K. G. Smith (1997). "Apoptosis and the B cell response to antigen." Int Rev Immunol **15**(1-2): 53-71.

Temin, H. M. and S. Mizutani (1970). "RNA-dependent DNA polymerase in virions of Rous sarcoma virus." Nature **226**(5252): 1211-1213.

Teoh, P. J., T. H. Chung, S. Sebastian, S. N. Choo, J. Yan, S. B. Ng, R. Fonseca and W. J. Chng (2014). "p53 haploinsufficiency and functional abnormalities in multiple myeloma." Leukemia **28**(10): 2066-2074.

Thabard, W., S. Barille, M. Collette, J. L. Harousseau, M. J. Rapp, R. Bataille and M. Amiot (1999). "Myeloma cells release soluble interleukin-6Ralpha in relation to disease progression by two distinct mechanisms: alternative splicing and proteolytic cleavage." Clin Cancer Res **5**(10): 2693-2697.

Thanendrarajan, S., E. Tian, P. Qu, P. Mathur, C. Schinke, F. van Rhee, M. Zangari, L. Rasche, N. Weinhold, D. Alapat, W. Bellamy, C. Ashby, S. Mattox, J. Epstein, S. Yaccoby, B. Barlogie, A. Hoering, M. Bauer, B. A. Walker, F. E. Davies and G. J. Morgan (2017). "The level of deletion 17p and bi-allelic inactivation of TP53 has a significant impact on clinical outcome in multiple myeloma." Haematologica **102**(9): e364-e367.

Thomas, S. J., J. A. Snowden, M. P. Zeidler and S. J. Danson (2015). "The role of JAK/STAT signalling in the pathogenesis, prognosis and treatment of solid tumours." Br J Cancer **113**(3): 365-371.

Tonegawa, S. (1983). "Somatic generation of antibody diversity." Nature **302**(5909): 575-581.

Tunyaplin, C., A. L. Shaffer, C. D. Angelin-Duclos, X. Yu, L. M. Staudt and K. L. Calame (2004). "Direct repression of prdm1 by Bcl-6 inhibits plasmacytic differentiation." J Immunol **173**(2): 1158-1165.

Turner, C. A., Jr., D. H. Mack and M. M. Davis (1994). "Blimp-1, a novel zinc finger-containing protein that can drive the maturation of B lymphocytes into immunoglobulin-secreting cells." Cell **77**(2): 297-306.

Uchiyama, H., B. A. Barut, A. F. Mohrbacher, D. Chauhan and K. C. Anderson (1993). "Adhesion of human myeloma-derived cell lines to bone marrow stromal cells stimulates interleukin-6 secretion." Blood **82**(12): 3712-3720.

Urashima, M., B. P. Chen, S. Chen, G. S. Pinkus, R. T. Bronson, D. A. Dedera, Y. Hoshi, G. Teoh, A. Ogata, S. P. Treon, D. Chauhan and K. C. Anderson (1997). "The development of a model for the homing of multiple myeloma cells to human bone marrow." Blood **90**(2): 754-765.

Usmani, S. Z., B. M. Weiss, T. Plesner, N. J. Bahlis, A. Belch, S. Lonial, H. M. Lokhorst, P. M. Voorhees, P. G. Richardson, A. Chari, A. K. Sasser, A. Axel, H. Feng, C. M. Uhlar, J. Wang, I. Khan, T. Ahmadi

and H. Nahi (2016). "Clinical efficacy of daratumumab monotherapy in patients with heavily pretreated relapsed or refractory multiple myeloma." Blood **128**(1): 37-44.

van Andel, H., K. A. Kocemba, M. Spaargaren and S. T. Pals (2019). "Aberrant Wnt signaling in multiple myeloma: molecular mechanisms and targeting options." Leukemia **33**(5): 1063-1075.

van den Akker, T. W., E. de Glopper-van der Veer, J. Radl and R. Benner (1988). "The influence of genetic factors associated with the immunoglobulin heavy chain locus on the development of benign monoclonal gammapathy in ageing IgH-congenic mice." Immunology **65**(1): 31-35.

Van Snick, J. (1990). "Interleukin-6: an overview." Annu Rev Immunol **8**: 253-278.

Van Weemen, B. K. and A. H. Schuurs (1971). "Immunoassay using antigen-enzyme conjugates." FEBS Lett **15**(3): 232-236.

Vanderkerken, K., K. Asosingh, P. Croucher and B. Van Camp (2003). "Multiple myeloma biology: lessons from the 5TMM models." Immunol Rev **194**: 196-206.

Vanderkerken, K., C. De Greef, K. Asosingh, B. Arteta, M. De Veerman, I. Vande Broek, I. Van Riet, M. Kobayashi, B. Smedsrod and B. Van Camp (2000). "Selective initial in vivo homing pattern of 5T2 multiple myeloma cells in the C57BL/KalwRij mouse." Br J Cancer **82**(4): 953-959.

Vanderkerken, K., H. De Raeve, E. Goes, S. Van Meirvenne, J. Radl, I. Van Riet, K. Thielemans and B. Van Camp (1997). "Organ involvement and phenotypic adhesion profile of 5T2 and 5T33 myeloma cells in the C57BL/KaLwRij mouse." Br J Cancer **76**(4): 451-460.

Vasanwala, F. H., S. Kusam, L. M. Toney and A. L. Dent (2002). "Repression of AP-1 function: a mechanism for the regulation of Blimp-1 expression and B lymphocyte differentiation by the B cell lymphoma-6 protooncogene." J Immunol **169**(4): 1922-1929.

Victora, G. D. and M. C. Nussenzweig (2012). "Germinal centers." Annu Rev Immunol **30**: 429-457.

Vlummens, P., K. De Veirman, E. Menu, E. De Bruyne, F. Offner, K. Vanderkerken and K. Maes (2019). "The Use of Murine Models for Studying Mechanistic Insights of Genomic Instability in Multiple Myeloma." Front Genet **10**: 740.

Walker, B. A., K. Mavrommatis, C. P. Wardell, T. C. Ashby, M. Bauer, F. Davies, A. Rosenthal, H. Wang, P. Qu, A. Hoering, M. Samur, F. Towfic, M. Ortiz, E. Flynt, Z. Yu, Z. Yang, D. Rozelle, J. Obenauer, M. Trotter, D. Auclair, J. Keats, N. Bolli, M. Fulciniti, R. Szalat, P. Moreau, B. Durie, A. K. Stewart, H. Goldschmidt, M. S. Raab, H. Einsele, P. Sonneveld, J. San Miguel, S. Lonial, G. H. Jackson, K. C. Anderson, H. Avet-Loiseau, N. Munshi, A. Thakurta and G. Morgan (2019). "A high-risk, Double-Hit, group of newly diagnosed myeloma identified by genomic analysis." Leukemia **33**(1): 159-170.

Waring, M. J. (1965). "Complex formation between ethidium bromide and nucleic acids." J Mol Biol **13**(1): 269-282.

Wei, A. and S. Juneja (2003). "Bone marrow immunohistology of plasma cell neoplasms." J Clin Pathol **56**(6): 406-411.

Weinstock, M. and I. M. Ghobrial (2013). "Extramedullary multiple myeloma." Leuk Lymphoma **54**(6): 1135-1141.

Wijdenes, J., W. C. Vooijs, C. Clement, J. Post, F. Morard, N. Vita, P. Laurent, R. X. Sun, B. Klein and J. M. Dore (1996). "A plasmocyte selective monoclonal antibody (B-B4) recognizes syndecan-1." Br J Haematol **94**(2): 318-323.

Wolniak, K. L., S. M. Shinall and T. J. Waldschmidt (2004). "The germinal center response." Crit Rev Immunol **24**(1): 39-65.

Wright, G., B. Tan, A. Rosenwald, E. H. Hurt, A. Wiestner and L. M. Staudt (2003). "A gene expression-based method to diagnose clinically distinct subgroups of diffuse large B cell lymphoma." Proc Natl Acad Sci U S A **100**(17): 9991-9996.

Wu, J., R. Irizarry, J. MacDonald, J. Gentry (2014). gcrma: Background adjustment using sequence information. **R package version 2.38.0.**

Xin, A., S. L. Nutt, G. T. Belz and A. Kallies (2011). "Blimp1: driving terminal differentiation to a T." Adv Exp Med Biol **780**: 85-100.

Yaccoby, S., B. Barlogie and J. Epstein (1998). "Primary myeloma cells growing in SCID-hu mice: a model for studying the biology and treatment of myeloma and its manifestations." Blood **92**(8): 2908-2913.

Yaccoby, S. and J. Epstein (1999). "The proliferative potential of myeloma plasma cells manifest in the SCID-hu host." Blood **94**(10): 3576-3582.

Yaccoby, S., W. Ling, F. Zhan, R. Walker, B. Barlogie and J. D. Shaughnessy, Jr. (2007). "Antibody-based inhibition of DKK1 suppresses tumor-induced bone resorption and multiple myeloma growth in vivo." Blood **109**(5): 2106-2111.

Yamaoka, K., P. Saharinen, M. Pesu, V. E. Holt, 3rd, O. Silvennoinen and J. J. O'Shea (2004). "The Janus kinases (Jaks)." Genome Biol **5**(12): 253.

Yamasaki, K., T. Taga, Y. Hirata, H. Yawata, Y. Kawanishi, B. Seed, T. Taniguchi, T. Hirano and T. Kishimoto (1988). "Cloning and expression of the human interleukin-6 (BSF-2/IFN beta 2) receptor." Science **241**(4867): 825-828.

Yeh, T. C., E. Dondi, G. Uze and S. Pellegrini (2000). "A dual role for the kinase-like domain of the tyrosine kinase Tyk2 in interferon-alpha signaling." Proc Natl Acad Sci U S A **97**(16): 8991-8996.

Yin, T., T. Taga, M. L. Tsang, K. Yasukawa, T. Kishimoto and Y. C. Yang (1993). "Involvement of IL-6 signal transducer gp130 in IL-11-mediated signal transduction." J Immunol **151**(5): 2555-2561.

Ying, M., D. Li, L. Yang, M. Wang, N. Wang, Y. Chen, M. He and Y. Wang (2010). "Loss of SOCS3 expression is associated with an increased risk of recurrent disease in breast carcinoma." J Cancer Res Clin Oncol **136**(10): 1617-1626.

Yoshida, K., T. Taga, M. Saito, S. Suematsu, A. Kumanogoh, T. Tanaka, H. Fujiwara, M. Hirata, T. Yamagami, T. Nakahata, T. Hirabayashi, Y. Yoneda, K. Tanaka, W. Z. Wang, C. Mori, K. Shiota, N. Yoshida and T. Kishimoto (1996). "Targeted disruption of gp130, a common signal transducer for the interleukin 6 family of cytokines, leads to myocardial and hematological disorders." Proc Natl Acad Sci U S A **93**(1): 407-411.

Yu, Q., W. J. Quinn, 3rd, T. Salay, J. E. Crowley, M. P. Cancro and J. M. Sen (2008). "Role of beta-catenin in B cell development and function." J Immunol **181**(6): 3777-3783.

Zhan, F., E. Tian, K. Bumm, R. Smith, B. Barlogie and J. Shaughnessy, Jr. (2003). "Gene expression profiling of human plasma cell differentiation and classification of multiple myeloma based on similarities to distinct stages of late-stage B-cell development." Blood **101**(3): 1128-1140.

Zhang, S. L., W. DuBois, E. S. Ramsay, V. Bliskovski, H. C. Morse, 3rd, L. Taddesse-Heath, W. C. Vass, R. A. DePinho and B. A. Mock (2001). "Efficiency alleles of the Pctr1 modifier locus for plasmacytoma susceptibility." Mol Cell Biol **21**(1): 310-318.

Zhang, Y., L. Tech, L. A. George, A. Acs, R. E. Durrett, H. Hess, L. S. K. Walker, D. M. Tarlinton, A. L. Fletcher, A. E. Hauser and K. M. Toellner (2018). "Plasma cell output from germinal centers is regulated by signals from Tfh and stromal cells." J Exp Med **215**(4): 1227-1243.

Zipper, H., H. Brunner, J. Bernhagen and F. Vitzthum (2004). "Investigations on DNA intercalation and surface binding by SYBR Green I, its structure determination and methodological implications." Nucleic Acids Res **32**(12): e103.

7 List of tables

Table 1: Overview of primers used for genotyping in this study 30
Table 2: Overview of primers used for qRT-PCR in this study 30
Table 3: Overview of antibodies used for western blot analysis in this study 31
Table 4: Overview of antibodies used for flow cytometric analysis in this study 31

8 List of figures

Figure 1: Classical IL-6 signaling (left) and trans-signaling (right) 2
Figure 2: Schematic structure of Janus kinases (JAKs) with their functional domains 3
Figure 3: Schematic structure of signal transducers and activators of transcription (STATs) with their functional domains 4
Figure 4: IL-6/gp130/JAK/STAT signaling 5
Figure 5: Schematic illustration of gp130 and the chimeric L-gp130 6
Figure 6: The Germinal Center (GC) reaction 9
Figure 7: Serum protein electrophoresis 12
Figure 8: Gene activation by the Cre/loxP system by L-gp130 as the gene of interest 18
Figure 9: Overview of the Cre-transgenic strains and their expression during B cell development and in hematopoietic stem cells 19
Figure 10: Generation of R26 fl rx L-gp130 mice 46
Figure 11: Overview of the experiment. 47
Figure 12: Expression of L-gp130 results in downstream activity 48
Figure 13: Flow cytometry gating strategy for the definition of distinct B cell subsets 49
Figure 14: Forced gp130 signaling promotes B cell differentiation in young *CD19;L-gp* mice 50
Figure 15: Forced gp130 signaling alters total WBC numbers in young mice 51
Figure 16: Expression and activity of STAT3 by hierarchical cluster analysis 54
Figure 17: Activation of gp130 signaling in B cells results in B cell malignancies 57
Figure 18: Serial transplantation of cells from *CD19;L-gp* tumors results in reestablishment of the disease 58
Figure 19: Gp130 activation during or post GC B cell differentiation results in lymphoma and plasmacytoma 60
Figure 20: SRBC immunization promotes the formation of a GC reaction 61
Figure 21: Activated gp130 collaborates with Myc to enforce plasmacytic differentiation 64
Figure 22: Conditional gp130 activation in hematopoietic stem/progenitor cells results in a highly aggressive B cell malignancy 68
Figure 23: Transcriptional programs in murine lymphomagenesis 70
Figure 24: The L-gp130 signature during progression of MM 71

9 List of publications

9.1 Articles in peer-reviewed journals

Schick M, Maurer S, Schneider L, Schnuck K, Rohleder E, Maurer C, Hofstetter J, Baluapuri A, **Scherger AK**, Slotta-Huspenina J, Weber J, Engleitner T, Maresch R, Slawska J, Lewis R, Istvanffy R, Habringer S, Steiger K, Baiker A, Miething C, Oostendorp R, Lenhof HP, Chapuy B, Bassermann F, Wolf E, Rad R, Müller S, Keller U – *A genomewide functional in vivo transposon screen identifies novel MYC-cooperating tumor suppressor genes.* **(Manuscript submitted)**

Biederstädt A, Hassan Z, Schneeweis C, Schick M, Schneider L, Muckenhuber A, Hong Y, Siegers G, Nilsson L, Wirth M, Dantes Z, Steiger K, Schunck K, Langston S, Lenhof HP, Coluccio A, Orben F, Slawska J, **Scherger AK**, Saur D, Müller S, Rad R, Weichert W, Nilsson J, Reichert M, Schneider G, Keller U – *SUMO pathway inhibition targets an aggressive pancreatic cancer subtype*. **(Gut, 2020)**

Scherger AK, Al-Maarri M, Maurer HC, Schick M, Maurer S, Öllinger R, Gonzalez-Menendez I, Martella M, Thaler M, Pechloff K, Steiger K, Sander S, Ruland J, Rad R, Quintanilla-Martinez L, Rose-John S, Wunderlich FT, Keller U – *Activated gp130 signaling selectively targets B cell differentiation to promote transformation of mature B cell lymphoma and plasmacytoma.* **(JCI Insight, 2019)**

Weber J, de la Rosa J, Grove CS, Schick M, Rad L, Baranov O, Strong A, Pfaus A, Friedrich MJ, Engleitner T, Lersch R, Öllinger R, Grau M, Gonzalez Menendez I, Martella M, Kohlhofer U, Banerjee R, Turchaninova MA, **Scherger A**, Hoffman GJ, Hess J, Kuhn LB, Ammon T, Kim J, Schneider G, Unger K, Zimber-Strobel U, Heikenwälder M, Schmidt-Supprian M, Yang F, Saur D, Liu P, Steiger K, Chudakov DM, Lenz G, Quintanilla-Fend L, Keller U, Vassiliou GS, Cadiñanos J, Bradley A, Rad R - *PiggyBac transposon tools for tumor suppressor screening identify B-cell lymphoma drivers in mice*. **(Nature Communications, 2019)**

9.2 Conference contributions

Scherger AK, Schick M, Maurer S, Steiger K, Al-Maarri M, Wunderlich FT, Rose-John S, Peschel C, and Keller U. Conditional gp130-JAK-STAT3 activation induces malignant transformation *in vivo.*

DGHO Jahrestagung, Stuttgart, 2017, Poster.

Scherger AK, Schick M, Steiger K, Al-Maarri M, Wunderlich FT, Rose-John S, Peschel C, and Keller U. Conditional gp130-JAK-STAT3 activation induces malignant transformation *in vivo.*

DKTK 4th Munich Cancer Retreat, Herrsching, 2017, Poster.

Scherger AK, Schick M, Steiger K, Al-Maarri M, Wunderlich FT, Rose-John S, Peschel C, and Keller U. Conditional gp130-JAK-STAT3 activation induces malignant transformation *in vivo.*

Aegean 2nd International Conference on Cytokine Signaling in Cancer, Crete, 2017, Poster.

10 Acknowledgements

This study is the result of more than four years of work in the group of Prof. Dr. Ulrich Keller. I am looking back on an intense time full of hard working, learning, fruitful discussions, curiosity, support, heaps of fun and craziness, and valuable experiences with remarkable colleagues who became precious friends to me. I am grateful for the last years and want to thank everyone who has made a contribution to the success of this study and who made this time exceptional!

First of all, I sincerely thank my supervisor Prof. Dr. Ulrich Keller. Uli, thank you for giving me the opportunity to work in your group on this interesting project. Thank you for time and support and discussions that let me outgrow myself.

A warm thank you to Prof. Dr. Christian Peschel as the former and Prof. Dr. Florian Bassermann as the current head of the III. Medical Department at Klinikum rechts der Isar for giving me the opportunity to conduct my doctoral thesis here.

Thank you also to Prof. Dr. Angelika Schnieke and Prof. Dr. Philipp Jost for being my second supervisor and mentor, respectively. Thank you for the time you spent on the committee meetings and for the suggestions you made to promote my project.

Thank you to the members of the animal facilities for keeping an eye on my mice during the course of my doctoral thesis.

Many thanks to all collaborators in Cologne, Kiel, Tübingen, and Munich who contributed to this study, especially to Carlo Maurer who did the analysis of all RNASeq data presented in this study.

I thank all members of the III. Medical Department, especially AG Oostendorp and AG Götze for scientific discussions and the friendly work atmosphere. Special thanks to my girls Resi, Judy and Mitch for your support and friendship over the last years, for some after-work drinks and lots of laugther and craziness.

Special thanks to the whole AG Keller crew with all current and former members who were always supportive in answering questions and helping me when I needed a hand with big experiments. And of course thank you for the social life after work.

I owe my biggest thank you to my lab buddy Markus Schick. Schicki, you make the “dynamic duo” complete and I could not have wished for a better collaboration partner in the lab. Thank you so much for your support throughout the years, for scientific discussions, for answering questions and explaining the world to me. Thank you for sharing heaps of ice cream, coffee, pizza, Leberkassemmeln and Brücken-Spezis, for making me laugh when I was down, and for your deep friendship.

Last but not least I want to sincerely thank my friends as well as my godparents and cousins and especially my parents and siblings: thank you for your encouragement and support in making me reach this important milestone. Thank you for your endless love and for always believing in me.